Article

Microbiota-mediated induction of beige adipocytes in response to dietary cues

https://doi.org/10.1038/s41586-026-10205-3

Received: 14 November 2024

Accepted: 28 January 2026

Published online: 04 March 2026

Open access

Check for updates

Takeshi Tanoue[1,2,3,20], Manabu Nagayama[1,2,4,20], Ayumi J. A. Roochana[1,20], Samuel Zimmerman[5,20], Orr Ashenberg[6], Tanvi Jain[6], Ryo Igarashi[7], Satoshi Sasajima[1], Kozue Takeshita[1], Nicola Hetherington[2,8], Nobuyuki Okahashi[2], Masahiro Ueda[2,9], Morichika Konishi[10], Yoshiaki Nakayama[10], Aki Minoda[2,8], Ashwin N. Skelly[1], Yasuhiko Minokoshi[11], Nicholas Pucci[12], Daniel R. Mende[12,13], Makoto Arita[2,13,14], Hironori Yamamoto[4], Shunji Watanabe[4], Kouichi Miura[4], Scott W. Behie[13], Wataru Suda[2], Toshiro Sato[7,13], Koji Atarashi[1,2,3,13], Mami Matsushita[15], Shingo Kajimura[16,17], Damian R. Plichta[5], Masayuki Saito[18], Ramnik J. Xavier[5,6,19] ✉ & Kenya Honda[1,2,3,14] ✉

Interactions between diet and the gut microbiota are fundamental to metabolic health, shaping energy balance and disease susceptibility[1–5]. However, the underlying mechanisms by which dietary and microbial factors converge to regulate host physiology remain unclear. Here we show that protein availability profoundly modulates the functional landscape of the gut microbiota and promotes remodelling of white adipose tissue (WAT). Specifically, low-protein diets (LPDs) robustly induce signature genes of browning in WAT to a similar extent to that seen in response to classical stimuli, such as cold exposure or β-adrenergic receptor activation[6–8]. LPD-mediated browning was markedly diminished in germ-free mice, and this defect was rescued by colonization with defined bacterial consortia made up of strains that were isolated and down-selected from the faeces of either LPD-fed mice or healthy human volunteers with ^{18}F-fluorodeoxyglucose positron emission tomography (FDG-PET)-confirmed brown- or beige-fat activity[9–12]. Microbiota-induced browning was mediated both by bile acids driving the activation of the farnesoid X receptor (FXR) in adipose progenitor cells, and by *nrfA*-encoding commensal-derived ammonia driving the expression of fibroblast growth factor 21 (FGF21) in hepatocytes. The bile acid–FXR and ammonia–FGF21 axes both have non-redundant, essential roles in promoting WAT browning. These findings highlight a mechanistic link between diet, gut microbial metabolism and adipose tissue remodelling, uncovering microbiota-dependent pathways by which the host responds to dietary cues.

Diet is a fundamental regulator of host physiology, influencing metabolism, immunity and susceptibility to a wide range of diseases[1–5]. The gut microbiota has emerged as a key mediator of dietary effects, contributing to interindividual variation in the nature, direction and magnitude of responses to nutritional and molecular inputs[13–15]. Among the many physiological processes that are influenced by diet–microbiota interactions, regulation of adipose tissue remodelling has emerged as an intriguing yet poorly characterized area. Unlike brown adipose tissue (BAT), which is enriched in mitochondria and expresses thermogenic proteins, such as uncoupling protein 1 (UCP1), WAT stores excess energy. However, notably, WAT retains considerable plasticity and can acquire brown-fat-like properties under specific conditions, such as cold exposure and catecholamine stimulation. This process, termed browning or beiging, gives rise to cells characterized by enhanced mitochondrial biogenesis and expression of thermogenic and lipid-oxidation-related genes[6,16–18]. Several dietary interventions—including caloric restriction, ketogenic diets and deprivation of methionine, leucine or cysteine—have been reported to activate BAT

[1]Department of Microbiology and Immunology, Keio University School of Medicine, Tokyo, Japan. [2]RIKEN Center for Integrative Medical Sciences, Yokohama, Japan. [3]City of Hope National Medical Center, Duarte, CA, USA. [4]Division of Gastroenterology, Department of Medicine, Jichi Medical University, Tochigi, Japan. [5]Infectious Disease and Microbiome Program, Broad Institute of MIT and Harvard, Cambridge, MA, USA. [6]Klarman Cell Observatory, Broad Institute of MIT and Harvard, Cambridge, MA, USA. [7]Department of Integrated Medicine and Biochemistry, Keio University School of Medicine, Tokyo, Japan. [8]Department of Human Biology, Radboud Institute for Molecular Life Sciences, Faculty of Science, University of Radboud, Nijmegen, The Netherlands. [9]JSR-Keio University Medical and Chemical Innovation Center, Keio University School of Medicine, Tokyo, Japan. [10]Laboratory of Microbial Chemistry, Kobe Pharmaceutical University, Kobe, Japan. [11]Division of Endocrinology and Metabolism, National Institute for Physiological Sciences, Okazaki, Japan. [12]Department of Medical Microbiology, Amsterdam UMC, University of Amsterdam, Amsterdam, The Netherlands. [13]Human Biology Microbiome Quantum Research Center (WPI-Bio2Q), Keio University, Tokyo, Japan. [14]Division of Physiological Chemistry and Metabolism, Graduate School of Pharmaceutical Sciences, Keio University, Tokyo, Japan. [15]Department of Nutrition, School of Nursing and Nutrition, Tenshi College, Sapporo, Japan. [16]Division of Endocrinology, Diabetes and Metabolism, Beth Israel Deaconess Medical Center and Harvard Medical School, Boston, MA, USA. [17]Howard Hughes Medical Institute, Chevy Chase, MD, USA. [18]Laboratory of Biochemistry, Faculty of Veterinary Medicine, Hokkaido University, Sapporo, Japan. [19]Center for Computational and Integrative Biology, Department of Molecular Biology, Massachusetts General Hospital and Harvard Medical School, Boston, MA, USA. [20]These authors contributed equally: Takeshi Tanoue, Manabu Nagayama, Ayumi J. A. Roochana, Samuel Zimmerman. ✉e-mail: xavier@molbio.mgh.harvard.edu; kenya@keio.jp

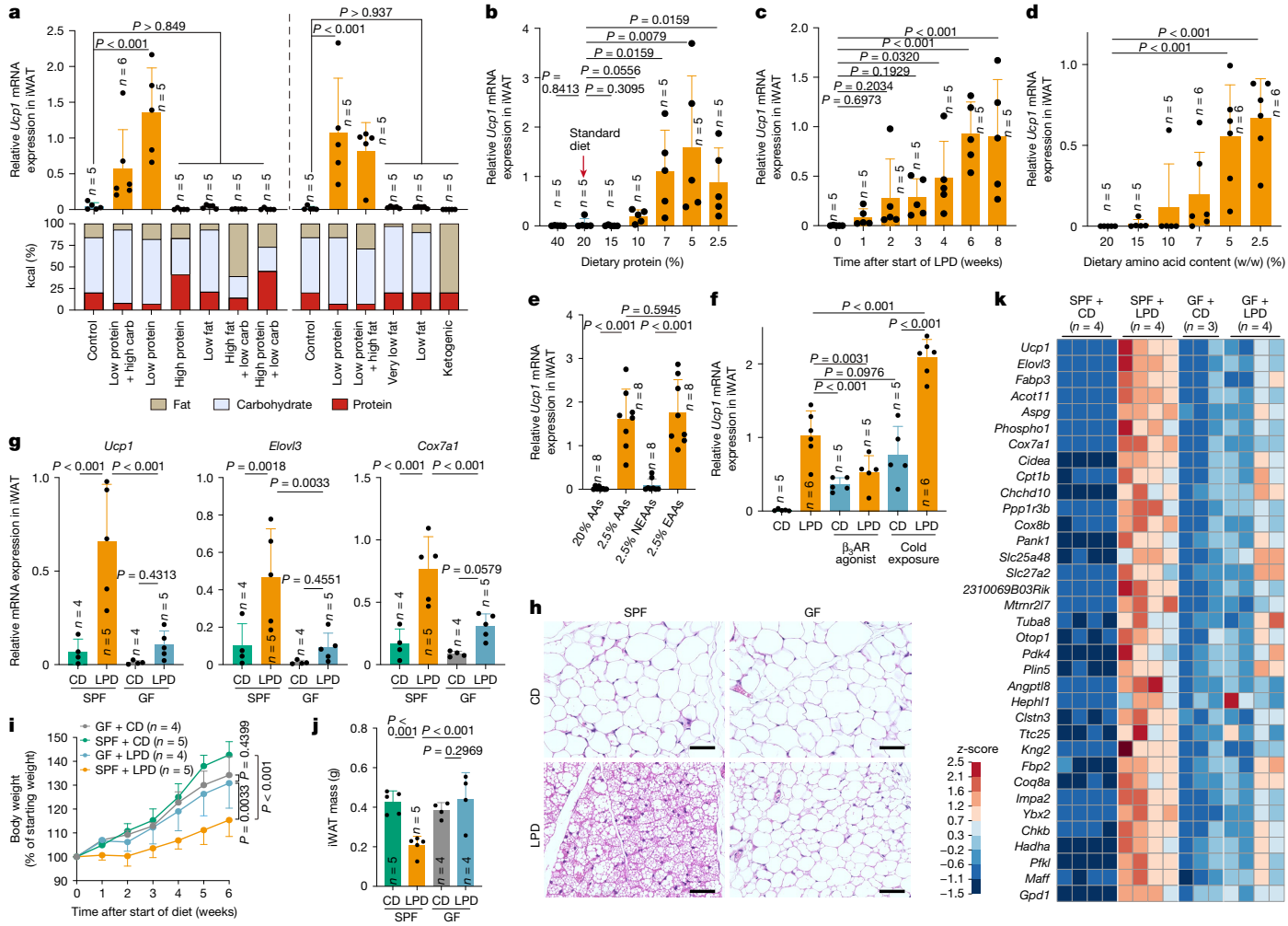

Fig. 1 | LPDs induce browning in a microbiota-dependent manner. a, SPF B6 male mice were fed diets with varying proportions of protein, carbohydrate (carb) and fat for 6 weeks. *Ucp1* mRNA expression in iWAT, normalized to *Ppib*, is shown together with each diet's macronutrient composition. The left and right panels represent two independent experiments. **b**–**e**, Relative *Ucp1* mRNA expression in iWAT in mice that were fed isocaloric diets containing the indicated protein concentrations for 6 weeks (**b**), a 7% LPD for the indicated durations (**c**), diets containing defined amino acids with varying total amino acid contents for 6 weeks (**d**) or diets containing 20% or 2.5% total amino acids (AAs), or with either EAAs or NEAAs reduced to 2.5%, for 6 weeks (**e**). **f**, SPF mice were fed a control diet (CD) or an LPD for 6 weeks and, during the final week, either received daily intraperitoneal injections of a β_3-adrenergic receptor (β_3AR) agonist (20 µg per mouse per day) or were exposed to cold (6 °C). **g**–**k**, SPF and GF mice were fed a CD or an LPD for 6 weeks. *Ucp1*, *Elovl3* and *Cox7a1* expression in iWAT (**g**), representative haematoxylin and eosin (H&E)-stained sections (**h**), body-weight change (**i**) and iWAT mass (**j**) are shown. Scale bars, 50 µm (**h**). **k**, Heat map showing genes enriched in iWAT of SPF + LPD mice compared with SPF + CD, GF + CD and GF + LPD mice (reads per kilobase per million reads (RPKM) ≥ 200, fold change ≥ 4, adjusted $P < 0.05$ with Benjamini–Hochberg correction). Each circle in the bar graphs represents an individual mouse. Data are mean ± s.d. Statistical tests: one-way ANOVA with Benjamini–Hochberg correction (**a**,**c**–**g**,**j**), two-tailed Mann–Whitney test for each comparison (**b**) and two-way ANOVA with Benjamini–Hochberg correction (**i**).

and induce WAT browning[19–24]. The gut microbiota is thought to have a role in mediating these responses, potentially through the production of bioactive metabolites and immunomodulatory effects[25–30]. However, which members of the microbiota are involved in particular dietary contexts, and how diet–microbiota interactions are translated into signals that drive beige-fat biogenesis, remain poorly defined. In this study, we identify two orthogonal pathways that link low protein intake, specific microbial metabolic activity and host signalling networks to promote WAT browning.

LPDs promote WAT browning

We first examined the effects of dietary modifications on WAT browning by formulating diets with varying proportions of protein, carbohydrate and fat. Although changes in fat content affected the total calorie count, all other diets were designed to be isocaloric. These diets were fed to specific-pathogen-free (SPF) C57BL/6 (B6) mice housed at room temperature (23 °C). Regardless of the lipid and carbohydrate content, feeding mice diets with low levels of protein significantly increased the expression of *Ucp1* and *Cox7a1* mRNA in the inguinal WAT (iWAT) (*Ucp1* expression is shown in Fig. 1a, with *Cox7a1* in Extended Data Fig. 1a. Throughout the manuscript, *Ucp1* data are shown in the main figures and additional beige markers are provided mainly in the Extended Data). mRNA expression was assessed using three distinct methods[31] with concordant results (Supplementary Fig. 1a). Feeding mice an LPD resulted in decreased iWAT mass (Supplementary Fig. 1b) and increased histological features of browning, including cells with multilocular lipid droplets, particularly in the central region adjacent to the inguinal lymph node (Extended Data Fig. 1b). B6 mice that were fed diets with a graded protein content showed a robust induction of *Ucp1*, *Elovl3* and *Cox7a1* in iWAT when dietary protein was reduced to 7% or less (a level approximately 60% lower than that of the control diet)

(Fig. 1b and Extended Data Fig. 1c–e). Time-course analysis showed that these genes were induced within 2 weeks on a 7% protein diet and plateaued by weeks 6–8 (Fig. 1c, Extended Data Fig. 1f and Supplementary Fig. 1c). RNA sequencing (RNA-seq) analysis revealed that a broad range of beige-fat signature genes were upregulated in iWAT, including those involved in mitochondrial function (such as *Cox7a1* and *Cox8b*), thermogenesis (such as *Elovl3*, *Dio2* and *Ucp1*) and lipid metabolism (such as *Cidea*, *Dio2*, *Cpt1b* and *Acott11*); this upregulation began within 1 week of LPD feeding and became progressively more pronounced over the next 6 weeks (Extended Data Fig. 1g,h). The iWAT transcriptional profile induced by LPD feeding closely resembled that induced by a β_3-adrenergic receptor agonist (Extended Data Fig. 1h). A reduction in dietary protein content also led to an increase in *Ucp1*, *Elovl3* and *Cox7a1* expression in interscapular BAT, although at lower magnitudes than that observed in iWAT (Extended Data Fig. 1i).

Feeding B6 mice a 7% protein diet for 6 weeks reduced body weight and whole-body fat volume, and enhanced glucose tolerance (Extended Data Fig. 2a–e). Mice showed no overt changes in appearance or behaviour (Supplementary Video 1), and did not exhibit increased faecal energy content or impaired lipid absorption (Extended Data Fig. 2f,g). In addition, whole-body lean volume and gastrocnemius muscle mass were mostly preserved (Extended Data Fig. 2h–j and Supplementary Video 2). These results indicate that the 6-week, 7% protein diet was generally well-tolerated and that the observed upregulation of browning markers and metabolic effects are unlikely to be driven mainly by pathological malabsorption or severe muscle wasting. Accordingly, this LPD protocol was used for all subsequent experiments, unless otherwise noted.

LPD feeding robustly induced signature genes of beige fat, even under thermoneutral conditions (30 °C) (Extended Data Fig. 2k). The LPD-induced formation of beige adipocytes in iWAT was observed across several mouse strains, including BALB/c and ICR, and was therefore not specific to B6 mice (Supplementary Fig. 2a). However, female or aged B6 mice showed attenuated browning, compared with male or young mice, respectively (Extended Data Fig. 2l,m). In addition, perigonadal WAT did not exhibit an induction of beige marker genes (Supplementary Fig. 2b). After reversion to a regular diet, beige marker expression and beige-adipocyte-like morphology declined (Extended Data Fig. 2n), indicating that LPD-induced browning in iWAT is both inducible and reversible. Increased expression of *Ucp1* and metabolic effects were also observed when mice were switched from a high-fat diet (HFD) either to an LPD (Extended Data Fig. 3a–e) or to a high-fat and low-protein diet (HFD to HF/LPD; Extended Data Fig. 3f–j), although the magnitude of this induction was attenuated with prolonged or greater fat exposure. Collectively, these results indicate that LPD-induced browning is robust but adipose-depot-specific, and modulated by age, sex and dietary context.

Because protein type and digestibility might influence outcomes, we next examined diets containing defined amino acids instead of natural proteins. Decreasing the dietary amino acid content led to a marked increase in beige marker expression in iWAT, with maximal induction, comparable to that observed with a 7% LPD, achieved at 5% or less amino acids (Fig. 1d and Extended Data Fig. 3k). We then formulated diets with decreased levels of essential amino acids (EAAs) or non-essential amino acids (NEAAs). Reducing EAAs recapitulated the induction of beige marker genes that was observed with total amino acid limitation, whereas restricting NEAAs had no discernible effect (Fig. 1e and Extended Data Fig. 3l). We next examined the effect of reducing each individual EAA in the diet. Reduction of isoleucine, leucine, phenylalanine, tryptophan, lysine, methionine or threonine resulted in modest and variable inductions of browning (Extended Data Fig. 3m). These results suggest that although restriction of individual EAAs has limited effects, concurrent restriction of several EAAs engages complementary pathways to drive a more robust browning response.

LPD-induced browning requires the microbiota

We next investigated the mechanistic underpinnings of LPD-mediated iWAT browning. Feeding mice an LPD robustly induced the expression of *Ucp1*, *Elovl3* and *Cox7a1*, to levels comparable with those induced by cold exposure (6 °C for 7 days) or treatment with a β3-adrenergic receptor agonist (Fig. 1f and Supplementary Fig. 3a). Notably, combining an LPD with cold exposure resulted in an additive increase in the expression of beige marker genes, suggesting that distinct—although possibly overlapping—mechanisms of browning are involved. Although immune cells have been implicated in cold-induced browning[32–38], LPD-induced browning was preserved across several immune-deficient mouse models, including those lacking αβ and γδ T cells, B cells, innate lymphocytes, type 1, 2 or 17 immune molecules, myeloid cells or lymphoid tissues (Extended Data Fig. 4a). We therefore focused on immune-independent mechanisms.

We next assessed the role of the gut microbiota in LPD-induced browning using germ-free (GF) mice. Compared with SPF mice, GF mice exhibited significantly reduced expression of *Ucp1*,*Elovl3*, and *Cox7a1* and fewer histological indicators of iWAT browning after being fed an LPD (Fig. 1g,h). In addition, although the LPD suppressed weight gain and WAT mass in SPF mice, no such effect was seen in GF mice (Fig. 1i,j). Low-level induction of *Ucp1* was occasionally observed in LPD-fed GF mice, suggesting that a microbiota-independent pathway exists, although this response was not robust (Supplementary Fig. 3b). RNA-seq of iWAT from LPD-fed GF mice revealed a reduction in the expression of several beige signature genes, compared with LPD-fed SPF mice, including *Ucp1*, *Cidea*, *Elovl3*, *Cox7a1*, *Cox8b*, *Clstn3* and *Acot11* (refs. 39–41) (Fig. 1k). Gene Ontology enrichment analysis highlighted the reduced expression of genes involved in mitochondrial biogenesis and lipid metabolism in LPD-fed GF versus SPF mice (Supplementary Fig. 3c). Similar trends were observed in mice that were fed a low-EAA diet (Supplementary Fig. 3d). Treating adult SPF mice with an antibiotic cocktail also led to a significant reduction in the expression of *Ucp1*, *Elovl3* and *Cox7a1* in iWAT (Supplementary Fig. 3e). These findings indicate that the microbiota is a key driver of LPD-mediated beige-adipocyte induction.

LPD–microbiota–FXR pathway in browning

We next aimed to identify microbiota-derived molecules that might contribute to iWAT browning. Non-targeted liquid chromatography–mass spectrometry (LC–MS) analysis of ileal and plasma samples from SPF and GF mice that were fed a control diet or an LPD revealed that an LPD increased the plasma levels of unconjugated bile acids, including cholic acid (CA) and muricholic acid (MCA), in SPF mice (Extended Data Fig. 4a). Subsequent targeted LC–MS analysis confirmed the increased plasma levels of CA, αMCA, βMCA and chenodeoxycholic acid (CDCA), as well as 7α- and 7β-dehydroxylation products[42], including 7-oxo-deoxycholic acid (7oxoDCA), ursocholic acid (UCA) and ursodeoxycholic acid (UDCA), in LPD-fed SPF mice compared with GF mice and control-diet-fed SPF mice (Fig. 2a and Extended Data Fig. 4b), although no such trends were seen in the intestinal contents (Supplementary Fig. 4a). These bile acids exhibited agonistic activity in an in vitro FXR reporter assay, indicating activation of this bile acid receptor (Supplementary Fig. 4b). Therefore, we next investigated whether FXR signalling was involved in browning. Mice deficient in FXR (encoded by *Nr1h4*) exhibited a significantly reduced induction of *Ucp1* and *Elovl3*, fewer morphologically beige cells in iWAT and increased weight gain during LPD feeding, compared with wild-type controls (Fig. 2b, Extended Data Fig. 4c–e and Supplementary Fig. 4c). By contrast, deletion of another prominent bile acid receptor, TGR5 (*Gpbar1*$^{-/-}$), did not affect LPD-induced browning (Fig. 2c, Extended Data Fig. 4d,e and Supplementary Fig. 4c). These findings indicate that microbiota-derived bile acids promote beige-adipocyte induction

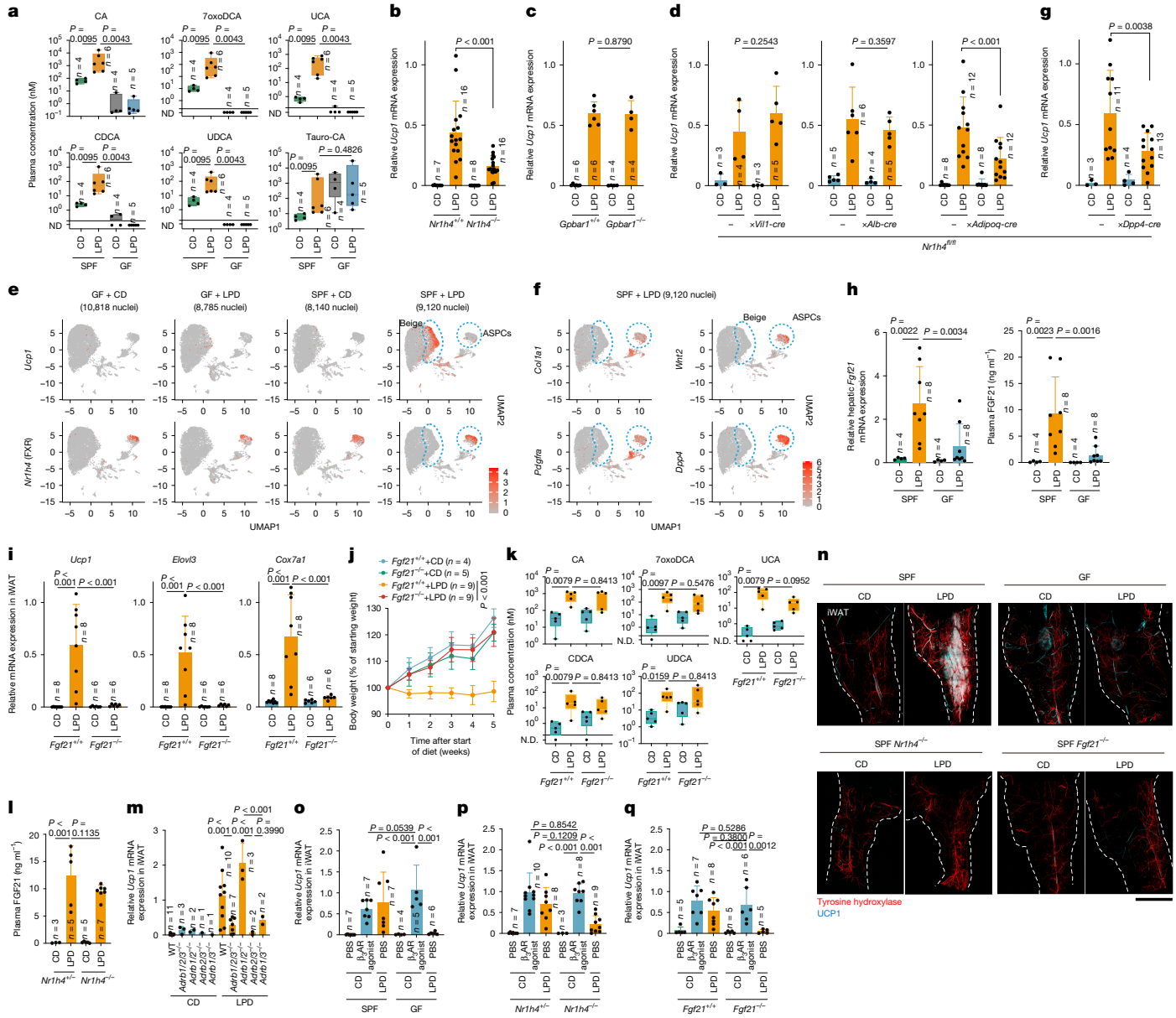

Fig. 2 | iWAT FXR and hepatic FGF21 contribute to LPD-mediated browning. **a**, Plasma bile acids in GF or SPF mice fed a CD or an LPD were quantified by LC–MS/MS. ND, not detected. **b**–**d**,**g**, SPF mice of the indicated genotypes were fed a CD or an LPD for 6 weeks, and iWAT *Ucp1* expression, normalized to *Ppib*, was measured. **e**,**f**, Uniform manifold approximation and projection (UMAP) plots of iWAT snRNA-seq data for *Ucp1* and *Nr1h4* (**e**) and for *Col1a1*, *Wnt2*, *Pdgfra* and *Dpp4* (**f**) from GF or SPF mice fed a CD or an LPD. Each dot represents a nucleus, and red indicates expression of the indicated gene, with colour intensity reflecting expression levels. Beige and ASPC clusters are outlined by blue dashed circles. **h**, Hepatic *Fgf21* mRNA expression and plasma FGF21 levels in GF or SPF mice fed a CD or an LPD. **i**–**k**, *Fgf21*$^{+/+}$ and *Fgf21*$^{-/-}$ littermates fed a CD or an LPD were analysed for iWAT gene expression (**i**), body-weight changes (**j**) and plasma bile acids (**k**). In **k**, $n = 5$ per group. **l**, Plasma FGF21 levels in *Nr1h4*$^{-/-}$ and *Nr1h4*$^{+/-}$ mice. **m**, iWAT *Ucp1* mRNA expression in SPF mice of the indicated genotypes (*Adrb1*$^{-/-}$*Adrb2*$^{-/-}$*Adrb3*$^{-/-}$ (*Adrb1/2/3*$^{-/-}$), *Adrb1*$^{-/-}$*Adrb2*$^{-/-}$ (*Adrb1/2*$^{-/-}$), *Adrb2*$^{-/-}$*Adrb3*$^{-/-}$ (*Adrb2/3*$^{-/-}$) or *Adrb1*$^{-/-}$*Adrb3*$^{-/-}$ (*Adrb1/3*$^{-/-}$)) after 6 weeks on a CD or an LPD. **n**, Representative whole-mount iWAT images stained for tyrosine hydroxylase and UCP1 with iDISCO processing; dashed lines indicate iWAT boundaries. Scale bar, 2 mm. **o**–**q**, Wild-type (WT) SPF and GF mice (**o**), or SPF mice of the indicated genotypes (**p**,**q**), were fed a CD or an LPD for 6 weeks and received a daily β_3-adrenergic receptor agonist or phosphate-buffered saline (PBS) during the final week. Relative iWAT *Ucp1* was measured. Circles represent individual mice; data are mean ± s.d. Box plots show median, interquartile range and range. Statistical analyses: one-way ANOVA with Benjamini–Hochberg correction (**b**–**d**,**g**–**i**,**l**,**m**,**o**–**q**), two-way ANOVA with Benjamini–Hochberg correction (**j**) and two-tailed Mann–Whitney test (**a**,**k**).

during LPD feeding at least in part through an FXR-dependent, TGR5-independent pathway.

Given the broad expression of FXR in the intestine, liver and WAT[43], we used tissue-specific *Nr1h4*-knockout mice to define the organ-specific contribution of FXR signalling to iWAT browning. Deleting FXR in intestinal epithelial cells (*Nr1h4*$^{fl/fl}$;*Vil1-cre*) or hepatocytes (*Nr1h4*$^{fl/fl}$;*Alb-cre*) did not affect LPD-induced *Ucp1* expression. By contrast, adipocyte-specific deletion of FXR (*Nr1h4*$^{fl/fl}$;*Adipoq-cre*) significantly reduced *Ucp1* and *Elovl3* expression and morphologically beige cells in iWAT (Fig. 2d, Extended Data Fig. 4e and Supplementary Fig. 4c), suggesting that FXR has a key role in adipose tissue. To identify FXR-expressing cell types in iWAT, we performed single-nucleus RNA-seq (snRNA-seq) of iWAT from GF and SPF mice fed a control diet or an LPD. A putative beige-cell cluster expressing *Ucp1* and *Elovl3* was detected almost exclusively in LPD-fed SPF mice (Fig. 2e and Extended Data Fig. 5a,b). Among bile acid receptors, FXR showed a restricted

pattern of expression and was enriched in cells expressing markers of adipose stem and progenitor cells (ASPCs), including *Wnt2* and *Dpp4* (refs. 44–46) (Fig. 2e,f and Extended Data Fig. 5a,b). Consistently, conditional deletion of FXR in *Dpp4*$^{+}$ cells (*Nr1h4*$^{fl/fl}$;*Dpp4-cre*) significantly attenuated the induction of *Ucp1* and *Elovl3* after LPD feeding (Fig. 2g and Supplementary Fig. 4c). Pseudotime analysis further suggested a de novo differentiation trajectory towards beige cells, characterized by a sequential induction of mitochondrial lipid metabolism and thermogenic genes (Supplementary Fig. 4d–f).

LPD-conditioned microbiota drives hepatic FGF21

Given the robust nature of LPD-induced browning, we hypothesized that multiple, complex pathways are involved in addition to the bile acid–FXR axis. Considering the central role of the liver in regulating metabolic responses to diet, we performed bulk RNA-seq and quantitative PCR (qPCR) on liver samples. In SPF but not in GF mice, LPD feeding for 1 or 6 weeks consistently induced a number of genes, including *Phgdh*, (*Psat1*, *Aldh1l2* and *Asns* (Extended Data Fig. 6a,b). As these genes function in serine biosynthesis, mitochondrial one-carbon metabolism and ammonia-dependent asparagine production[47,48], their induction implicates the gut microbiota in linking dietary protein restriction to hepatic nitrogen assimilation and recycling. These genes are known to be regulated by activating transcription factor 4 (ATF4)[49,50], and, consistently, other ATF4-inducible genes (*Mthfd2, Nupr1*, *Chac1* and *Gdf15*) were similarly upregulated in a microbiota-dependent manner (Extended Data Fig. 6a,b). Notably, this transcriptional response was not induced by treatment with a β_3-adrenergic receptor agonist (Extended Data Fig. 6b), highlighting the unique nature of LPD-induced microbiota-dependent signalling in the liver.

Notably, *Fgf21*, another ATF4-inducible gene[51], was markedly upregulated in the livers of SPF mice, but not GF mice, as early as 1 week after LPD initiation, with corresponding increases in circulating FGF21 (Fig. 2h and Extended Data Fig. 6b). *Fgf21*$^{-/-}$ mice phenocopied GF mice, showing a minimal induction of beige marker genes in iWAT and no suppression of weight gain during LPD feeding (Fig. 2i,j). However, administering recombinant FGF21 was insufficient to induce iWAT browning in control-diet-fed GF mice (Supplementary Fig. 5a), indicating that additional microbiota-dependent signals, including the bile acid–FXR axis, are required. Indeed, the gene-expression profiles of iWAT from *Fgf21*$^{-/-}$ and *Nr1h4*$^{-/-}$ mice showed distinct patterns (Supplementary Fig. 5b), and *Nr1h4* and *Klb* (encoding a crucial component of the FGF21 receptor) were expressed in distinct cell populations within iWAT (Extended Data Fig. 5b). Moreover, LPD feeding resulted in comparable plasma bile acid profiles in *Fgf21*$^{-/-}$ and wild-type mice (Fig. 2k), and, conversely, plasma FGF21 levels were not significantly altered between *Nr1h4*$^{-/-}$ and wild-type mice (Fig. 2l). These findings suggest that FXR and FGF21 act through parallel, non-redundant pathways that collectively contribute to beige cell induction in iWAT.

To identify the hepatic cell types that express *Fgf21*, we performed snRNA-seq on liver tissue. *Fgf21* and other ATF4-dependent genes were detected in hepatocyte clusters from LPD-fed SPF mice, but not in other liver cell types or in GF or control-diet-fed mice (Extended Data Fig. 7). A similar pattern of expression was observed for *Cyp39a1* and *Csad* (Extended Data Fig. 7). Given the roles of CYP39A1 in non-canonical bile acid biosynthesis and CSAD in taurine synthesis[52], these findings suggest that hepatocytes respond to LPD feeding by coordinately upregulating not only *Fgf21*, but also genes involved in bile acid production.

Microbiota–FXR–FGF21–sympathetic neuron axis

As catecholamine signalling is central to adipose browning[6,16,17,40,53–55], we next assessed LPD-mediated beige-cell induction in mice deficient in β_1- (*Adrb1*), β_2- (*Adrb2*) or β_3- (*Adrb3*) adrenergic receptors. Loss of β_3-adrenergic signalling, either alone or combined with β_1 or β_2 deficiency, resulted in a severe impairment in beige-cell induction, whereas deletion of β_1 and β_2 had no effect (Fig. 2m and Extended Data Fig. 8a), suggesting that LPD-induced browning relies specifically on β_3-adrenergic receptor signalling. Consistently, whole-mount immunostaining of iWAT revealed a pronounced remodelling of tyrosine hydroxylase-positive sympathetic neurons and vasculature in SPF but not in GF wild-type mice in response to an LPD (Fig. 2n and Extended Data Fig. 8b). Specifically, sympathetic neurons developed finer, denser networks, particularly in regions with a strong accumulation of UCP1-expressing cells. By contrast, LPD-fed *Fgf21*$^{-/-}$ and *Nr1h4*$^{-/-}$ SPF mice exhibited markedly reduced sympathetic innervation, resembling the pattern observed in GF mice (Fig. 2n and Extended Data Fig. 8c). Notably, administration of a β_3-adrenergic receptor agonist increased *Ucp1* and *Cox7a1* expression in control-diet-fed GF mice as well as *Nr1h4*$^{-/-}$ and *Fgf21*$^{-/-}$ mice to levels comparable with those in LPD-fed SPF mice (Fig. 2o–q and Extended Data Fig. 8d–f). These findings suggest that FXR and FGF21 signal through distinct pathways that converge on the promotion of sympathetic innervation and β_3-adrenergic signalling during LPD-induced browning.

Browning induced by 20 bacterial strains in mice

To assess whether LPD-induced iWAT browning is transmissible via the microbiota, we transplanted small-intestinal luminal contents from LPD-fed SPF donor mice (donors A and B) into GF mice (Fig. 3a). Browning was observed in recipient mice irrespective of the transplant source, but only when recipients were fed an LPD (Fig. 3b), indicating that ongoing diet–microbiota interactions are required. Similar results were obtained using faecal transplants (Supplementary Fig. 6a). To identify a bacterial community capable of mediating browning, we selected mouse B28, which exhibited the strongest induction of *Ucp1* after receiving small-intestinal contents from LPD-fed mouse B and being maintained on an LPD (Fig. 3b and Supplementary Fig. 6b). Transferring small-intestinal contents from mouse B28 to new GF recipients recapitulated the robust iWAT browning upon LPD feeding (Fig. 3c and Supplementary Fig. 6c). We selected mouse B28-1, which exhibited the strongest beige adipocyte induction, for subsequent analyses (Fig. 3c). From the small-intestinal contents of mouse B28-1, we isolated 18 bacterial strains (mu18-mix) (Fig. 3d). However, colonizing GF mice with the mu18-mix was insufficient to induce browning (Fig. 3e). Adding two further isolates, *Blautia* sp. (St.27G3) and *Turicibacter* sp. (St.80E1), yielded a 20-strain consortium (mu20-mix) that robustly induced browning after LPD feeding, reaching levels comparable to those of SPF mice (Fig. 3f,g), indicating that these two strains are required for the full beige-inducing activity of the consortium. GF mice inoculated with the mu20-mix and fed an LPD showed increased plasma levels of CA, CDCA, 7oxoDCA, UCA and UDCA (Fig. 3h), as well as FGF21 (Fig. 3i). By contrast, *Nr1h4*$^{-/-}$ and *Fgf21*$^{-/-}$ GF mice inoculated with the mu20-mix exhibited markedly reduced beige-cell induction (Fig. 3j), further supporting the requirement for FXR and FGF21 signalling in LPD-induced browning mediated by defined members of the microbiota.

Four human-derived isolates promote browning

Having confirmed that a small microbial community is sufficient to promote LPD-induced browning, we next sought to identify human-associated microorganisms that are capable of exerting this activity. To this end, we recruited 25 healthy volunteers and performed ^{18}F-fluorodeoxyglucose positron emission tomography (FDG-PET), which detects beige or brown adipose depots[9–12]. Approximately 40% of volunteers exhibited supraclavicular FDG accumulation (Fig. 4a). We transplanted faecal samples from the top four FDG-positive volunteers (T17, T10, T19 and T18) into GF mice and placed the mice on either a control diet or an LPD (Extended Data Fig. 9a). In exGF mice colonized with microbiota from donors T17, T10 or T19, LPD feeding robustly

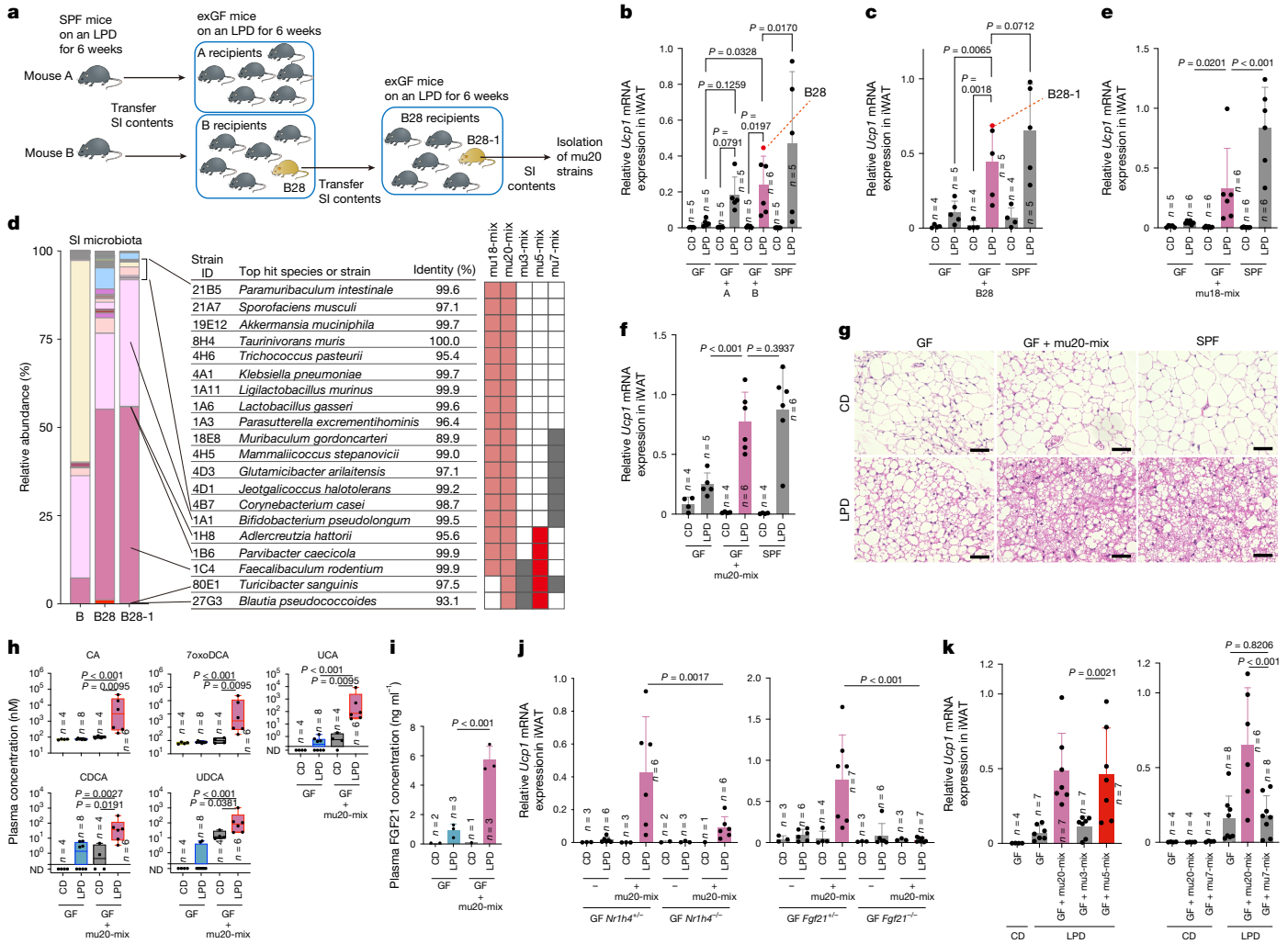

Fig. 3 | Mouse-derived microbial isolates promote LPD-induced browning. **a**, Schematic illustrating the strategy to isolate browning-inducing commensal strains from the gut microbiota of SPF mice. SI, small intestine. **b**,**c**,**e**,**f**, GF mice were colonized with ileal microbiota from LPD-fed SPF mouse A, SPF mouse B (**b**) or exGF mouse B28 (**c**), or with defined bacterial consortia (mu18-mix in **e** or mu20-mix in **f**). Mice were then fed an LPD for 6 weeks, and relative iWAT *Ucp1* expression was measured by qPCR. **d**, The ileal microbiota compositions of mouse B, mouse B28 and mouse B28-1 were determined by 16S rRNA gene sequencing. The 20 strains isolated from mouse B28-1 are listed. **g**, Representative H&E-stained iWAT sections from the indicated groups. Scale bars, 50 μm. **h**,**i**, Plasma bile acid (**h**) and FGF21 (**i**) concentrations in the indicated mice were quantified by LC–MS/MS and by enzyme-linked immunosorbent assay (ELISA), respectively. **j**, iWAT *Ucp1* expression in GF *Nr1h4*$^{-/-}$ or GF *Fgf21*$^{-/-}$ mice inoculated with mu20-mix or vehicle control and fed a CD or an LPD for 6 weeks. **k**, GF mice were colonized with the indicated mouse-derived bacterial consortia (mu20-mix, mu3-mix, mu5-mix or mu7-mix) and fed a CD or an LPD for 6 weeks. iWAT *Ucp1* expression and hepatic *Fgf21* expression were measured. Circles represent individual mice; data are mean ± s.d. Box plots show median, interquartile range and range. Statistics: one-way ANOVA with Benjamini–Hochberg correction for multiple comparisons (**b**,**c**,**e**,**f**,**i**–**k**) or two-tailed Mann–Whitney test for each comparison (**h**).

induced *Ucp1* expression and morphologically beige adipocytes in iWAT (Fig. 4b and Extended Data Fig. 9b). Faecal microbiota transplantation from donor T18 was much less effective, probably due to unsuccessful engraftment of key effector strains. We also transplanted GF mice with faecal samples from donors FF2 and T07, who exhibited intermediate or no FDG accumulation, respectively. Mirroring the human phenotype, FF2 recipient mice exhibited an intermediate degree of browning, whereas T07 recipients showed no evidence of browning (Fig. 4c and Extended Data Fig. 9c).

Next, we isolated 33 strains from faecal samples from T10 microbiota-recipient mice (T10-4 and T10-5) and another 33 strains from T19 microbiota-recipient mice (T19-5 and T19-6) (Fig. 4b,h and Extended Data Fig. 9d). GF mice were colonized with each of these 33-strain mixtures. Mice that were colonized with the T19-derived 33-strain mixture exhibited robust beige-cell induction after LPD feeding, whereas those colonized with the T10-derived mixture showed substantially less induction (Fig. 4d and Extended Data Fig. 9e). Mice that were colonized with the T19-derived 33-mix exhibited increased plasma levels of CA, 7oxoDCA, UCA, CDCA and UDCA, as well as FGF21 (Fig. 4e,f). By contrast, *Nr1h4*$^{-/-}$ or *Fgf21*$^{-/-}$ GF mice inoculated with the T19-derived 33-mix failed to significantly upregulate *Ucp1* in iWAT (Fig. 4g), indicating that these strains promote beige-cell induction through activation of both the FXR and the FGF21 pathway, similar to the mu20-mix.

To identify a minimal effector consortium, we divided the 33 T19-derived strains into 2 phylogenetic groups: a 19-strain group comprising *Bacteroides*, *Enterococcus*, *Erysipelotrichaceae* and other phyla (19 BEEO), and a 14-strain group comprising *Ruminococcaceae* and *Lachnospiraceae* (14 RL) (Fig. 4h). Gnotobiotic mice colonized with the 19 BEEO-mix recapitulated the robust induction of *Ucp1* in iWAT that was observed with the parental 33-mix, whereas mice colonized with the 14 RL-mix did not (Fig. 4i). We further subdivided the 33 T19-derived

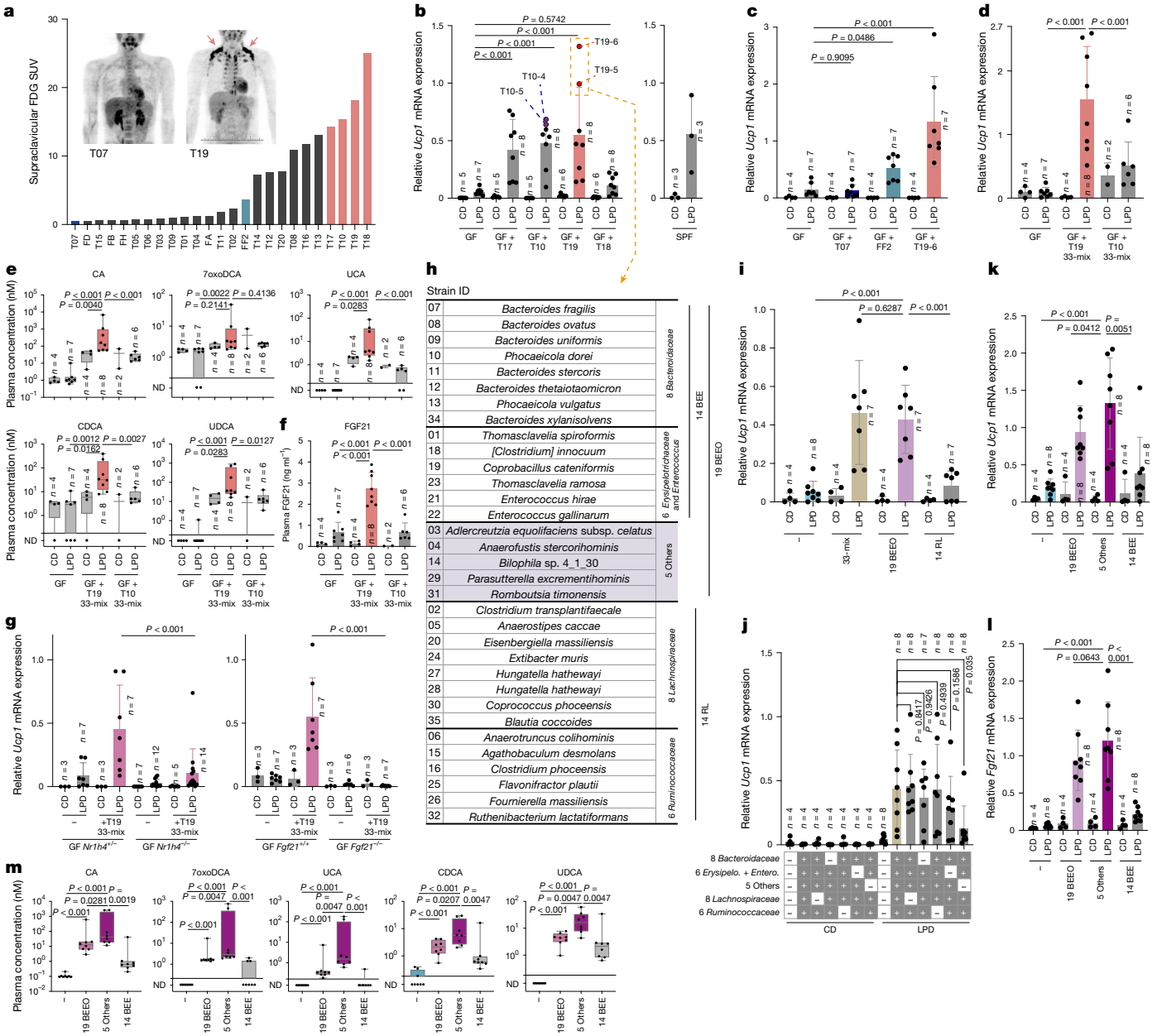

Fig. 4 | Down-selection of human-derived bacterial strains that promote LPD-mediated browning. a, Standardized uptake values (SUV) of FDG in the supraclavicular regions of each volunteer. Columns highlighted in red and blue indicate samples that were selected for follow-up analysis, and representative FDG-PET images are shown as inserts. **b**–**f**, GF B6 mice were colonized with faecal microbiota from the indicated individuals (**b**,**c**) or with defined bacterial consortia (**d**) and then fed either a CD or an LPD for 6 weeks. Relative iWAT *Ucp1* expression, normalized to *Ppib*, was determined by qPCR (**b**–**d**). Plasma bile acids (**e**) and FGF21 (**f**) were quantified by LC–MS/MS and ELISA, respectively. **g**, iWAT *Ucp1* expression in GF *Nr1h4*$^{-/-}$ and *Fgf21*$^{-/-}$ mice colonized with the T19-derived 33-mix and fed a CD or an LPD. **h**, List of the 33 T19-derived strains, as determined by 16S rRNA sequencing. **i**–**m**, GF B6 mice were colonized with the indicated bacterial consortia selected from the 33 T19-derived strains and fed a CD or an LPD for 4 weeks. In **j**, the presence (+) or absence (–) of each bacterial group in the consortium is indicated. Expression of *Ucp1* in iWAT (**i**-**k**) and *Fgf21* in the liver (**l**), normalized to *Ppib*, was measured by qPCR. **m**, Plasma bile acid concentrations in LPD-fed gnotobiotic mice were quantified by LC–MS/MS ($n = 8$ per group). Circles represent individual mice; bar heights indicate exact SUV values (**a**) or mean ± s.d. (**b**–**d**,**f**,**g**,**i**–**l**). Box plots show median, interquartile range and data range. Statistics: one-way ANOVA with Benjamini–Hochberg correction for multiple comparisons (**b**–**d**,**f**,**g**,**i**–**l**) or two-tailed Mann–Whitney test for each comparison (**e**,**m**).

strains into 5 phylogenetic groups (Fig. 4h) and assessed the effect of excluding each on iWAT browning. Excluding the five strains classified as other phyla (5 Others) led to the greatest reduction in *Ucp1* induction (Fig. 4j). We thus compared the effects of colonization with the 5 Others-mix versus the remaining 14 strains from the 19 BEEO group (14 BEE). The 5 Others-mix efficiently induced beige marker genes in an LPD-dependent manner, whereas the 14 BEE strains produced only a modest effect (Fig. 4k and Extended Data Fig. 9f). Colonization with the 5 Others-mix, but not the 14 BEE-mix, also increased hepatic *Fgf21* mRNA expression and plasma bile acid concentrations to levels comparable with those observed in mice colonized with the parental 19 BEEO-mix (Fig. 4l,m).

Additional dropout experiments were performed by inoculating GF mice with all possible four-strain permutations of the 5 Others-mix, each omitting one of the five strains. Notably, omitting *Romboutsia timonensis* (St.31) prevented engraftment of the remaining four strains and markedly reduced beige-cell induction (Fig. 5a and Extended Data Fig. 10a), suggesting that *R. timonensis* acts as a supporter strain that

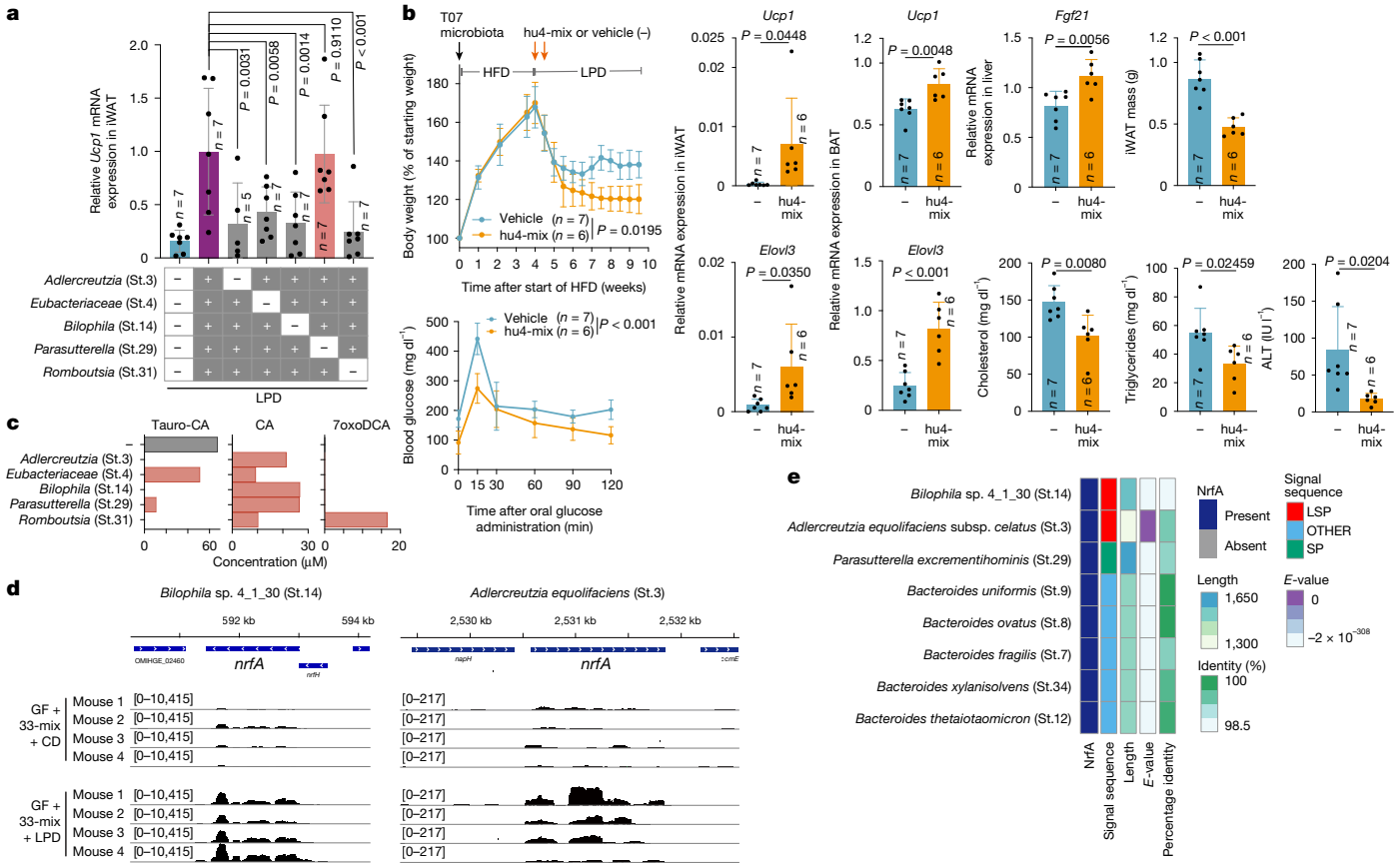

Fig. 5 | Identification of four human-derived isolates that promote browning. **a**, GF B6 mice were colonized with four-strain permutations of the 5 Others-mix; included strains are indicated by + and the excluded strain by –. Mice were fed an LPD for 4 weeks, and iWAT *Ucp1* expression, normalized to *Ppib*, was measured by qPCR. **b**, GF mice were inoculated with faecal microbiota from participant T07, fed a HFD (60% kcal fat, 20% protein) for 4 weeks, then switched to an LPD and given two oral doses of the hu4 strains or vehicle control (–). Longitudinal changes in body weight are shown. An oral glucose tolerance test (OGTT) was performed after 4 weeks on the LPD. After 6 weeks on the LPD, *Ucp1* and *Elovl3* expression in iWAT and BAT, hepatic *Fgf21* expression, iWAT mass and plasma cholesterol, triglycerides and ALT were assessed. IU, international units. **c**, In vitro bile acid metabolic capacity of individual members of the 5 Others-mix after incubation with 50 μM tauro-CA. **d**, Metatranscriptomic analysis of bacterial RNA from the caecal contents of gnotobiotic mice colonized with the T19-derived 33-mix and fed a CD or an LPD. Reads mapped to the *nrfA* loci of *Bilophila* sp. 4_1_30 (St.14) and *A. equolifaciens* (St.3) are shown. **e**, NrfA homologues and predicted signal peptides in human isolates. eggNOG-mapper was used for annotation, and SignalP 6.0 was used to identify signal peptides. Percentage identity indicates similarity to the closest NrfA protein. *E*-value represents the expected value. Length denotes the aligned protein length. SP, standard signal peptide. Circles represent individual mice; data are mean ± s.d. (**a**,**b**) or exact bile acid concentrations (**c**). Statistics: one-way ANOVA with Benjamini–Hochberg correction (**a**), two-way ANOVA (**b**, line graphs) and two-tailed unpaired *t*-test (**b**, bar graphs).

facilitates colonization by the others. Excluding *Adlercreutzia equolifaciens* (St.3), *Eubacteriaceae* sp. (St.4) or *Bilophila* sp. 4_1_30 (St.14) did not impair colonization by the remaining strains but substantially affected their ability to induce iWAT browning (Fig. 5a and Extended Data Fig. 10a). By contrast, omitting *Parasutterella excrementihominis* (St.29) had no effect on beige-cell induction (Fig. 5a). Therefore, whereas the *Parasutterella* strain is dispensable, all four remaining strains (*Adlercreutzia*, *Eubacteriaceae*, *Bilophila* and *Romboutsia*; hereafter referred to as 'hu4' strains) are essential for the observed LPD-mediated browning effect by human-associated strains.

To assess the metabolic effect of the hu4-strain consortium, GF mice were inoculated with faeces from participant T07, whose microbiota lacked browning capacity, and were fed a HFD. Mice were then treated with an LPD alone or combined with two oral doses of the hu4 strains. Whereas the LPD alone was somewhat efficacious, combination treatment with the hu4 strains led to significantly greater body-weight loss, increased expression of *Ucp1* and *Elovl3* in both iWAT and BAT, increased hepatic *Fgf21* expression, reduced iWAT mass, decreased levels of plasma cholesterol, triglyceride and alanine transaminase (ALT) and improved glucose tolerance (Fig. 5b). These effects occurred with minimal reduction in muscle mass and no increase in plasma creatine kinase levels (Extended Data Fig. 10b), suggesting that WAT browning mediated by specific microbiota members enhances the metabolic effects of LPD feeding without overt muscle damage.

Microbial ammonia production induces hepatic FGF21

To elucidate how the hu4 strains promote LPD-induced browning, we examined their bile-acid-metabolizing capabilities. All four strains exhibited bile salt hydrolase activity, converting tauro-CA to CA in vitro (Fig. 5c). Furthermore, the supporter *R. timonensis* (St.31) strain encodes a putative 7α-hydroxysteroid dehydrogenase (7αHSDH) (Extended Data Fig. 10c) and uniquely converted tauro-CA into 7oxoDCA (Fig. 5c), which may facilitate colonization by the other strains and FXR activation in iWAT.

We next performed genome sequencing of the 33 T19-derived strains (Supplementary Table 1) and transcriptomic profiling of caecal microbiota from gnotobiotic mice colonized with this consortium and fed either a control diet or an LPD. LPD feeding selectively upregulated nitrogen-metabolism-related genes in the 19-BEEO and hu4 strains, but not in the 14-BEE or 14-RL strains (Extended Data Fig. 10d). Notably, expression of *nrfA*, which encodes and enzyme that catalyses the

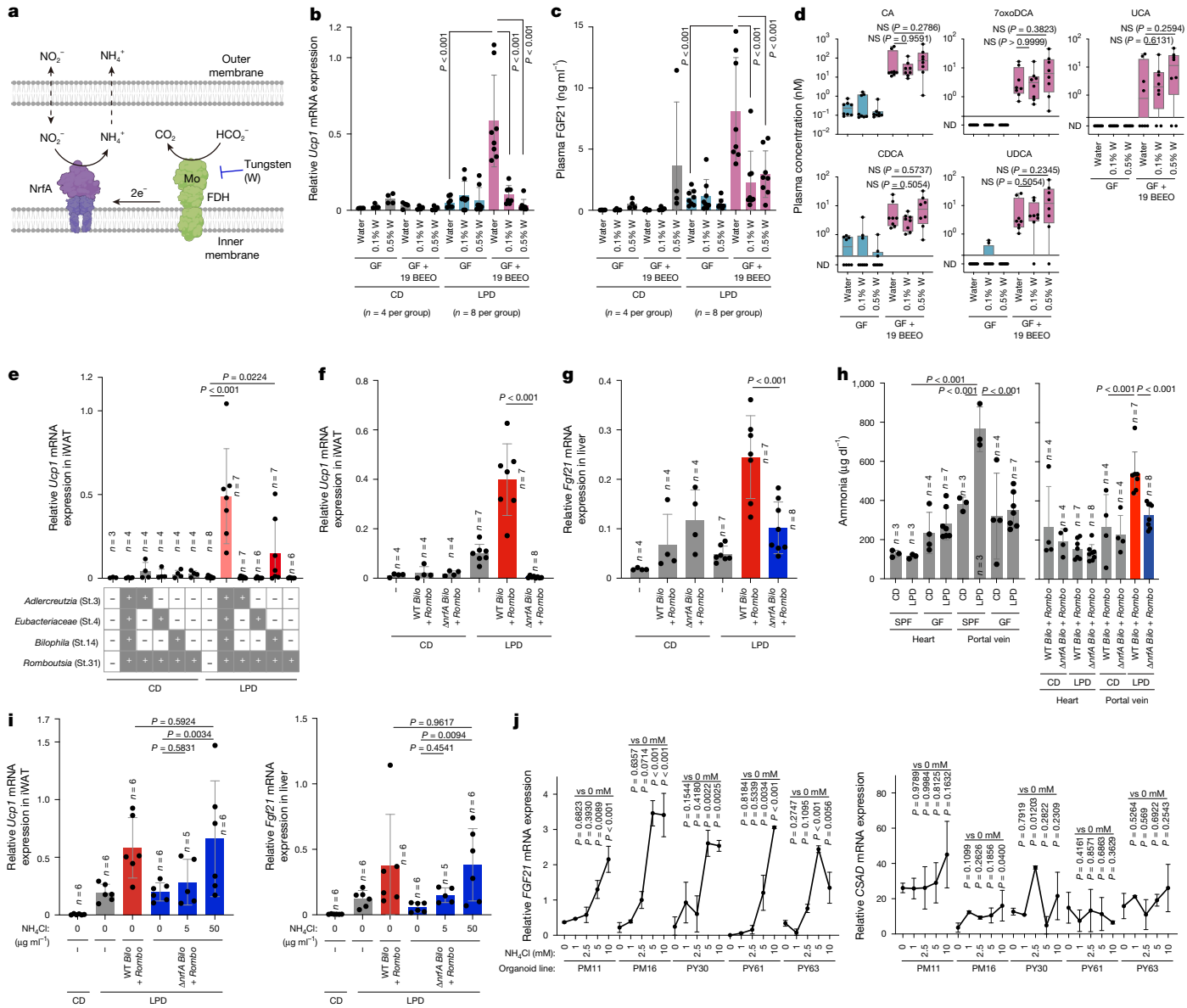

Fig. 6 | Microbial *nrfA*-dependent ammonia production promotes FGF21 expression. a, Schematic illustrating nitrite reduction by NrfA in conjunction with formate dehydrogenase (FDH). Mo, molybdopterin. **b**–**d**, GF B6 mice were colonized with 19 BEEO-mix and fed a CD or an LPD for 3 weeks. During the final 2 weeks, mice received 0.1% or 0.5% sodium tungstate dihydrate (W) in the drinking water. Relative iWAT *Ucp1* expression (**b**), plasma FGF21 levels (**c**) and plasma bile acid concentrations (**d**) were assessed. In **d**, $n = 8$ per group. **e**, GF mice colonized with two strains selected from the hu4-mix (included, +; excluded, –) were fed a CD or an LPD for 4 weeks, and iWAT *Ucp1* expression was quantified. **f**,**g**, GF mice were colonized with Δ*nrfA* or wild-type *Bilophila* sp. 4_1_30 (St.14) together with *Romboutsia timonensis* (St.31) (*Rombo*) and fed a CD or an LPD for 4 weeks; iWAT *Ucp1* (**f**) and hepatic *Fgf21* (**g**) expression were measured by qPCR. **h**, Ammonia concentration in portal and peripheral blood from CD- or LPD-fed SPF and GF mice, and from GF mice colonized with *R. timonensis* plus wild-type or Δ*nrfA Bilophila*. **i**, Ammonium chloride (NH_4Cl) was administered in the drinking water to the indicated gnotobiotic mice, and iWAT *Ucp1* and hepatic *Fgf21* expression were assessed. **j**, Hepatocyte organoids derived from five human donors were stimulated with the indicated concentrations of NH_4Cl, and *FGF21* and *CSAD* mRNA expression was analysed by qPCR ($n = 2$ per group). Circles represent individual mice; data are mean ± s.d. Box plots show median, interquartile range and data range. Statistics: one-way ANOVA with Benjamini–Hochberg correction (**b**,**c**,**e**–**j**) and two-tailed Mann–Whitney test (**d**). NS, not significant.

reduction of nitrite into ammonia, was greatly increased in *Bilophila* sp. 4_1_30 (St.14) and *A. equolifaciens* (St.3) upon LPD feeding (Fig. 5d). Unlike most *nrfA* homologues, the *nrfA* genes in these strains uniquely contain lipoprotein signal peptides (LSPs) (Fig. 5e), a feature that is rare in the human microbiome and mostly restricted to Desulfobacterota (Extended Data Fig. 10e and Supplementary Table 2). Such signal peptides are predicted to localize NrfA to the inner membrane, enabling periplasmic dissimilatory nitrate reduction to ammonium (Fig. 6a). NrfA uses formate as an electron donor through its partner enzyme, formate dehydrogenase (FDH)[56]. FDH contains a molybdopterin cofactor in its active site, which can be inhibited by treatment with tungsten[57]. Adding tungsten to the drinking water significantly suppressed both iWAT browning and plasma FGF21 levels in mice colonized with the 19 BEEO-mix, without altering strain engraftment or plasma bile acid levels (Fig. 6b–d and Extended Data Fig. 11a).

To further assess the role of NrfA in WAT browning, we generated a *nrfA*-deficient *Bilophila* sp. 4_1_30 (St.14) mutant (Supplementary Fig. 7). This Δ*nrfA* mutant exhibited defective ammonia production in vitro, compared with the *nrfA*-sufficient (wild-type) *Bilophila* strain, which produced high levels of ammonia in protein-restricted

settings (Extended Data Fig. 11b). In vivo, co-colonization of GF mice with the wild-type *Bilophila* strain and bile-acid-producing *R. timonensis* (St.31) induced significant browning, although the magnitude was substantially less than that observed with the complete hu4 strains (Fig. 6e). By contrast, co-colonization with *R. timonensis* and the Δ*nrfA Bilophila* mutant failed to induce browning (Fig. 6f and Extended Data Fig. 11d), despite comparable intestinal engraftment of the Δ*nrfA* and wild-type strains (Extended Data Fig. 11c). Notably, Δ*nrfA Bilophila*-colonized mice exhibited reduced hepatic expression of *Fgf21* (Fig. 6g), whereas induction of hepatic *Csad* and *Cyp39a1* expression and plasma bile acids was preserved or even enhanced (Extended Data Fig. 11e,f), suggesting that *nrfA*-mediated nitrogen metabolism specifically promotes *Fgf21* induction, likely via ammonia production. Consistent with this, LPD feeding increased the levels of ammonia in the portal vein, but not in the peripheral blood, of SPF B6 mice and gnotobiotic mice colonized with wild-type *Bilophila* and *R. timonensis*. By contrast, no such increase was observed in GF mice or in mice colonized with the Δ*nrfA* strain (Fig. 6h). Supplementation with ammonium chloride rescued hepatic *Fgf21* and iWAT *Ucp1* and *Elovl3* expression in mice colonized with *R. timonensis* and Δ*nrfA Bilophila* (Fig. 6i and Extended Data Fig. 11g). Moreover, stimulating human hepatocyte organoids with ammonia[58] induced the expression of *FGF21* in a dose-dependent manner without affecting bile acid biosynthesis genes (Fig. 6j). These results suggest that microbiota-derived ammonia enters the portal circulation and selectively induces hepatic *FGF21* expression, thereby contributing to WAT browning.

Having elucidated the roles of human-derived, nitrogen-metabolizing *Bilophila* and bile-acid-modifying *Romboutsia* in browning, we revisited the mu20-mix. Two strains, *Adlercreutzia* sp. (St.1H8) and *Parvibacter caecicola* (St.1B6) were found to carry LSP-containing *nrfA* homologues and produced ammonia in vitro (Extended Data Fig. 12a,b). In addition, *Faecalibaculum rodentium* (St.1C4) was found to be capable of bile acid deconjugation as well as 7α- and 3α-dehydroxylation, producing CA, 7oxoDCA and 3oxoCA from tauro-CA (Extended Data Fig. 12c). We thus selected these three strains and combined them with *Blautia* sp. (St.27G3) and *Turicibacter* sp. (St.80E1). The resulting five-strain consortium (mu5-mix) robustly increased portal ammonia levels, hepatic *Fgf21* mRNA expression and iWAT browning, comparable to the levels induced by the parental mu20-mix (Fig. 3k and Extended Data Fig. 12d). By contrast, exclusion of the two *nrfA*-positive strains (mu3-mix) or colonization with a random seven-strain mixture (mu7-mix) did not elicit these effects. These findings suggest that diverse microbial consortia, derived from either the human or the mouse microbiota, can promote adipose tissue browning in mice fed an LPD, provided that they possess both ammonia-producing and bile-acid-modifying capacities.

Discussion

This study identifies low protein intake as a dietary context in which specific gut microorganisms engage coordinated host pathways to promote adipose tissue browning (see also Supplementary Discussion). By combining gnotobiotic models with defined human- and mouse-derived bacterial consortia, we show that distinct microbial communities can elicit a shared browning phenotype, provided that they encode complementary functional capacities of bile acid modification and ammonia production. These functions engage two host pathways: activation of FXR in adipose progenitor populations and induction of hepatic FGF21. These pathways probably act in parallel and are non-redundant, because disruption of either axis compromises browning, whereas activation of one alone is insufficient.

Our findings support a model in which protein scarcity is sensed by specific members of the microbiota, which respond accordingly, leading to increased levels of systemic bile acids and hepatic ammonia. This activates FXR and FGF21 signalling, which together drive sympathetic innervation, adipose remodelling and metabolic adaptation. Host–microbiota cooperation in nitrogen conservation and the maintenance of amino acid homeostasis through ammonia production represents an evolutionarily conserved adaptive strategy under conditions of protein scarcity[59]. This framework illustrates how the gut microbiota functions as an active interpreter of dietary composition, linking nutrient availability to coordinated host physiological responses.

Despite these advances, several key limitations remain. Mechanistically, it will be crucial to determine how the microbiota senses low-protein conditions; how the LPD-conditioned microbiota preferentially increases certain bile acids in the systemic circulation; how specific members of the microbiota influence multiple organs; whether and how FXR signalling promotes adipose progenitor differentiation; and how FGF21, FXR and possibly other factors lead to a substantial remodelling of sympathetic neurons. Although an LPD consistently induced metabolic changes, including weight loss and improved glucose tolerance, the directionality of the relationship between *Ucp1* upregulation and weight loss is difficult to dissect. The specific contribution of beige adipocytes to overall metabolic effects needs to be addressed in future studies. *Ucp1* mRNA expression is highly dynamic and does not necessarily indicate active thermogenesis. Indeed, reports suggest that the anti-obesity activity of FGF21 is mediated at least in part by UCP1-independent pathways[60]. As such, the LPD-activated pathways involving FGF21 induction, bile acid signalling, WAT browning and additional factors are likely to contribute to both UCP1-dependent and UCP1-independent metabolic outcomes, the quantitative deconvolution of which warrants further investigation.

Online content

Any methods, additional references, Nature Portfolio reporting summaries, source data, extended data, supplementary information, acknowledgements, peer review information; details of author contributions and competing interests; and statements of data and code availability are available at https://doi.org/10.1038/s41586-026-10205-3.

1. Sonnenburg, J. L. & Backhed, F. Diet–microbiota interactions as moderators of human metabolism. *Nature* **535**, 56–64 (2016).
2. Lynch, S. V. & Pedersen, O. The human intestinal microbiome in health and disease. *N. Engl. J. Med.* **375**, 2369–2379 (2016).
3. Nicholson, J. K. et al. Host–gut microbiota metabolic interactions. *Science* **336**, 1262–1267 (2012).
4. Barratt, M. J., Ahmed, T. & Gordon, J. I. Gut microbiome development and childhood undernutrition. *Cell Host Microbe* **30**, 617–626 (2022).
5. Zhang, F. et al. Dietary urbanization destabilizes host-gut microbiome homeostasis and informs precision nutrition for human health. *Cell Metab.* **37**, 2128–2148 (2025).
6. Cannon, B. & Nedergaard, J. Brown adipose tissue: function and physiological significance. *Physiol. Rev.* **84**, 277–359 (2004).
7. Harms, M. & Seale, P. Brown and beige fat: development, function and therapeutic potential. *Nat. Med.* **19**, 1252–1263 (2013).
8. Wu, J. et al. Beige adipocytes are a distinct type of thermogenic fat cell in mouse and human. *Cell* **150**, 366–376 (2012).
9. Virtanen, K. A. et al. Functional brown adipose tissue in healthy adults. *N. Engl. J. Med.* **360**, 1518–1525 (2009).
10. Saito, M. et al. High incidence of metabolically active brown adipose tissue in healthy adult humans: effects of cold exposure and adiposity. *Diabetes* **58**, 1526–1531 (2009).
11. Zhang, F. et al. An adipose tissue atlas: an image-guided identification of human-like BAT and beige depots in rodents. *Cell Metab.* **27**, 252–262 (2018).
12. Lidell, M. E. et al. Evidence for two types of brown adipose tissue in humans. *Nat. Med.* **19**, 631–634 (2013).
13. Carter, M. M. et al. A gut pathobiont regulates circulating glycine and host metabolism in a twin study comparing vegan and omnivorous diets. Preprint at *medRxiv* https://doi.org/10.1101/2025.01.08.25320192 (2025).
14. Carmody, R. N., Varady, K. & Turnbaugh, P. J. Digesting the complex metabolic effects of diet on the host and microbiome. *Cell* **187**, 3857–3876 (2024).
15. Bae, M. et al. Metatranscriptomics-guided discovery and characterization of a polyphenol-metabolizing gut microbial enzyme. *Cell Host Microbe* **32**, 1887–1896 (2024).
16. Kajimura, S., Spiegelman, B. M. & Seale, P. Brown and beige fat: physiological roles beyond heat generation. *Cell Metab.* **22**, 546–559 (2015).
17. Chouchani, E. T., Kazak, L. & Spiegelman, B. M. New advances in adaptive thermogenesis: UCP1 and beyond. *Cell Metab.* **29**, 27–37 (2019).
18. Nedergaard, J., Ricquier, D. & Kozak, L. P. Uncoupling proteins: current status and therapeutic prospects. *EMBO Rep.* **6**, 917–921 (2005).
19. Hasek, B. E. et al. Remodeling the integration of lipid metabolism between liver and adipose tissue by dietary methionine restriction in rats. *Diabetes* **62**, 3362–3372 (2013).

20. Wanders, D. et al. UCP1 is an essential mediator of the effects of methionine restriction on energy balance but not insulin sensitivity. *FASEB J.* **29**, 2603–2615 (2015).
21. Wang, F. et al. Activation of GCN2 in macrophages promotes white adipose tissue browning and lipolysis under leucine deprivation. *FASEB J.* **35**, e21652 (2021).
22. Srivastava, S., Baxa, U., Niu, G., Chen, X. & Veech, R. L. A ketogenic diet increases brown adipose tissue mitochondrial proteins and UCP1 levels in mice. *IUBMB Life* **65**, 58–66 (2013).
23. Lee, A. H. et al. Cysteine depletion triggers adipose tissue thermogenesis and weight loss. *Nat. Metab.* **7**, 1204–1222 (2025).
24. Varghese, A. et al. Unravelling cysteine-deficiency-associated rapid weight loss. *Nature* **643**, 776–754 (2025).
25. Zietak, M. et al. Altered microbiota contributes to reduced diet-induced obesity upon cold exposure. *Cell Metab.* **23**, 1216–1223 (2016).
26. Chevalier, C. et al. Gut microbiota orchestrates energy homeostasis during cold. *Cell* **163**, 1360–1374 (2015).
27. Worthmann, A. et al. Cold-induced conversion of cholesterol to bile acids in mice shapes the gut microbiome and promotes adaptive thermogenesis. *Nat. Med.* **23**, 839–849 (2017).
28. Cani, P. D. & Van Hul, M. Gut microbiota in overweight and obesity: crosstalk with adipose tissue. *Nat. Rev. Gastroenterol. Hepatol.* **21**, 164–183 (2024).
29. Li, G. et al. Intermittent fasting promotes white adipose browning and decreases obesity by shaping the gut microbiota. *Cell Metab.* **26**, 672–685 (2017).
30. Li, B. et al. Microbiota depletion impairs thermogenesis of brown adipose tissue and browning of white adipose tissue. *Cell Rep.* **26**, 2720–2737 (2019).
31. Nedergaard, J. & Cannon, B. Diet-induced thermogenesis: principles and pitfalls. *Methods Mol. Biol.* **2448**, 177–202 (2022).
32. Brestoff, J. R. et al. Group 2 innate lymphoid cells promote beiging of white adipose tissue and limit obesity. *Nature* **519**, 242–246 (2015).
33. Lee, M. W. et al. Activated type 2 innate lymphoid cells regulate beige fat biogenesis. *Cell* **160**, 74–87 (2015).
34. Nguyen, K. D. et al. Alternatively activated macrophages produce catecholamines to sustain adaptive thermogenesis. *Nature* **480**, 104–108 (2011).
35. Villarroya, F., Cereijo, R., Villarroya, J., Gavalda-Navarro, A. & Giralt, M. Toward an understanding of how immune cells control brown and beige adipobiology. *Cell Metab.* **27**, 954–961 (2018).
36. Kohlgruber, A. C. et al. γδ T cells producing interleukin-17A regulate adipose regulatory T cell homeostasis and thermogenesis. *Nat. Immunol.* **19**, 464–474 (2018).
37. Hu, B. et al. γδ T cells and adipocyte IL-17RC control fat innervation and thermogenesis. *Nature* **578**, 610–614 (2020).
38. Rao, R. R. et al. Meteorin-like is a hormone that regulates immune-adipose interactions to increase beige fat thermogenesis. *Cell* **157**, 1279–1291 (2014).
39. Sharma, A. K., Khandelwal, R. & Wolfrum, C. Futile cycles: emerging utility from apparent futility. *Cell Metab.* **36**, 1184–1203 (2024).
40. Wang, W. & Seale, P. Control of brown and beige fat development. *Nat. Rev. Mol. Cell Biol.* **17**, 691–702 (2016).
41. Zeng, X. et al. Innervation of thermogenic adipose tissue via a calsyntenin 3β–S100b axis. *Nature* **569**, 229–235 (2019).
42. Ridlon, J. M. & Gaskins, H. R. Another renaissance for bile acid gastrointestinal microbiology. *Nat. Rev. Gastroenterol. Hepatol.* **21**, 348–364 (2024).
43. Wahlstrom, A., Sayin, S. I., Marschall, H. U. & Backhed, F. Intestinal crosstalk between bile acids and microbiota and its impact on host metabolism. *Cell Metab.* **24**, 41–50 (2016).
44. Rodeheffer, M. S., Birsoy, K. & Friedman, J. M. Identification of white adipocyte progenitor cells in vivo. *Cell* **135**, 240–249 (2008).
45. Merrick, D. et al. Identification of a mesenchymal progenitor cell hierarchy in adipose tissue. *Science* **364**, eaav2501 (2019).
46. Burl, R. B. et al. Deconstructing adipogenesis induced by β3-adrenergic receptor activation with single-cell expression profiling. *Cell Metab.* **28**, 300–309 (2018).
47. Lomelino, C. L., Andring, J. T., McKenna, R. & Kilberg, M. S. Asparagine synthetase: function, structure, and role in disease. *J. Biol. Chem.* **292**, 19952–19958 (2017).
48. Ryoo, H. D. The integrated stress response in metabolic adaptation. *J. Biol. Chem.* **300**, 107151 (2024).
49. Kilberg, M. S., Shan, J. & Su, N. ATF4-dependent transcription mediates signaling of amino acid limitation. *Trends Endocrinol. Metab.* **20**, 436–443 (2009).
50. Kress, J. K. C. et al. The integrated stress response effector ATF4 is an obligatory metabolic activator of NRF2. *Cell Rep.* **42**, 112724 (2023).
51. Laeger, T. et al. Metabolic responses to dietary protein restriction require an increase in FGF21 that Is delayed by the absence of GCN2. *Cell Rep.* **16**, 707–716 (2016).
52. Li-Hawkins, J., Lund, E. G., Bronson, A. D. & Russell, D. W. Expression cloning of an oxysterol 7α-hydroxylase selective for 24-hydroxycholesterol. *J. Biol. Chem.* **275**, 16543–16549 (2000).
53. Frontini, A. & Cinti, S. Distribution and development of brown adipocytes in the murine and human adipose organ. *Cell Metab.* **11**, 253–256 (2010).
54. Cohen, P. & Kajimura, S. The cellular and functional complexity of thermogenic fat. *Nat. Rev. Mol. Cell Biol.* **22**, 393–409 (2021).
55. Fischer, A. W., Schlein, C., Cannon, B., Heeren, J. & Nedergaard, J. Intact innervation is essential for diet-induced recruitment of brown adipose tissue. *Am. J. Physiol. Endocrinol. Metab.* **316**, E487–E503 (2019).
56. Wang, X. et al. The role of the NADH-dependent nitrite reductase, Nir, from *Escherichia coli* in fermentative ammonification. *Arch. Microbiol.* **201**, 519–530 (2019).
57. Zhu, W. et al. Precision editing of the gut microbiota ameliorates colitis. *Nature* **553**, 208–211 (2018).
58. Igarashi, R. et al. Generation of human adult hepatocyte organoids with metabolic functions. *Nature* **641**, 1248–1257 (2025).
59. Regan, M. D. et al. Nitrogen recycling via gut symbionts increases in ground squirrels over the hibernation season. *Science* **375**, 460–463 (2022).
60. Stanic, S. et al. Prolonged FGF21 treatment increases energy expenditure and induces weight loss in obese mice independently of UCP1 and adrenergic signaling. *Biochem. Pharmacol.* **221**, 116042 (2024).

Methods

Mice

SPF C57BL/6 (B6), BALB/c and ICR mice were purchased from Japan SLC, CLEA Japan and the Jackson Laboratory Japan. Male B6 mice aged 7 to 17 weeks were used unless otherwise specified. GF male B6 mice were purchased from Sankyo Labo Service Corporation and CLEA Japan. GF rederivation of SPF mutant mice was done at the gnotobiotic facilities of RIKEN and Keio University. In brief, in vitro fertilization (IVF) was used to generate embryos (typically using eggs and sperm from heterozygous pairs), which were then transplanted into IQI pseudo-pregnant female recipients. After embryo transfer, the recipient females underwent Caesarean sections on embryonic day 18. The intact uterine horns containing pups were passed through a germicidal bath, after which the pups were delivered into flexible plastic GF isolators and suckled by GF lactating foster mothers. This method enabled the generation of GF cohorts of 10–40 mice, all born on the same date (littermates or equivalents), thereby supporting consistent experimental conditions. *Fgf21*$^{-/-}$ mice were generated as previously described[61]. Triple-knockout mice lacking the β_1-, β_2- and β_3-adrenergic receptors (*Adrb1*$^{-/-}$*Adrb2*$^{-/-}$*Adrb3*$^{-/-}$) were used with permission from B. Lowell[62]. *Il4*$^{-/-}$ mice (G4 mice) were supplied by W. E. Paul[63]. R26:lacZbpA^{flox}DTA mice were provided by D. Riethmacher[64] and subsequently crossed with *Il5-cre* or *Lyz2-cre*e mice. *Nr1h4*$^{-/-}$, *Gpbar1*$^{-/-}$, *Nr1h4*$^{fl/fl}$, *Vil1-cre*, *Alb-cre*, *Adipoq-cre*, *Tcrb*$^{-/-}$, *Tcrd*$^{-/-}$, *Tbx21*$^{-/-}$, *Rorc*$^{-/-}$ (homozygous of *Rorc(γt)*-EGFP mice), *Il5-cre* and *Lta*$^{-/-}$ mice were purchased from the Jackson Laboratory. *Rag2*$^{-/-}$*Il2rg*$^{-/-}$ mice were obtained from Taconic. *Il33*$^{-/-}$ mice were obtained from RIKEN BRC with permission from S. Nakae. *Dpp4-cre* (*Dpp4*-RFP, -cre) mice were obtained from RMRC. Unless otherwise indicated, mice were housed under controlled conditions, including a temperature range of 23–25 °C, a humidity of 40–60% and a 12-h light–dark cycle. In the experiment at thermoneutral conditions, SPF mice were kept in an incubator (MIR-154, PHCbi, Japan) at 30 °C according to previous work[65]. Magnetic resonance imaging (MRI) data collection was outsourced to PRIMETECH and collected using an M7 Compact MRI system (Aspect Imaging). Autoclaved water and gamma-irradiated (50 kGy) sterilized food were provided ad libitum throughout the experiments. Unlike autoclaving, gamma irradiation avoids heat-induced alterations in food components. The specific diets and durations of each experiment are detailed in the corresponding figure panels. Mice were randomly allocated into experimental groups. All animal experiments were approved by the Institutional Animal Care and Use Committee of Keio University and the RIKEN Yokohama Institute.

Experimental diets

All experimental diets were obtained from Research Diets or Oriental Yeast. The control diet used in this study was a 50-kGy-irradiated AIN-93G diet (product D19090404) containing 20 kcal% protein (mineral acid casein), 64 kcal% carbohydrate and 16 kcal% fat. Unless otherwise specified, the LPD was an isocaloric AIN-93G-based diet containing 7 kcal% protein, 77 kcal% carbohydrate and 16 kcal% fat (product D20121501; see Supplementary Tables 3 and 4). Diets with varying proportions of protein, carbohydrate and fat were formulated based on the AIN-93G diet, with the exception of the ketogenic diet and the ketogenic–control diet, which have a lower fat content than AIN-93G does. The ketogenic diet and ketogenic–control diets (products D20012303 and D20012304 from Research Diets, respectively) use cocoa butter as the main fat source, with the protein concentration adjusted to 20 kcal% to match the AIN-93G diet. Because the ketogenic–control diet contains only 10% fat, which is lower than the fat content of AIN-93G, it is referred to as the low-fat diet in Fig. 1a. For experiments using defined amino acid diets, natural protein (mineral acid casein) was replaced with pure amino acids, aligned with the amino acid composition of the protein. The total amino acid concentration was then adjusted, ranging from 20 to 2.5 kcal%, or set to 2.5% kcal content for individual EAAs, while maintaining the levels of other amino acids at 20%, and isocaloric conditions were maintained by varying the amount of carbohydrate (see Supplementary Table 5).

Model of HFD-induced obesity

SPF C57BL/6 mice were at first fed an HFD for 2, 4 or 9 weeks. For HFD-to-CD versus HFD-to-LPD experiments, HFD32 (CLEA Japan; 60 kcal% fat and 20 kcal% protein) was used. For the HFD-to-HF/LPD versus HFD-to-HFD experiments, an AIN-93G-based HFD (32 kcal% fat and 20 kcal% protein) was used (Supplementary Table 6). Mice were then switched to one of the following diets for 4 or 6 weeks: control diet (20% fat and 20% protein), LPD (20 kcal% fat and 7 kcal% protein) or HF/LPD (32 kcal% fat and 7 kcal% protein). Quantification of plasma ALT, cholesterol and triglycerides was outsourced to Oriental Yeast. Oral glucose tolerance tests (OGTTs) were performed 7 days before euthanasia. For the hu4-mix treatment experiments, GF mice were inoculated with faecal microbiota from human participant T07 and fed a HFD (HFD32) for four weeks, then switched to an LPD. On days 0 and 3 after the diet switch, mice were given two oral doses of the hu4 strains or vehicle control. After 6 weeks on the LPD, mRNA expression of *Ucp1* in iWAT and BAT, iWAT mass, hepatic *Fgf21* mRNA expression and plasma levels of cholesterol, triglycerides and ALT were assessed. An OGTT was performed after 3 weeks of LPD feeding.

Measuring faecal calories

Faecal caloric content was measured using bomb calorimetry, as previously described[66]. In brief, faecal samples were dried overnight at 60 °C, weighed and analysed for energy content using a bomb calorimeter (Parr 6100EA with Semimicro Bomb) calibrated with standard benzoic acid (6,320 cal g^{-1}).

Cold exposure and treatments with a β_3-adrenergic receptor agonist, tungsten, ammonium chloride and recombinant FGF21

For cold exposure, mice were housed at 6 °C for 7 days. For treatment with a β_3-adrenergic receptor agonist, mice were administered CL316,243 daily by intraperitoneal injection (20 μg per mouse per dose, SIGMA C5976) for seven consecutive days. For tungsten treatment, mice were provided with 0.22-μm filter-sterilized sodium tungstate dihydrate ($Na_2WO_4/2H_2O$, Nacalai Tesque 32011-25) in their drinking water at concentrations of 0.1% or 0.5% for 2 weeks. Throughout the treatment period, mice had ad libitum access to the tungsten-containing water, and both the remaining water volume and the health status of the mice were carefully monitored. On the basis of daily observations, mice in the 0.1% tungsten treatment group did not exhibit any noticeable changes in food or water consumption. By contrast, those in the 0.5% tungsten group showed signs of adverse effects, including mildly reduced appetite. For ammonium chloride (NH_4Cl) treatment, mice were given 0.22-μm filter-sterilized NH_4Cl (Nacalai Tesque 02423-65) in their drinking water at concentrations of 5 or 50 μg ml^{-1} for 5 weeks, corresponding to the full duration of LPD feeding. Administration of NH_4Cl at either concentration did not result in any noticeable changes in food or water intake. For recombinant FGF21 treatment, GF B6 mice were fed a control diet for 1 week. On days 5, 6 and 7, they received intraperitoneal injections of recombinant human FGF21 (12 μg per mouse, twice daily, BioLegend 553804) or PBS.

qPCR

To evaluate mRNA expression, whole iWAT (excluding inguinal lymph nodes), gonadal WAT (gWAT), BAT and 30–50 mg of liver tissue were homogenized using 1.4-mm ceramic beads. Total RNA was extracted using TRIzol reagent (Invitrogen) following the manufacturer's protocol. For iWAT and gWAT lysates, the lipid fraction was removed at the first step by centrifugation. For qPCR analysis, cDNA was synthesized from 0.5 μg of total RNA using ReverTra Ace qPCR RT Master Mix

(TOYOBO), and qPCR was performed with Thunderbird SYBR qPCR Mix (TOYOBO) on a LightCycler 480 II (Roche). The following primer pairs were used:

Ppib: 5′-GGAGATGGCACAGGAGGAA-3′ and 5′-GCCCGTAGTGCTTCAGCTT-3′;

Ucp1: 5′- CACCTTCCCGCTGGACACT −3′ and 5′-CCCTAGGACACCTTTATACCTAATGG-3′;

Elovl3: 5′-TGTTGGCCAGACCTACATGA-3′ and 5′-GGCCCACTGTAAACATCACTG-3′;

Cidea: 5′-ATCACAACTGGCCTGGTTACG-3′ and 5′-TACTACCCGGTGTCCATTTCT-3′;

Cox7a1: 5′-AGCTGCTGAGGACGCAAAAT-3′ and 5′-CTTCTCTGCCACACGGTTTT-3′;

Cox8b: 5′-GAACCATGAAGCCAACGACT-3′ and 5′-GCGAAGTTCACAGTGGTTCC-3′;

Phgdh: 5′-ATGGCCTTCGCAAATCTGC-3′ and 5′-AGTTCAGCTATCAGCTCCTCC-3′;

Psat1: 5′-TGCCACACTCGGTATTGTTG-3′ and 5′-CAGCTAGCAATTCCCTCACAA-3′;

Aldh1l2: 5′-AAAGAGGGCCACCGAGTAGT-3′ and 5′-TTCATCGAGGGAACTTGAAC-3′;

Asns: 5′-AAGATGGGTTTCTGGCTGTG-3′ and 5′-ACAGACGCAACTTTGCCATT-3′;

Gdf15: 5′-GAACCAAGTCCTGACCCAGC-3′ and 5′-GCTTCAGGGGCCTAGTGATG-3′;

Fgf21: 5′-CCTGGGTGTCAAAGCCTCTA-3′ and 5′-TCCTCCAGCAGCAGTTCTCT-3′;

Cyp39a1: 5′-TTCTCACCAATAGCAATCGCC-3′ and 5′-GTCATTCGGTTTCCCATAGCAA-3′;

Csad: 5′-GCCGGACTGTGATTCACTACA-3′ and 5′-GTGTTGAGGCTCTCCGTGAT-3′.

The assessment of mRNA expression was performed using three independent methods: relative abundance, fold change and total per-depot mRNA. For the assessment of relative abundance, C_t values were converted into quantities using linear equations derived from standard curves, which were generated from serial dilutions of cDNA samples containing high copy numbers of the target gene. In cases in which no samples with high copy numbers or obvious positive controls were available, the ΔΔCt method was used. *Ppib* (peptidylprolyl isomerase B) served as the housekeeping gene for normalization, enabling the calculation of relative expression levels for each target gene. Fold change was calculated by dividing the relative abundance value of each individual by the mean value of the control diet group. For the assessment of total per-depot mRNA, 2^{-Ct} values were calculated for each depot[31].

Bulk RNA-seq analysis of iWAT and liver

Libraries were prepared using the TruSeq Stranded mRNA Library Prep Kit (Illumina) following the manufacturer's instructions. Sequencing was performed by Macrogen Japan using a NovaSeq 6000 platform (Illumina) with 100-bp paired-end reads and a run scale of 4 Gb per sample. Sequenced reads were mapped to the mouse reference genome (mm10) and normalized to reads per kilobase per million reads (RPKM) using Strand NGS software v.2.7 (Strand Life Sciences). The summarized data were then assessed by statistical models (one-way ANOVA with Tukey's HSD and the Benjamini–Hochberg for multiple gene correction) or STAR, featureCounts and DESeq2.

OGTTs

For the OGTTs, mice were fasted overnight and then orally administered glucose at a dose of 1.2 g per kg body weight (note that although we acknowledge that dosing according to lean mass might better reflect glucose utilization[67], particularly by skeletal muscle, which is a major site of glucose uptake, we adopted body-weight-normalized dosing in accordance with previous studies[68–70]). Blood samples were taken from the tail before and at 15, 30, 60, 90 and 120 min after glucose administration. Blood glucose levels were measured using GlucoCard G Black sensors and blood glucose test strips (G sensor, Arkray).

Histological analysis

Freshly collected tissues were fixed in 4% paraformaldehyde (PFA), embedded in paraffin and sectioned into 5-µm slices before undergoing haematoxylin and eosin (H&E) staining. For immunostaining, tissues were first deparaffinized three times in xylene and then rehydrated. The sections were blocked for 60 min in PBS containing 5% goat serum, 1% bovine serum albumin and 0.5% Tween 20. After rinsing in PBS, the slides were incubated overnight at 4 °C with Alexa Fluor 647-conjugated anti-UCP1 antibody (rabbit, EPR20381, Abcam ab225489, 1:200). After further washes, the sections were stained with DAPI, mounted and imaged using a BZ-X810 microscope (Keyence).

Whole-mount immunostaining

iWAT was post-fixed overnight in 4% PFA and stored in 80% ethanol at 4 °C until iDISCO processing. Immunohistochemical staining was performed following the detailed iDISCO experimental protocol, adapted from a previous report[71] with modifications. iWAT samples were dehydrated through a graded methanol/H_2O series (20%, 40%, 60%, 80% and 100%; 1 h each), followed by overnight incubation at room temperature in a 66% dichloromethane (DCM) and 33% methanol solution on a rocker (Multi Bio 3D programmable mini-shaker; Biosan). Tissues were then washed twice in 100% methanol and treated with 6% H_2O_2 in methanol overnight at 4 °C. After overnight incubation, tissues were rehydrated in a series of 1 h methanol /H_2O washes, then washed in fresh PBS overnight on a rocker at room temperature. Tissues were washed with PTx.2 solution (0.2% Triton X-100 in PBS) twice on a rocker at 1-h intervals. Samples were then incubated in permeabilization solution (400 ml PTx.2, 11.5 g glycine and 100 ml dimethyl sulfoxide (DMSO)) for 2 days at 37 °C in a shaker (Bioshaker, BR-43FL). This was followed by incubation in blocking solution (42 ml PTx.2, 5 ml DMSO and 3 ml normal donkey serum (NDS)) at 37 °C for 2 days in the shaker. Tissues were then incubated with primary antibodies (chicken anti-TH (1:400, Milipore, AB9702), rabbit anti-UCP1 (1:400, Abcam, ab225489) and goat anti-CD31 (1:300, Novus Biologicals, AF3628)) in primary incubation solution (92 ml PTwH (1 ml of 10 mg ml^{-1} heparin stock solution, 2 ml Tween 20 dissolved in 1 l PBS), 5 ml DMSO and 3 ml NDS) on a shaking incubator at 25 °C for seven days. After primary antibody staining, tissues underwent six 1-h washes in PTwH and were then subjected to secondary antibody staining (Alexa Fluor 555 donkey anti-chicken IgY (1:300, Thermo Fisher Scientific, A-78949) and Alexa Fluor 488 donkey anti-goat IgG (1:300, Thermo Fisher Scientific, A-11055)) in secondary incubation solution (PTwH with 3% NDS) for 10 days at 25 °C on a shaker. Samples underwent another PTwH wash step and were incubated overnight at room temperature on a rocker with fresh PTwH solution. An additional round of methanol dehydration was performed (as described above) and then samples were incubated overnight in 100% methanol on a rocker at room temperature. Next, tissues were submerged in a 66% DCM and 33% methanol solution for 3 h. After that, the samples underwent two 100% DCM washes and were placed in dibenzyl ether for 3 days on a rocker at room temperature for clearing. A ZEISS Lightsheet 7 microscope or Miltenyi Biotec UltraMicroscope Blaze were used to generate three-dimensional images of iWAT tissues with a zoom factor of 5× or 20×. Images of TH and UCP1 labelling were collected for all samples using ZEN black, ZEN blue and Arivis software.

Blood FGF21 and ammonia measurement

Plasma samples were collected from mice under appropriate anaesthesia through cardiac puncture or portal vein sampling. For portal vein collection, blood was drawn using a syringe fitted with a 30G needle. All plasma samples were stored at −80 °C until analysis. FGF21 levels were measured using the Mouse FGF-21 DuoSet ELISA kit (R&D), following the manufacturer's instructions. Ammonia levels in portal vein

and cardiac blood samples were measured by Oriental Yeast using the CicaLiquid NH_3 kit (Kanto Chemical).

Western blot analysis

Mouse iWAT was snap-frozen in liquid nitrogen, the proteins were extracted using RIPA buffer and the final protein concentration was adjusted to 4 μg $μl^{-1}$. For SDS–PAGE and blotting, the Novex NuPAGE SDS-PAGE Gel system (Thermo Fisher Scientific) and Trans-Blot Turbo system (Bio-Rad, 1704150) were used according to the manufacturer's instructions. iBind Western Systems (Thermo Fisher Scientific) were used for staining throughout the study. The antibodies used in this study are as follows: rabbit anti-mouse UCP1 (Abcam, ab10983, 1:1,000), mouse monoclonal anti-β-actin antibody (Sigma, A1978, 1:1,000), goat anti-rabbit IgG HRP-linked (Cell Signaling, 7074, 1:2,000) and horse anti-mouse IgG, HRP-linked (Cell Signaling, 7076, 1:2,000). Chemi-Lumi One (Nacalai Tesque) was used for the chemiluminescence assays and the Fusion FX (Vilber) was used for imaging.

FXR reporter assay

The FXR stimulating activity of bile acids was assessed using the GeneBLAzer FXR-UAS-bla HEK 293T Cell Agonist Assay (Thermo Fisher Scientific), following the manufacturer's protocol. In brief, cells were seeded in black-walled, clear-bottomed 384-well assay plates at a density of 1×10^4 cells per well and incubated overnight at 37 °C in a 5% CO_2 atmosphere. Bile acids (CDCA, UDCA, CA, 7oxoCA, UCA, DCA, tauro-βMCA or tauro-CA, all sourced from Cayman) were added at concentrations ranging from 20 to 0.61 μM. After overnight incubation at 37 °C, cells were treated with the FRET blue/green-enabled substrate CCF4-AM and incubated for an additional 2 h at room temperature in the dark. Fluorescence was measured using a TECAN microplate reader at emission wavelengths of 460 nm (blue) and 530 nm (green), with an excitation wavelength of 409 nm. The blue/green emission ratio for each well was calculated by dividing the background-subtracted blue emission values by the green emission values, as per the manufacturer's instructions. Data from cells exhibiting abnormal morphology, indicative of cellular toxicity at higher bile acid concentrations, were excluded from the analysis.

snRNA-seq analysis of iWAT

Approximately 50 mg of mouse iWAT was dissected from the region surrounding the inguinal lymph nodes (excluding the nodes themselves), cut into about 20 pieces and stored in liquid nitrogen until use. Nuclei were isolated from frozen samples using the 10x Chromium Nuclei Isolation kit according to the manufacturer's protocol. An aliquot of nuclei from each sample was stained with trypan blue or acridine orange–propidium iodide (Logos Biosystems), and a haemocytometer and LUNA-FX7 were used to identify and count intact nuclei. Nuclei from three or four mice were pooled and immediately loaded on the 10x Chromium controller (10x Genomics) according to the manufacturer's protocol. For each sample (GF + CD, GF + LPD, SPF + CD, SPF + LPD; $n = 2$ pools; 8 samples in total), 20,000 nuclei were loaded in one channel of a Chromium Chip (10x Genomics). The Chromium Next GEM Single Cell 3′ v.3.1 Chemistry (dual index) was used to process all samples. cDNA and gene-expression libraries were generated according to the manufacturer's instructions. cDNA and gene-expression-library fragment sizes were assessed with DNA High Sensitivity Screen tape (Agilent). Gene-expression libraries were multiplexed and sequenced on the NovaSeq 6000 (Illumina) at Macrogen Japan using the 150-bp paired-end mode. The Cell Ranger v.7.0 pipeline from 10x Genomics was used to align reads to the mm10 genome assembly and produce feature matrices. To adjust for downstream effects of ambient RNA expression within mouse nuclei, we used CellBender v.0.1.0 (ref. 72) to remove counts due to ambient RNA molecules from the count matrices and estimate the true nuclei. Seurat v.4.3.0 (ref. 73) was used for quality control, analysis of individual feature matrices, integrated analysis of all eight samples (dim = 8, resolution = 0.5 for liver, dim = 30, resolution = 1.2 for iWAT) and generation of the UMAP plot.

Trajectory inference analysis

To study differentiation within the adipose cell subsets, we performed trajectory analysis using Slingshot[74]. We first subsetted our Seurat object to include only mature iWAT adipocyte clusters in SPF LPD-treated cells (adipocyte 10, adipocyte 03, adipocyte 07, adipocyte 05, adipocyte 09, adipocyte 02, beige adipocyte, adipocyte 12, adipocyte 11, adipocyte 01, adipocyte 06, adipocyte 08 and adipocyte 04). After subsetting, we converted the Seurat object into a SingleCellExperiment object (v.1.26.0) using the as.SingleCellExperiment function and computed pseudotime lineages using Slingshot (v.2.12.0) on the UMAP embeddings[75]. We next computed a cell–cell transition matrix and identified lineage driver genes using CellRank[76]. The Seurat object, along with Slingshot pseudotime coordinates, was converted to an AnnData object with Seurat's Convert function for analysis in Python. Of the four lineages identified by Slingshot, we selected cells belonging to the beige-adipocyte lineage (lineage 2). Within this lineage, we computed cell–cell transition probabilities using the PseudotimeKernel in CellRank (v.2.0.5), which incorporates both a *k*-nearest neighbours (k-NN) graph (30 principal components and 50 nearest neighbours) and the Slingshot pseudotime ordering. We used the resulting cell–cell transition matrix to estimate fate probabilities and identify key driver genes within the beige-cell lineage. We fit the generalized perron cluster cluster analysis (GPCCA) estimator on the pseudotime kernel, assigning beige adipocyte as the terminal state. We finally computed beige-adipocyte fate probabilities and identified genes correlated with these fate probabilities using the compute_lineage_drivers function, with default parameter settings. To further study these lineage driver genes, we visualized their expression along the beige-cell lineage and performed pathway enrichment analysis. We visualized gene-expression trends by fitting the expression of lineage driver genes along pseudotime using generalized additive models.

snRNA-seq analysis in liver

Nuclei were collected from frozen liver tissues (approximately 50–60 mg) using Singulator 100 (S2 Genomics, with the inbuilt program Single-Shot Standard Nuclei Isolation V2) and buffers according to the 10x Genomics protocol (Demonstrated Protocol: Nuclei Isolation for Single Cell Multiome ATAC + GEX Sequencing). The resulting suspensions including nuclei were filtered through a 30-μm strainer, stained with acridine orange–propidium iodide (Logos Biosystems), and counted in a LUNA-FX7 to identify intact nuclei. Nuclei were immediately loaded onto the 10x Chromium controller (10x Genomics) according to the manufacturer's protocol. For each sample (GF + CD, GF + LPD, SPF + CD, SPF + PD; $n = 2$ mice; 8 samples in total), 8,000 nuclei were loaded onto one channel of a Chromium Chip (10x Genomics). The Chromium Next GEM Single Cell 3′ v.3.1 Chemistry (single index) was used to process all samples.

FDG-PET scans

Twenty-five healthy male volunteers (age: 20 to 47 years) were recruited to investigate the role of the gut microbiota in beige-cell accumulation. All participants were thoroughly briefed on the study and provided written informed consent. The protocols were approved by the Institutional Research Ethics Review Board of Tenshi College (Sapporo, Japan) (UMIN000016361). Human brown- and beige-cell activity was assessed using a FDG-PET scan (Aquiduo, Toshiba Medical Systems) following standardized non-shivering cold exposure, as described previously[77,78]. All individuals fasted for 12 h before undergoing the PET-CT scan. After 1 h of cold exposure, volunteers received an intravenous injection of ^{18}F-FDG (1.66–5.18 MBq per kg body weight) and remained in the cold room for an additional hour. Brown- and beige-cell activity

was evaluated by measuring the standardized uptake value (SUV) of ^{18}F-FDG and Hounsfield units from −300 to −10 in the supraclavicular region using Fusion software (Toshiba Medical Systems). Faecal samples were collected from all participants and stored at Keio University following the protocol approved by the Institutional Review Boards (approval number 20150075).

Bacterial isolation and generation of gnotobiotic mice

Human and mouse faecal samples and intestinal contents were suspended in an equal volume (w/v) of PBS containing 20% glycerol, snap-frozen in liquid nitrogen and stored at −80 °C until use. To inoculate into GF mice, the frozen stocks were thawed, suspended in mGAM broth and filtered through a 100-μm cell strainer, and an aliquot (approximately 2–5 mg in 250 μl per mouse) was orally inoculated into GF mice. To identify beige-cell-inducing bacterial strains associated with mice or humans, small-intestinal contents from the B28-1 mouse or faecal samples from mice colonized with T10 or T19 human microbiota were serially diluted in PBS and plated onto non-selective and selective agar plates. EG, BHK and BBE media were used for the isolation of human-derived strains, and BL, mucin, YCFA-GSC, marine and TSA were used in addition for the isolation of mouse-derived strains. After incubating under anaerobic conditions (80% N_2, 10% H_2 and 10% CO_2) in an anaerobic chamber (Coy Laboratory Products) or under aerobic conditions at 37 °C for 2 to 7 days, individual colonies were picked. The full-length 16S rRNA gene region was amplified using universal primers (27Fmod: 5′-AGRGTTTGATYMTGGCTCAG-3′, 1492R: 5′-GGYTACCTTGTTACGACTT-3′) and Sanger sequenced. The resulting strain sequences corresponding to the first half (approximately 0.8 kb) were aligned and compared using BLAST to identify closely related species or strains. Individual isolates were classified as a strain if their 16S rRNA gene sequences exhibited 100% identity. The sequences were also compared with amplicon sequence variants (ASVs) identified in small-intestinal samples from mouse B28-1 and faecal samples from mice T10-4, T10-5, T19-5 and T19-6 to identify their corresponding ASVs. Note that the 16S rRNA gene sequences of mouse B28-1-derived St.27G3 and St.80E1 are most similar to those of *Blautia pseudococcoides* and *Turicibacter sanguinis* but share only 93% and 97% similarity, respectively, indicating that they represent previously undefined strains. For convenience, we refer to these isolates as *Blautia* sp. (St.27G3) and *Turicibacter* sp. (St.80E1) throughout this manuscript. The closest species of human-derived St.4 was *Anaerofustis stercorihominis*, but with less than 98% sequence identity, indicating that this also represents previously undefined strain. We refer to this isolate as *Eubacteriaceae* sp. (St.4).

To prepare bacterial mixtures for inoculation into GF mice, individual strains were cultured to confluence in mGAM broth or BHKRS agar, and equal volumes of the resulting bacterial suspensions were mixed. Specific supplements were added to support the growth of certain strains: 0.1% fumarate, 0.1% formate and 0.5 μg ml^{-1} vitamin K were added for *Parasutterellaceae* (St.1A3); 0.1% fumarate, 0.1% formate, 0.5 μg ml^{-1} vitamin K and 0.1 mg ml^{-1} sodium sulfate were added for *Blautia* sp. (St.27G3), *Eggerthellaceae* (St.1H8) and *Taurinovorans muris* (8H4); and 1 mg ml^{-1} glycine and 1 mg ml^{-1} glutamate were added for *Parvibacter caecicola* (St.1B6). For *Bilophila* sp. 4_1_30 (St.14) and *Ruthenibacterium lactatiformans* (St.32), cultures were supplemented with 0.1% fumarate, 0.1% formate, 0.5 μg ml^{-1} vitamin K, 0.1 mg ml^{-1} sodium sulfate, 1 mg ml^{-1} glycine and 1 mg ml^{-1} glutamate. In some experiments, 1% taurine was added for *Bilophila* sp. 4_1_30 (St.14) or 1% arginine was added for *Adlercreutzia* (St.3). The bacterial mixtures were administered orally to GF mice, delivering approximately 1×10^8 to 1×10^9 colony-forming units (CFU) of each strain in 250 μl of medium per mouse. All mice receiving the same mixture of bacterial strains were housed together in a single gnotobiotic isolator. Gnotobiotic mice were analysed 4 or 6 weeks after inoculation unless otherwise indicated. Colonization was evaluated through direct smears of faecal suspensions and qPCR analysis of faecal and caecal DNA, using the extraction method described in the '16S rRNA gene amplicon sequencing' section below. Strain-specific primers were used:

Mouse-derived 20 strains:

St.1A1: 5′-ACATGCAAGTCGAACGGGAT-3′, 5′-CTCATGTGGAACATCCGGCA-3′

St.1A11: 5′-TGCTTGCACTCACCGATAAA-3′, 5′-CGGTATTAGCACCTGTTTCCA-3′

St.1A3: 5′-GAACGGTAACAGCGAGGAAA-3′, 5′-CATCCTTTCGGATGGTTGTC-3′

St.1A6: 5′-CGAGCGAGCTTGCCTAGATG-3′, 5′-CACGTGTTACTCACCCGTCC-3′

St.1B6: 5′-CAGTGGGGACGATGGTGAC-3′, 5′-CGCTCCCTACGTATTACCGC-3′

St.C4: 5′-AAGGCCTTCGGGTCGTAAAG-3′, 5′-GCACGTAGTTAGCCGTGACT-3′

St.1H8: 5′-GGAATAGAGTGGCGAACGGG-3′, 5′-CATCCCTTGCCGTCGGG-3′

St.4A1: 5′-GAAACTGCCTGATGGAGGGG-3′, 5′-GAAGGTCCCCCACTTTGGTC-3′

St.4B7: 5′-GACGAAGCCACTTGTGGTGA-3′, 5′-ATTTCACAGACGACGCGACA-3′

St.4D1: 5′-GGCGGATTTATCTGCCGCTC-3′, 5′-CTATGCATCGTCGCCTTGGT-3′

St.4D3: 5′-GGGAAGAAGCCCCTTTTGGG-3′, 5′-TTGCGCCCTACGTATTACCG-3′

St.4H5: 5′-GATAACTCCGGGAAACCGGG-3′, 5′-ACAGCCGAAACCGTCTTTCA-3′

St.4H6: 5′-ACAGCCGAAACCGTCTTTCA-3′, 5′-TCTCCACATGGAGGGGGAAG-3′

St.8H4: 5′-ACGTATGTGGGAAAGACGGC-3′, 5′-AACCATCGTCGCCTTGGTAG-3′

St.18E8: 5′-AAAGGAGGGGAGTCAGCAAT-3′, 5′-ACAGAGTCCTCTGCTTCACCA-3′

St.19E12: 5′-CGGCACATGATACTGCGAGA-3′, 5′-TTAATGTCCAGGAACCCGCC-3′

St.21A7: 5′-GCGAAGCACTTTGATTGGAT-3′, 5′-CGCGGTCTTATGCGGTATTA-3′

St.21B5: 5′-TGAAGGCTTGCCTTTACCAG-3′, 5′-ATGTCCCGTCGATGCATTAT-3′

St.27G3: 5′-GCAAGTCGAACGAAGCATTT-3′, 5′-TGTTGTCCCCCTGTGTAAGG-3′

St.80E1: 5′-ATGCAAGTCGAGCGAACCAC-3′, 5′-TAGCGATCGTTTCCAATCGT-3′

Human-derived T19 33 strains:

St.1: 5′-TGGCGAACGGGTGAGTAATA-3′, 5′-CACCATGCAGTGTCCATACCT-3′

St.2: 5′-AGTAACGCGTGGGTAACCTG-3′, 5′-TGCGATACTGTGCGCTTATG-3′

St.3: 5′-TTCGGCCGTGTATAGAGTGG-3′, 5′-GTATTAGCCGCCGTTTCCAG-3′

St.4: 5′-AACGGGTGAGTAACGCGTAG-3′, 5′-ATCATGCGATAGCGTGGTCT-3′

St.5: 5′-GCCCTATACAGGGGGATAACA-3′, 5′-TACTGCCAGGGCTTTTCACA-3′

St.6: 5′-GAGCAACCTGCCTTTCAGAG-3′, 5′-GATTGCTCCTTTGGTTGCAG-3′

St.7: 5′-AAAGCTTGCTTTCTTTGCTG-3′, 5′-AACCATGCGGAATCATTATGC-3′

St.8: 5′-GTTTGCTTGCAACTGAAGATGG-3′, 5′-AAAGGCTATTCCGGAGTTATCG-3′

St.9: 5′-CGGGTGAGTAACACGTATCCA-3′, 5′-TGCGGAAGAATTATGCCATC-3′

St.10: 5′-CGTATCCAACCTGCCGTCTA-3′, 5′-TCATGCGGACATGTGAACTC-3′

St.11: 5′-AAGCTTGCTTTGATGGATGG-3′, 5′-TTCGAAAGGCTATCCCAGTG-3′
St.12: 5′-ACGTATCCAACCTGCCGATA-3′, 5′-CAAGACCATGCGGTCTGATT-3′
St.13: 5′-TTAGCTTGCTAAGGCCGATG-3′, 5′-CCTTTCAGAAGGCTGTCCAA-3′
St.14: 5′-GGGTGAGTAACGCGTGGATA-3′, 5′-ATCGGGAGCGTATTCGGTAT-3′
St.15: 5′-TGAGTAACGCGTGAGCAATC-3′, 5′-TCAAGAGATGCCTCCCAAAC-3′
St.16: 5′-TGGGGAATAACAGGTGGAAA-3′, 5′-GAGCGATAAATCTTTGGCAGTC-3′
St.18: 5′-CATGTGTCCGGGATAACTGC-3′, 5′-CCTTGATGGGCGCTTTAATA-3′
St.19: 5′-TGGCGAACGGGTGAGTAATA-3′, 5′-CCCTTCACCTATGCGGTCTT-3′
St.20: 5′-CTGTACCGGGGGATAACACTT-3′, 5′-CCACCGGAGTTTTTCACACT-3′
St.21: 5′-GGAAAAAGAAGAGTGGCGAAC-3′, 5′-CGGTATTAGCACCTGTTTCCA-3′
St.22: 5′-TTTTCTTTCACCGGAGCTTG-3′, 5′-CGCCTTTCAACTTTCTTCCA-3′
St.23: 5′-TGGCGAACGGGTGAGTAATA-3′, 5′-TGTCCGTACCTATGCGGTCT-3′
St.24: 5′-GATGAAGGATATGGCGACTGA-3′, 5′-GGCCTTATGCGGTATTAGCA-3′
St.25: 5′-GATTCGTCCAACGGATTGAG-3′, 5′-GCATCATGCGGTATTAGCACT-3′
St.26: 5′-AACGGGTGAGTAACACGTGAG-3′, 5′-TTGCTCCTTTTCCCTCTGTG-3′
St.27: 5′-AGTAACGCGTGGGTAACCTG-3′, 5′-ACCGGAGTTTTTCACACCAG-3′
St.28: 5′-GCGGATCTTCGGAAGTTTTC-3′, 5′-ACCGGAGTTTTTCACACCAG-3′
St.29: 5′-TGGCGAACGGGTGAGTAATA-3′, 5′-GTCCCCCTCTTTCTTCCGTA-3′
St.30: 5′-AGTAACGCGTGGGTAACCTG-3′, 5′-CCACCGGAGTTTTTCACACT-3′
St.31: 5′-AGCGATTCTCTTCGGAGAAG-3′, 5′-GCAAAAGCTTTGATACTTCT-3′
St.32: 5′-TTTCAGTGGGGGACAACATT-3′, 5′-AAATCCTTTGACCCCTGTGC-3′
St.34: 5′-TTAGTTTGCTTGCAAACTAAAG-3′, 5′-CCATGCGGTTTTAATATACC-3′
St.35: 5′-GACGGATTTCTTCGGATTGA-3′, 5′-ACCGGAGTTTTTCACACCAG-3′.

16S rRNA gene amplicon sequencing

Frozen small-intestinal and caecal contents and faecal pellets from mice were thawed and suspended in 500 ml TE10 (10 mM Tris-HCl, 10 mM EDTA) buffer containing RNase A (final concentration of 100 μg ml^{-1}, Invitrogen) and lysozyme (final concentration 3.0 mg ml^{-1}, Sigma). The suspension was incubated for 1.5 h at 37 °C with gentle mixing. Then, sodium dodecyl sulfate (final concentration 1%) and proteinase K (final concentration 2 mg ml^{-1}, Nacalai) were added to the suspension and the mixture was incubated for 1 h at 55 °C. High-molecular-mass DNA was extracted with phenol:chloroform:isoamyl alcohol (25:24:1), precipitated with isopropanol, washed with 75% ethanol and resuspended in 50–200 ml of TE or sterile Milli-Q water. PCR was performed using 27Fmod 5′-AGRGTTTGATYMTGGCTCAG-3′ and 338R 5′-TGCTGCCTCCCGTAGGAGT-3′ to the V1–V2 region of the 16S rRNA gene. Amplicons generated from each sample (around 330 bp) were subsequently purified using AMPure XP (Beckman Coulter). DNA was quantified using a Quant-iT Picogreen dsDNA assay kit (Invitrogen) and a TBS-380 Mini-Fluorometer (Turner Biosystems). The 16S metagenomic sequencing was performed using MiSeq according to the Illumina protocol. Two paired-end reads were merged using the fastq-join program based on overlapping sequences. Reads with an average quality value of less than 25 and inexact matches to both universal primers were filtered out. Filter-passed reads were used for further analysis after trimming off both primer sequences. For each sample, 3,000 quality filter-passed reads were rearranged in descending order according to the quality value, and then the trimmed reads were uploaded to the DADA2 R package v.1.18.0 to construct ASVs using the filterAndTrim function with standard parameters (maxN = 0, truncQ = 2 and maxEE = 2). Possible chimeric reads were removed with the removeBimeraDenovo function of DADA2. Taxonomic assignment of each ASV was made by searching by similarity against the National Center for Biotechnology Information RefSeq and genome database using the GLSEARCH program.

Bacterial whole-genome sequencing

Whole-genome sequencing was performed using the Sequel II system (PacBio). The library was prepared using the SMRTbell Express template preparation kit v.2.0 (PacBio) following DNA shearing to a target length of 10–15 kb using gTUBE (Covaris). The PacBio reads were converted to HiFi reads using CCS software v.6.2.0. The HiFi reads for the mouse-derived strains were assembled using both Canu v.2.1.1 and Flye v.2.9 with the following parameters: Canu (-pacbio-hifi, genomeSize = 2.5 M, minReadLength = 2200) and Flye (-g 2.5 m, --min-overlap 2200, --pacbio-hifi). Contigs from the Canu assembly were used as genomes for analysis when consensus was reached between the two assemblers. The generated consensus contigs generated were checked for circularization to remap the HiFi reads by Minimap2 v.2.24-r1122. For human-derived strains, HiFi reads were assembled using Hifiasm v.0.19.5-r587 with default parameters. Contigs aligned to other contigs with 99% identity or higher and 95% coverage or higher were considered as bubble contigs. Contigs with low depth (less than 5) and bubble contigs were eliminated. The genes were predicted and annotated using Bakta v.1.5.1 (ref. 79). Further functional annotation was performed using eggNOG-mapper (version emapper-2.1.10)[80] based on eggNOG orthology data[81] and a DIAMOND search algorithm[82].

Bile acid and metabolomics analysis

For untargeted metabolomic analysis, plasma and ileal samples were suspended in 400 μl methanol per 100 μl plasma volume or per 100 mg of ileal contents. A 40-μl aliquot was subjected to a single-layer extraction, followed by untargeted LC–QTOF/MS analysis as previously described[83]. For targeted metabolomic analysis focusing on bile acids, 30 ml of plasma was mixed with 968.5 ml of 0.2 M NaOH and sonicated for 10 min in a vial containing 1.5 ml of the internal standards (d4-CA, d4-GCDCA, d4-TCDCA, d4-CDCA-3S and d4-LCA; each at 10 μM). Ileal content samples were resuspended in 20 or 2,000 times the volume of water. One hundred millilitres of the diluted luminal suspension was homogenized in 897 ml of 0.2 M NaOH by ultrasonication for1 h in a screw-cap glass vial containing 3 ml deuterium-labelled internal standards (d4-CA, d4-GCDCA, d4-TCDCA, d4-CDCA-3S and d4-LCA; 10 mM each). After 1 h of incubation at room temperature, the pH was adjusted to 8.0 using 12 M HCl and mixed with 110 μl of 0.5 M EDTA/0.5 M Tris-HCl. The pH was checked and adjusted as needed with 17 μl of 12 M HCl. The mixture was centrifuged at 15,000 rpm for 10–20 min, and the supernatant was loaded onto a solid-phase extraction cartridge (Agilent Bond Elut C18, 100 mg/3 ml), preconditioned with 1 ml of methanol and 3 ml of water, repeated three times. The cartridge was washed with 1 ml of water, and the bile acids were eluted with 600 μl of 90% ethanol. For quantification of bile acids, 2 μl of the eluted sample was injected into a liquid chromatography–electrospray ionization–tandem mass spectrometry (LC–ESI–MS/MS) system (Triple Quad 6500+ tandem mass spectrometer, equipped with an ESI probe and Exion LC AD ultra-high-pressure liquid chromatography

system; SCIEX). An InertSustain C18 separation column (150 mm × 2.1 mm ID, 2 µm particle size; GL Sciences) was used, maintained at 40 °C. The eluent consisted of a mixture of double-distilled water with 0.01% formic acid, 10 mM ammonium acetate and 20% acetonitrile (mixture A), and a mixture of 30% acetonitrile and 70% methanol (mixture B). Separation was achieved using a linear gradient elution at a flow rate of 0.2 ml per min, with the following gradient profile: 30–45% B (0–14 min), 45–65% B (14–25 min), 65–75% B (25–35 min), 75–100% B (35–35.1 min), 100% B (35.1–40 min), 100–30% B (40–40.1 min) and 30% B (40.1–45 min). The total run time was 45 min. LC–ESI–MS/MS was operated under the following conditions. For positive-ion multiple reaction monitoring (MRM) mode: ion spray voltage, 5,500 V; interface temperature, 400 °C; curtain gas, 25 psi; collision gas (nitrogen), 10 psi; ion source gas 1, 60 psi; and ion source gas 2, 40 psi. For negative-ion MRM mode: ion spray voltage, −4,500 V; interface temperature, 400 °C; curtain gas, 25 psi; collision gas (nitrogen) 10 psi; ion source gas 1, 60 psi; and ion source gas 2, 40 psi. Data acquisition was performed using Analyst v.1.71, and data analysis was done with SCIEX OS-MQ v.2.1.0.55343. Samples with values below the limit of detection are designated as not detected (ND), and a value corresponding to one-half of the detection limit was imputed for statistical analyses.

Measurement of orally administered $^{13}C_4$-palmitic acid in plasma

SPF C57BL/6 mice were fed a control diet or an LPD for 7 weeks. After fasting for 3 h, palmitic acid-1,2,3,4-$^{13}C_4$ (Sigma), suspended in corn oil (Sigma), was orally administered at a dose of 250 mg per kg body weight. Plasma samples were collected at 0, 0.5, 1, 2, 4, 6, 9 and 24 h after administration and stored at −80 °C until fatty acid extraction. Twenty microlitres of plasma was mixed with 200 µl of methanol containing 5 ng ml^{-1} d_4-linoleic acid as an internal standard, vortexed and incubated for 10 min at 4 °C. After centrifugation at 15,000 rpm for 5 min at 4 °C, the supernatant was transferred to a new 1.5-ml tube containing 800 µl of 0.1 % formic acid, and the mixture was applied to a polymeric reversed-phase sorbent column (Oasis HLB, 60 mg, 3 cc, Waters; WAT094226). The column was sequentially washed with 3 ml of 0.1% formic acid, 3 ml of 15% ethanol and 1 ml hexane, and the analytes were eluted with 600 µl methanol. The eluate was evaporated to dryness, and the residue was reconstituted in 40 µl methanol and transferred to an LC–MS vial. Quantification of plasma $^{13}C_4$-palmitic acid was done using an LC–ESI–MS/MS system composed of an ExionLC AD system (AB SCIEX) coupled to a Triple Quad 6500+ mass spectrometer (AB SCIEX) equipped with an ESI source. Chromatographic separation was done on a CORTECS UPLC C18 column (150 × 2.1 mm, 1.6 µm particle size; Waters) maintained at 40 °C. The injection volume was 2 ml per sample. Gradient elution was performed using a binary solvent system consisting of eluent A (ultrapure water containing 0.1% formic acid and 5 mM ammonium acetate) and eluent B (acetonitrile) under the following conditions: 0 min, 58% B; 5 min, 60% B; 10 min, 70% B; 20 min, 78% B; 25 min, 100% B; 30 min, 100% B; 30.1 min, 58% B; and 35 min, 58% B. The flow rate was set to 0.3 ml per min. Mass-spectrometry conditions were as follows: curtain gas, 25 psi; collision gas, 9 psi; ion spray voltage, −4,500 V; temperature, 300 °C; ion source gas 1, 50 psi; and ion source gas 2, 80 psi. Data acquisition was performed using Analyst (AB SCIEX), and data analysis was done using SCIEX OS-MQ (AB SCIEX).

In vitro bile acid transformation

Individual bacterial strains, derived from mouse and human microbiota, were streaked on BHK agar plates. A single colony of each strain was inoculated into mGAM broth, with supplements added for certain strains to support growth (as described above). Overnight cultures were then diluted 100 times and incubated with 50 µM taurocholic acid (tauro-CA) at 37 °C for 48 h in mGAM or mGAM-based medium containing varying concentrations of mGAM protein, as indicated. All culturing and assays were done in an anaerobic chamber (Coy Laboratory Products) with an atmosphere of 80% N_2, 10% H_2 and 10% CO_2. After 48 h, 200 µl of each bacterial suspension was collected for bile acid extraction. To each 40-µl aliquot of the suspension, 33 µl of 6.0 M NaOH, 10 µM internal standard and 924 µl of Milli-Q water were added, followed by 10 min of sonication. Then, 110 µl of 0.5 M EDTA/0.5 M Tris buffer (pH 8) and 17 µl of 12 M HCl were added, adjusting the pH to neutral as needed. Samples were purified on columns pre-activated with 1 ml methanol and washed twice with 3 ml Milli-Q water. After loading, samples were washed six times with 3 ml Milli-Q water, and residual water was removed by adjusting the flow rate. Finally, 600 µl of 90% ethanol was applied to elute bile acids, and samples were collected in vials for LC–MS/MS quantification.

In vitro ammonia production

Individual bacterial strains of both mouse and human origin were evaluated for their capacity to produce ammonia in vitro. Strains were first revived from glycerol stocks and streaked onto BHK agar plates under anaerobic conditions. After 3 days of incubation at 37 °C, a single colony from each strain was inoculated into mGAM broth supplemented with a supplement mix (0.1% fumarate, 0.1% formate, 0.5 µg ml^{-1} vitamin K, 0.1 mg ml^{-1} sodium sulfate and 1% taurine). After 2 to 3 days of anaerobic incubation at 37 °C, the cultures were diluted in either complete mGAM (containing all supplements) or 10% mGAM (diluted with Milli-Q water and supplemented with the same mixture). Samples were incubated for 1 h at 37 °C under anaerobic conditions in individual sealed tubes to prevent cross-contamination by gaseous ammonia. Bacterial growth kinetics were monitored throughout the incubation period. Culture supernatants were diluted 25-fold with Milli-Q water, and ammonia levels were measured using the Urease Activity Assay Kit (Sigma-Aldrich, MAK120) according to the manufacturer's instructions.

Bacterial metatranscriptomic analysis

Extraction of total RNA from the caecal contents of T19-derived 33-mix-colonized mice fed either a control diet or an LPD was done using the NucleoSpin RNA kit (Macherey-Nagel) according to the manufacturer's instructions. Libraries for RNA-seq were prepared using TruSeq Stranded mRNA Library Prep (Illumina) and sequenced using HiSeq X (Illumina) or NovaSeqXPlus at Macrogen Japan using the 150-bp paired-end mode. The sequenced paired-end reads were quality-controlled using Trimmomatic[84] v.0.39 with '2:30:10 LEADING:20 TRAILING:20 SLIDINGWINDOW:4:20 MINLEN:30' parameters. The quality-controlled reads were mapped to concatenated reference genome sequences of the T19-derived 33 stains using STAR v.2.7.10b with 'outFilterMultimapNmax: 20 alignIntronMax: 1' parameters. Aligned sorted bam files were generated using SAMtools v.1.19.2 and visualized using Integrative Genomics Viewer v.2.17.4. The read counts for each gene were obtained using featureCounts[85] Rsubread 2.12.3 with 'countMultiMappingReads=TRUE,fraction=TRUE' parameters and normalized by bacterial abundance using the absolute DNA level of each strain compared to the total bacteria quantified by qPCR using 16S rRNA primers as previously described[86]. The differential expression analysis was performed using DESeq2 v.1.38.3 (ref. 87) with cut-off adjusted $P < 0.05$. Upregulated genes of St.3, St.4, St.14 and St.31 were used for enrichment analysis using the enricher function of clusterProfiler v.1.38.3 (ref. 88) against all KEGG pathways included in (1) metabolism, (2) genetic information processing, (3) environmental information processing and (4) cellular processes.

Generation of *Bilophila* sp. 4_1_30 (St.14) mutants

The *nrfA* (gene id: OMIHGE_02465) gene-deletion mutant of *Bilophila* sp. 4_1_30 (St.14) was generated in a manner similar to that used for the *Nitratidesulfovibrio vulgaris* 'marker-exchange' mutant, as previously described[89,90] and as shown in Supplementary Fig. 7. First, a Δ*upp* mutant *Bilophila* strain lacking uracil phosphoribosyltransferase (*upp*, gene ID: OMIHGE_01720) was generated. Subsequently, a marker-exchange mutant (Δ*upp*, Δ*nrfA*::(*cat upp*)) was generated from the parent Δ*upp*

strain by electroporation-mediated plasmid introduction and selection with 5-fluorouracil (5-FU) and chloramphenicol. To generate the Δ*upp* mutant, approximately 0.9-kb sequences flanking the coding region were amplified by PCR (primers are listed in Supplementary Table 7) and cloned into the PstI and SalI sites of the pBluescriptIISK+ using HiFi DNA Assembly (NEB) as per the manufacturer's protocol, to ultimately generate a *upp* deletion cassette. The electroporation was carried out in a total volume of 80 ml with an ELEPO21 Electroporator (Nepa Gene) in 1-mm gapped electroporation cuvettes at 1,500–2,000 V with the default settings. The cells were allowed to recover in 1 ml mGAM broth supplemented with 1 % taurine overnight at 37 °C, after which 50 µl of the bacterial suspension was plated on mGAM agar containing 1% taurine and 40 mg ml^{-1} 5-FU and incubated for 4 days under anaerobic conditions. The 5-FU-resistant colonies were selected and the deletion of the *upp* gene was verified both by PCR and by culturing on mGAM agar containing 40 mg ml^{-1} 5-FU. To generate a *nrfA* mutant *Bilophila* strain, a marker-exchange plasmid was constructed containing the pUC origin of replication, the ampicillin resistance gene (for selection in *Escherichia coli* DH5α), a 1.5-kb region upstream of the *nrfA* gene, the chloramphenicol resistance gene (*cat*, encoding chloramphenicol acetyltransferase) and its promoter, a *upp* gene cassette driven by the kanamycin resistance gene promoter (*PaphIIa*), and a 1.5-kb region downstream of the *nrfA* gene. The marker-exchange plasmid was introduced into the Δ*upp* strain by electroporation under the same conditions described above. Bacterial cells were allowed to recover overnight in mGAM broth supplemented with 1% taurine. Subsequently, 50 µl of the bacterial suspension was plated onto mGAM agar containing 1% taurine and 80 µg ml^{-1} chloramphenicol, and incubated for 5 days under anaerobic conditions. The resulting colonies were picked and suspended in mGAM in 1.5-ml tubes, and each suspension was spotted onto two mGAM agar plates: one containing 80 µg ml^{-1} chloramphenicol alone and the other containing 80 µg ml^{-1} chloramphenicol and 40 µg ml^{-1} 5-FU. Colonies that were resistant to chloramphenicol and sensitive to 5-FU were selected, and deletion of the *nrfA* gene was confirmed by PCR and Sanger sequencing. In Fig. 6f–i and Extended Data Fig. 11, the Δ*upp*, Δ*nrfA*::(*cat upp*) strain is referred to as Δ*nrfA*, and the parental Δ*upp* strain is referred to as wild type.

Protein homology search for 7αHSDH

We used mmseq2 (version ffb05619cadadd8655b8719818ed566caaa6d0a6) to align three experimentally validated 7αHSDH protein sequences to all proteins from *R. timonensis* (St.31), *A. equolifaciens* (St.3), *Bilophila* sp. 4_1_30 (St.14), and *Eubacteriaceae* sp. (St.4). The protein from each isolate that aligned best to each reference protein was plotted in a heat map using the pheatmap package.

Protein homology search to NrfA

All proteins encoded in the genomes of the 33 human isolates were annotated using eggNOG-mapper (v.2.1.12). Proteins annotated as NrfA were further analysed using SignalP 6.0 to identify and categorize putative signal sequences. If multiple proteins within a genome were annotated as NrfA, only the one most homologous to the eggNOG-mapper-assigned reference NrfA was included in the analysis. SP stands for the 'standard' secretory signal peptide putatively transported by the Sec translocon and cleaved by signal peptidase I, whereas LSP indicates the lipoprotein signal peptide known to be transported by the Sec translocon and cleaved by signal peptidase II. Percentage identity indicates sequence homology to the closest NrfA reference protein assigned by eggNOG-mapper, as calculated by DIAMOND BLASTP. The *E*-value (expected value), also computed by DIAMOND BLASTP, represents the number of chance alignments with an equal or greater bit score. Length refers to the predicted length of the protein from each isolate that best aligns to NrfA, as determined by eggNOG-mapper.

In Extended Data Fig. 10e, Unified Human Gastrointestinal Genome (UHGG) v.2.0.2 reference genome eggNOG annotations were downloaded from https://ftp.ebi.ac.uk/pub/databases/metagenomics/mgnify_genomes/human-gut/v2.0.2/species_catalogue/. GTDB-Tk v.2.4.0 was used to identify and align 120 bacterial genes across all UHGG reference genomes. FastTree with the parameter '-lg' was used to create the phylogenetic tree. All proteins in UHGG annotated as NrfA by eggNOG annotation were also run through SignalP to annotate the signal sequence.

Similarly, all predicted proteins from the genome sequences of the 20 mouse-derived isolates were annotated using eggNOG-mapper (v.2.1.12). Proteins annotated as NrfA homologues were aligned to the NrfA protein of human *Bilophila* sp. 4_1_30 (St.14) using BLASTP, and their signal sequences were classified with SignalP.

Human hepatocyte organoids

To evaluate the induction of FGF21 in vitro, we used human hepatocyte organoids, as previously described[58]. In brief, organoids were established from commercially available cryopreserved primary human hepatocytes cultured in Matrigel at 37 °C and 5% CO_2. Organoids were cultured for 14 days in expansion medium consisting of Advanced DMEM/F12 supplemented with penicillin–streptomycin, 10 mM HEPES, 2 mM GlutaMAX, 1× B27 (Thermo Fisher Scientific), 10 nM gastrin I (Sigma), 1 mM *N*-acetylcysteine (FUJIFILM Wako Pure Chemical), 20% afamin/WNT3A serum-free conditioned medium[91], 5% RSPO1-conditioned medium[92], 50 ng ml^{-1} mouse recombinant EGF (Thermo Fisher Scientific), 25 ng ml^{-1} human recombinant HGF (PeproTech), 100 ng ml^{-1} human recombinant FGF-10 (PeproTech), 25 ng ml^{-1} mouse recombinant noggin (PeproTech), 5 µM A83-01 (Tocris), 10 µM forskolin (Cayman Chemical) and 20 ng ml^{-1} oncostatin M (PeproTech). Subsequently, the cultures were transitioned to differentiation medium, which excluded afamin/WNT3A, RSPO1, noggin and oncostatin M but was supplemented with 10 ng ml^{-1} growth hormone (PeproTech), 10 ng ml^{-1} prolactin (PeproTech), 100 ng ml^{-1} cortisol (Selleck) and 10 µM DAPT (Selleck). Ammonium chloride (FUJIFILM Wako Pure Chemical) was added to the differentiation medium at the indicated concentrations. After 14 days of differentiation, organoids were collected and subjected to qPCR with reverse transcription (RT–qPCR). cDNA was synthesized from 0.1 µg total RNA and qPCR was performed as described above. The following primer pairs were used: *GUSB*: 5′-AGCCACTACCCCTATGCAGA-3′ and 5′-CCCTACGCACCACTTCTTCC-3′; *FGF21*: 5′-ACTCCAGTCCTCTCCTGCAA-3′ and 5′-TGAATAACTCCCGGCTTCAAGG-3′; and *CSAD*: 5′-TACCCGGATTGCAAGCAGAG-3′ and 5′-CCATACCAATCTGCCTCTCCAG-3′. *GUSB* (glucuronidase beta) served as the housekeeping gene for normalization, enabling calculation of the relative expression of *FGF21* and *CSAD*.

Statistical analysis

Statistical analyses were performed using Strand NGS v.2.7 and DAVID for bulk RNA-seq data, R (v.4) for metatranscriptomic analyses and Microsoft Excel and GraphPad Prism software v.9 for all other analyses. Comparisons between two groups were done using either the two-tailed unpaired Student's *t*-test (parametric) or the Mann–Whitney test (non-parametric), as appropriate. One-way analysis of variance (ANOVA) followed by Benjamini–Hochberg correction for multiple comparisons was used for all comparisons between three or more groups, except for bile acid concentration comparisons, which were analysed using the two-tailed Mann–Whitney test for each comparison between two groups. For time-course analysis of body weight, relative gene expression and blood glucose, two-way ANOVA with Benjamini–Hochberg correction was used.

Reporting summary

Further information on research design is available in the Nature Portfolio Reporting Summary linked to this article.

Data availability

Genome sequences of the 20 mouse-derived and 33 human (T19)-derived strains and metatranscriptomes have been deposited in the DNA Data Bank of Japan under BioProject PRJDB19530. Data of bulk RNA-seq and snRNA-seq are deposited in the DNA Data Bank of Japan under BioProject PRJDB19694. We used the mm10 (GRCm38) mouse genome. Source data are provided with this paper.

Code availability

No special code was developed for this analysis.

61. Hotta, Y. et al. Fibroblast growth factor 21 regulates lipolysis in white adipose tissue but is not required for ketogenesis and triglyceride clearance in liver. *Endocrinology* **150**, 4625–4633 (2009).
62. Bachman, E. S. et al. βAR signaling required for diet-induced thermogenesis and obesity resistance. *Science* **297**, 843–845 (2002).
63. Hu-Li, J. et al. Regulation of expression of *IL-4* alleles: analysis using a chimeric *GFP*/*IL-4* gene. *Immunity* **14**, 1–11 (2001).
64. Brockschnieder, D., Pechmann, Y., Sonnenberg-Riethmacher, E. & Riethmacher, D. An improved mouse line for Cre-induced cell ablation due to diphtheria toxin A, expressed from the Rosa26 locus. *Genesis* **44**, 322–327 (2006).
65. Nagai, M. et al. High body temperature increases gut microbiota-dependent host resistance to influenza A virus and SARS-CoV-2 infection. *Nat. Commun.* **14**, 3863 (2023).
66. Reho, J. J. et al. Methods for the comprehensive in vivo analysis of energy flux, fluid homeostasis, blood pressure, and ventilatory function in rodents. *Front. Physiol.* **13**, 855054 (2022).
67. Alquier, T. & Poitout, V. Considerations and guidelines for mouse metabolic phenotyping in diabetes research. *Diabetologia* **61**, 526–538 (2018).
68. Vinue, A. & Gonzalez-Navarro, H. Glucose and insulin tolerance tests in the mouse. *Methods Mol. Biol.* **1339**, 247–254 (2015).
69. Zhao, P. et al. TBK1 at the crossroads of inflammation and energy homeostasis in adipose tissue. *Cell* **172**, 731–743 (2018).
70. Al Rijjal, D. & Wheeler, M. B. A protocol for studying glucose homeostasis and islet function in mice. *STAR Protoc.* **3**, 101171 (2022).
71. Huesing, C., Muenzberg, H., Burk, D. & Torres, H. iDISCO protocol for whole-mount immunostaining and volume imaging. *protocols.io* https://doi.org/10.17504/protocols.io.wzuff6w (2021).
72. Fleming, S. J. et al. Unsupervised removal of systematic background noise from droplet-based single-cell experiments using CellBender. *Nat. Methods* **20**, 1323–1335 (2023).
73. Butler, A., Hoffman, P., Smibert, P., Papalexi, E. & Satija, R. Integrating single-cell transcriptomic data across different conditions, technologies, and species. *Nat. Biotechnol.* **36**, 411–420 (2018).
74. Street, K. et al. Slingshot: cell lineage and pseudotime inference for single-cell transcriptomics. *BMC Genomics* **19**, 477 (2018).
75. Amezquita, R. A. et al. Orchestrating single-cell analysis with Bioconductor. *Nat. Methods* **17**, 137–145 (2020).
76. Weiler, P., Lange, M., Klein, M., Pe'er, D. & Theis, F. CellRank 2: unified fate mapping in multiview single-cell data. *Nat. Methods* **21**, 1196–1205 (2024).
77. Yoneshiro, T. et al. Recruited brown adipose tissue as an antiobesity agent in humans. *J. Clin. Invest.* **123**, 3404–3408 (2013).
78. Yoneshiro, T. et al. BCAA catabolism in brown fat controls energy homeostasis through SLC25A44. *Nature* **572**, 614–619 (2019).
79. Schwengers, O. et al. Bakta: rapid and standardized annotation of bacterial genomes via alignment-free sequence identification. *Microb. Genom.* **7**, 000685 (2021).
80. Cantalapiedra, C. P., Hernandez-Plaza, A., Letunic, I., Bork, P. & Huerta-Cepas, J. eggNOG-mapper v2: functional annotation, orthology assignments, and domain prediction at the metagenomic scale. *Mol. Biol. Evol.* **38**, 5825–5829 (2021).
81. Huerta-Cepas, J. et al. eggNOG 5.0: a hierarchical, functionally and phylogenetically annotated orthology resource based on 5090 organisms and 2502 viruses. *Nucleic Acids Res.* **47**, D309–D314 (2019).
82. Buchfink, B., Reuter, K. & Drost, H. G. Sensitive protein alignments at tree-of-life scale using DIAMOND. *Nat. Methods* **18**, 366–368 (2021).
83. Okahashi, N., Ueda, M., Yasuda, S., Tsugawa, H. & Arita, M. Global profiling of gut microbiota-associated lipid metabolites in antibiotic-treated mice by LC-MS/MS-based analyses. *STAR Protoc* **2**, 100492 (2021).
84. Bolger, A. M., Lohse, M. & Usadel, B. Trimmomatic: a flexible trimmer for Illumina sequence data. *Bioinformatics* **30**, 2114–2120 (2014).
85. Liao, Y., Smyth, G. K. & Shi, W. featureCounts: an efficient general purpose program for assigning sequence reads to genomic features. *Bioinformatics* **30**, 923–930 (2014).
86. Zhang, Y., Thompson, K. N., Huttenhower, C. & Franzosa, E. A. Statistical approaches for differential expression analysis in metatranscriptomics. *Bioinformatics* **37**, i34–i41 (2021).
87. Love, M. I., Huber, W. & Anders, S. Moderated estimation of fold change and dispersion for RNA-seq data with DESeq2. *Genome Biol.* **15**, 550 (2014).
88. Wu, T. et al. clusterProfiler 4.0: a universal enrichment tool for interpreting omics data. *Innovation* **2**, 100141 (2021).
89. Keller, K. L., Bender, K. S. & Wall, J. D. Development of a markerless genetic exchange system for *Desulfovibrio vulgaris* Hildenborough and its use in generating a strain with increased transformation efficiency. *Appl. Environ. Microbiol.* **75**, 7682–7691 (2009).
90. Hillesland, K. L. et al. Erosion of functional independence early in the evolution of a microbial mutualism. *Proc. Natl Acad. Sci. USA* **111**, 14822–14827 (2014).
91. Mihara, E. et al. Active and water-soluble form of lipidated Wnt protein is maintained by a serum glycoprotein afamin/α-albumin. *eLife* **5**, e11621 (2016).
92. Ootani, A. et al. Sustained in vitro intestinal epithelial culture within a Wnt-dependent stem cell niche. *Nat. Med.* **15**, 701–706 (2009).
93. Abe, I. et al. Lipolysis-derived linoleic acid drives beige fat progenitor cell proliferation. *Dev. Cell* **57**, 2623–2637.e2628 (2022).
94. Zückert, W. R. Secretion of bacterial lipoproteins: through the cytoplasmic membrane, the periplasm and beyond. *Biochim. Biophys. Acta* **1843**, 1509–1516 (2014).
95. Goh, C. E. et al. Nitrite generating and depleting capacity of the oral microbiome and cardiometabolic risk: results from ORIGINS. *J. Am. Heart Assoc.* **11**, e023038 (2022).

Acknowledgements K.H. is funded through the Japan Agency for Medical Research and Development (AMED) Moonshot Research and Development programme (JP22zf0127007), the AMED NEDDTrim programme (JP21ae0121041), the AMED LEAP programme (JP20gm0010003), a Grant-in-Aid for Specially Promoted Research from JSPS (20H05627), a Stand Up to Cancer grant (SU2C Convergence 3.1416 Research Team) and the Wellcome Leap's Dynamic Resilience programme (jointly funded by Temasek Trust). T.T. is supported by the research fund of the Mitsukoshi Health and Welfare Foundation, Chugai Foundation for Innovative Drug Discovery Science, Keio University Medical Science Fund and a Grant-in-Aid for Scientific Research (B) from JSPS (25K02703). R.J.X. is supported by grants from the Klarman Cell Observatory and the National Institutes of Health (NIH) (DK043351, AI172147, DK 127171 and HL157717). We thank M. Kumamoto, R. Takeda, Y. Tokifuji and S. Okamoto for animal maintenance and experiments, J.-C. Chang for supporting snRNA-seq analysis and J. Kuramoto and M. Shimoda for H&E staining.

Author contributions K.H., T.T., M.N., S.Z., O.A., A.N.S., S.K., D.R.P. and R.J.X. designed experiments, analysed data and co-wrote the paper with S.W.B., O.A., T.J., and M.S. T.T., M.N. and A.J.A.R. performed bacterial and animal experiments. S.S., M.U., N.O., M.A. and K.A. performed metabolomic analyses. S.Z., O.A., T.J., N.P., D.R.M., D.R.P., W.S. and R.J.X. performed bioinformatic analyses. T.T., O.A., T.J., N.H. and A.M. performed snRNA-seq analysis. R.I. and T.S. performed human hepatocyte organoid experiments. M.N., K.T., H.Y., S.W., K.M., K.A., M.M., M.S., M.K., Y.N. and Y.M. provided essential materials.

Competing interests K.H. is a scientific advisory board member of Vedanta Biosciences, 4BIO Capital and Taxa. M.U. is an employee of JSR Corporation. R.J.X. is a co-founder of Jnana Therapeutics and Celsius Therapeutics, scientific advisory board member at Nestlé and board director at MoonLake Immunotherapeutics. D.R.P. is an employee of Novonesis. The remaining authors declare no competing interests.

Additional information

Supplementary information The online version contains supplementary material available at https://doi.org/10.1038/s41586-026-10205-3.

Correspondence and requests for materials should be addressed to Ramnik J. Xavier or Kenya Honda.

Peer review information *Nature* thanks Lawrence Kazak and the other, anonymous, reviewer(s) for their contribution to the peer review of this work. Peer reviewer reports are available.

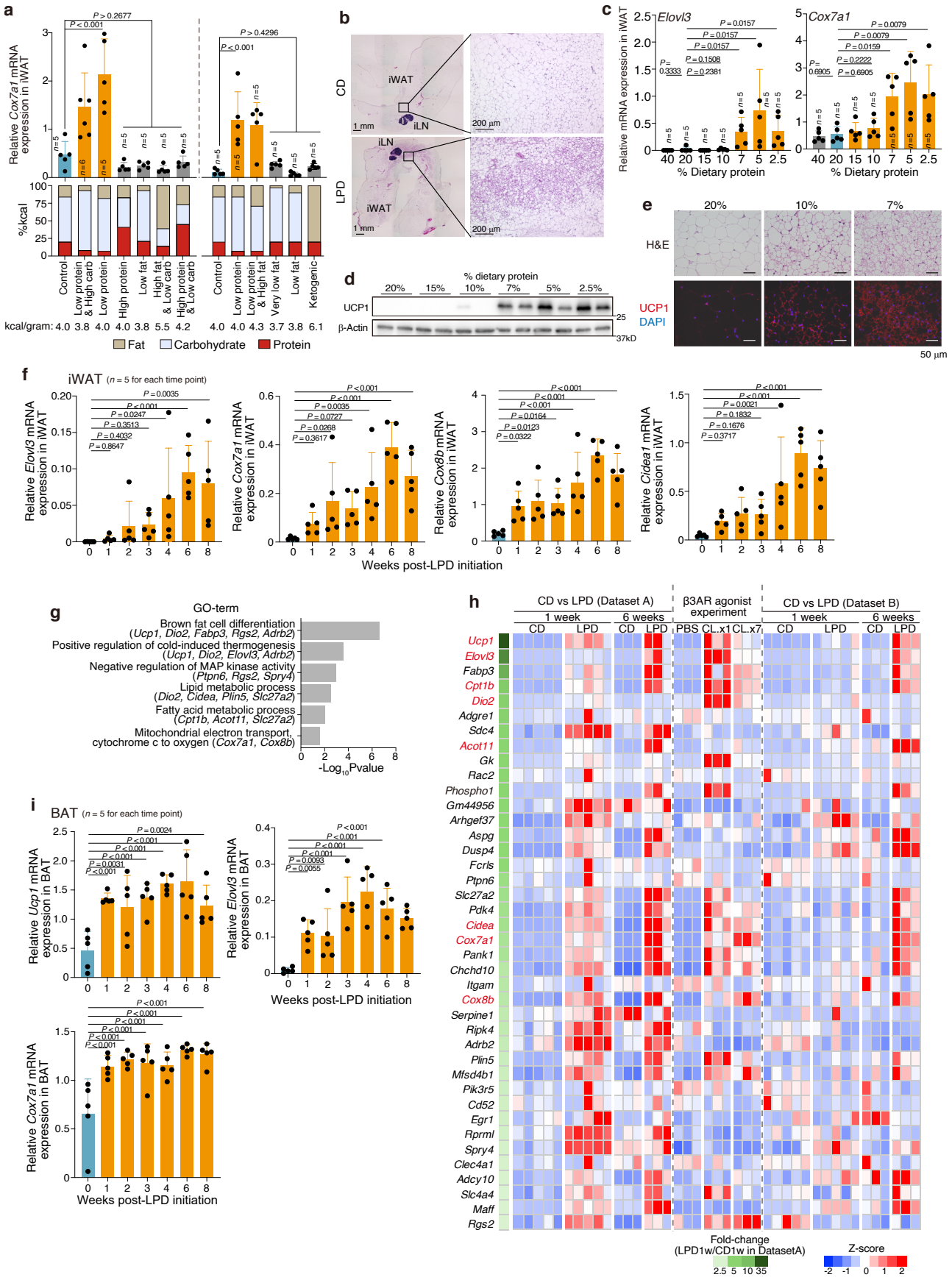

Extended Data Fig. 1 | See next page for caption.

Extended Data Fig. 1 | LPDs induce beige cells in iWAT. a, SPF B6 male mice were fed diets with varying proportions of protein, carbohydrates, and fat for 6 weeks. *Cox7a1* mRNA expression in iWAT, normalized to *Ppib*, is shown along with stacked bar graphs representing each diet's macromolecular composition and total energy content (kcal/g). The left and right panels show results from two independent experiments. **b**, H&E staining of iWAT from mice fed either a control diet (CD, 20% protein content) or a LPD (7% protein content) for 6 weeks. **c**–**e**, SPF B6 mice were fed isocaloric diets containing various concentrations of protein for 6 weeks. iWAT browning was assessed by evaluating *Elovl3*, and *Cox7a1* expression (**c**), UCP1 protein expression via western blotting (**d**), as well as by examining cellular morphology through H&E staining and immunostaining with an anti-UCP1 antibody and DAPI (**e**). **f**, SPF B6 mice were fed a 7% LPD for the indicated durations, and mRNA expression of the indicated genes in iWAT was quantified by qPCR. **g**,**h**, RNA was extracted from iWAT of mice fed a CD or an LPD for the indicated duration, and gene expression were determined by RNA-seq. GO terms of the genes are shown (**g**). Heat map shows relative expression of genes upregulated in mice fed an LPD versus a CD for one week (≥2.5-fold with RPKM ≥ 200). Fold change (LPD1w/CD1w in DatasetA) is indicated by the green heat map. Data include two independent diet experiments (datasets A and B), as well a positive control experiment in which β3-adrenergic receptor (β3AR) agonist CL316,243 was administered intraperitoneally (20 μg total per mouse, given as a single injection ["CL.x1"] or daily for 7 consecutive days ["CL.x7"]) (**h**). **i**, SPF B6 mice were fed an LPD for the indicated durations, and mRNA expression of the indicated genes in interscapular brown adipose tissue (BAT) was quantified by qPCR. Each circle represents an individual mouse and the height of each bar represents the mean ± s.d. or -Log_{10} Fisher's Exact P-value (**g**). Statistical test: one-way ANOVA with Benjamini–Hochberg correction for multiple comparisons (**a**,**f**,**i**), two-tailed Mann–Whitney test for each comparison (**c**) or a two-sided Fisher's Exact test in DAVID (**g**).

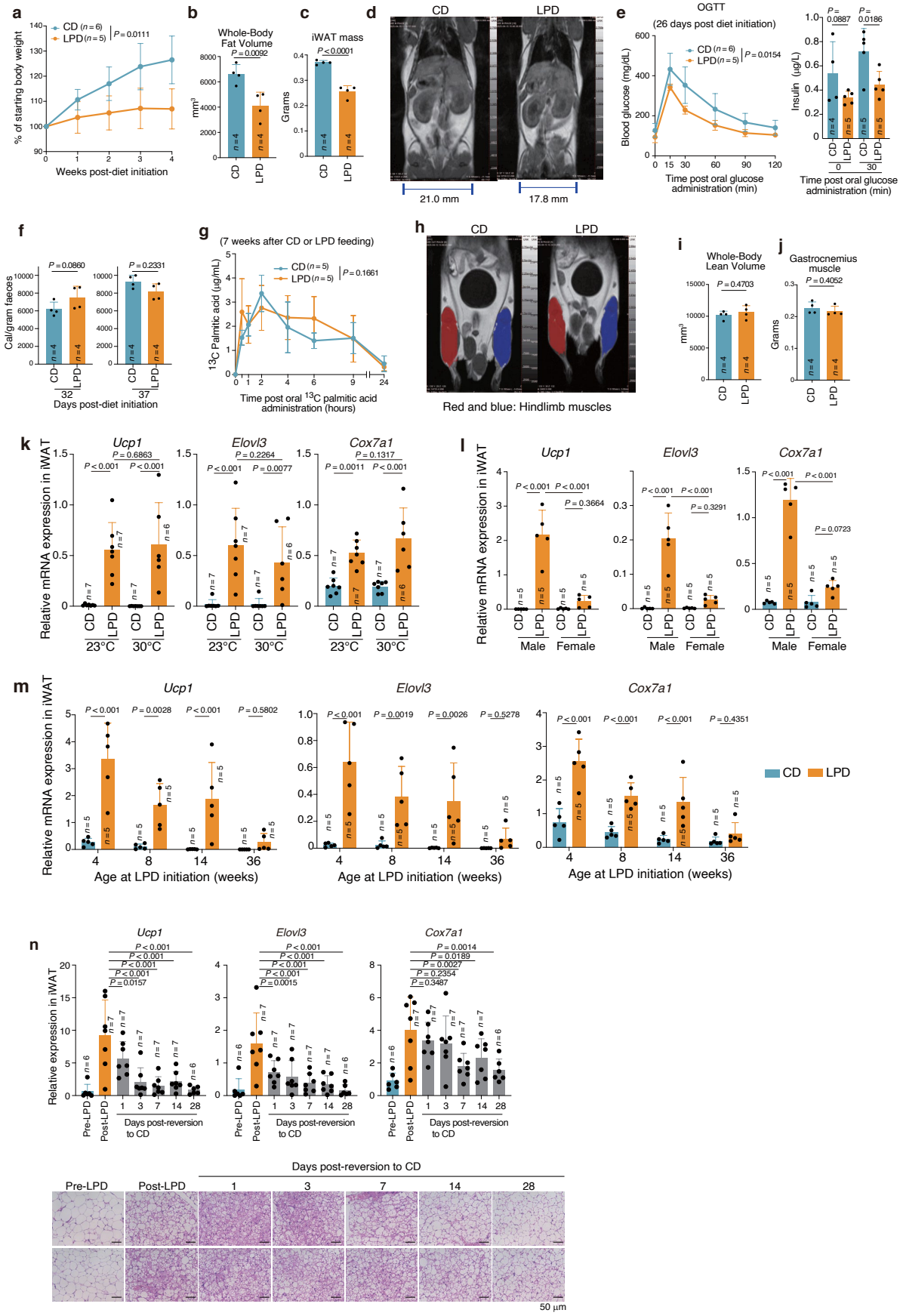

Extended Data Fig. 2 | See next page for caption.

Extended Data Fig. 2 | Context-dependent iWAT browning induced by LPDs. **a**–**j**, SPF B6 mice were fed a 7% LPD or a 20% protein CD for 6 weeks or for the indicated durations. Shown are body-weight changes from diet initiation to 4 weeks (**a**); MRI-evaluated whole-body fat mass (**b**); iWAT mass (**c**); representative T1-weighted MRI images (fat appears white) (**d**), plasma glucose and insulin levels during OGTT (**e**), faecal energy contents evaluated on day 32 and 37 (**f**), plasma levels of orally administered ^{13}C-labelled palmitic acid (**g**); representative T1-weighted MRI images of hindlimb muscles (**h**); MRI-evaluated whole-body lean volume (**i**); and gastrocnemius muscle mass (**j**). **k**–**m**, Relative mRNA expression of *Ucp1*, *Elovl3*, and *Cox7a1* in iWAT in SPF B6 mice fed either a CD or an LPD. Shown are data from mice housed at the indicated temperatures (**k**); 7-week-old male and female mice (**l**); or male mice aged 4, 8, 14, or 36 weeks at diet initiation (**m**). **n**, Eight-week-old male SPF B6 mice were fed an LPD for 6 weeks and then switched back to a CD for the indicated duration. *Ucp1*, *Elovl3*, and *Cox7a1* mRNA expression and histological analysis of iWAT were performed at the indicated time points. Each circle in bar graphs represents an individual mouse, and bars show mean ± s.d. In line graphs, the mean ± s.d is shown. Statistical analyses: two-way ANOVA (**a**,**e**, left; **g**,**m**), two-tailed unpaired t-test (**b**,**c**,**f**,**i**,**j**), one-way ANOVA with Benjamini–Hochberg correction for multiple comparisons (**e**, right; **k**,**l**,**n**).

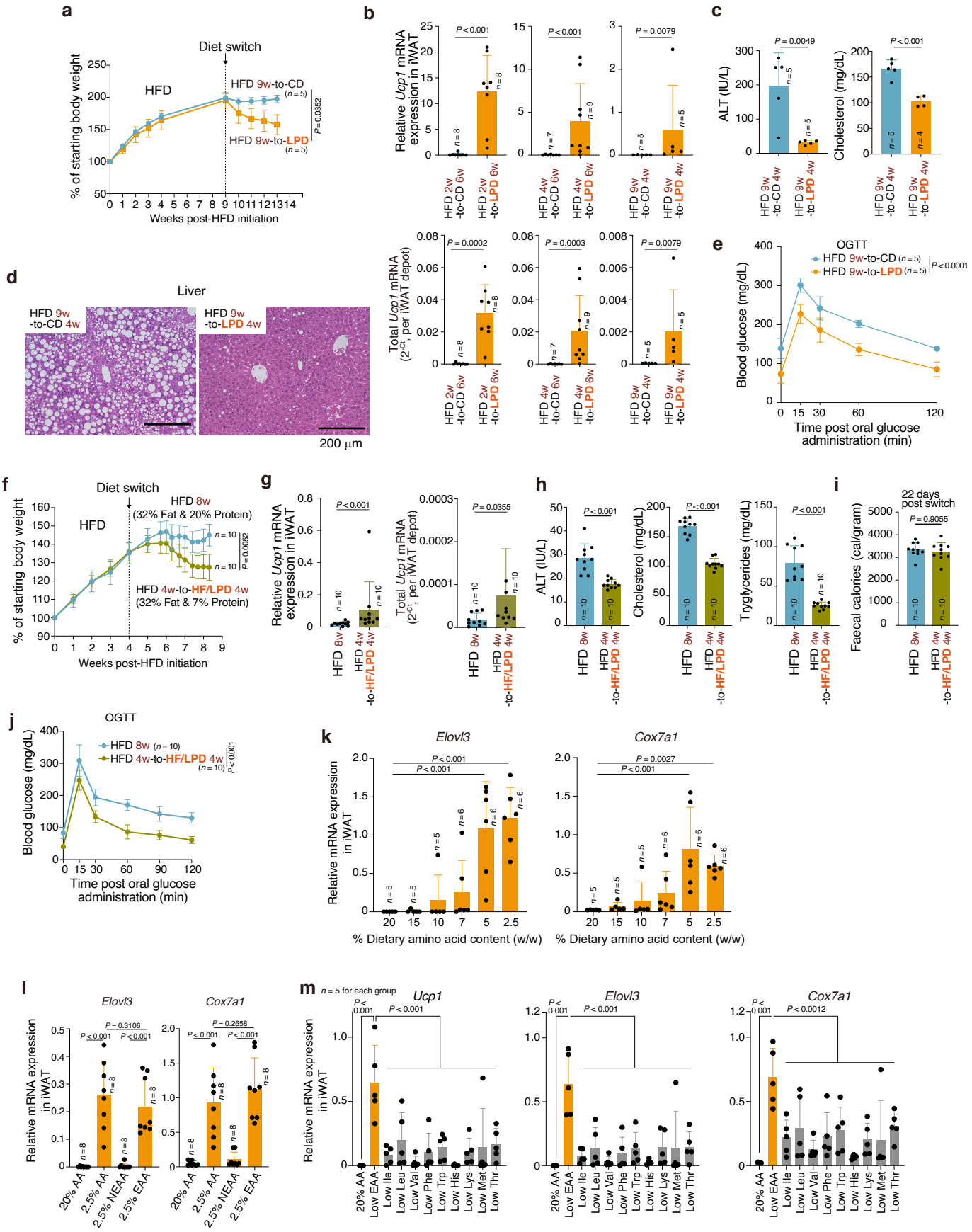

Extended Data Fig. 3 | See next page for caption.

Extended Data Fig. 3 | Metabolic effects of LPDs during or after HFD feeding. **a**–**j**, SPF B6 mice were initially fed an HFD [either 60% kcal fat (**a**–**e**) or 32% kcal fat (**f**–**j**), both containing 20% protein] for 2, 4 or 9 weeks, and were subsequently switched to a CD (20% fat, 20% protein), an LPD (20% fat, 7% protein), or a HF/LPD (32% fat, 7% protein) for the indicated durations. Longitudinal body-weight changes are shown as the percentage of body weight relative to that at the initiation of HFD feeding (**a**,**f**). End-point analyses include *Ucp1* expression in iWAT, normalized to *Ppib* or total mRNA per iWAT depot (**b**,**g**); plasma levels of ALT, cholesterol, and triglycerides (**c**,**h**); liver histology assessed by H&E staining (**d**); and faecal energy content measured by bomb calorimetry (**i**). OGTTs were performed 7 days prior to euthanasia (**e**,**j**). LPD feeding was associated with improvements in HFD-induced obesity, hepatic steatosis, and glucose intolerance without altering faecal caloric content; however, whether the induction of WAT browning directly contributes to these metabolic improvements remains unclear. **k**–**m**, Eight-week-old SPF B6 male mice were fed diets containing purified amino acids in place of natural protein for 6 weeks. Total dietary amino acid content ranged from 20% (equivalent to a standard diet) to 2.5% (**k**); diets contained 20% or 2.5% total amino acids, or 2.5% essential or NEAAs (**l**); or total amino acids were maintained at 20% while the indicated EAAs was reduced to 2.5% kcal (**m**). mRNA expression of the indicated genes in iWAT was quantified by qPCR and normalized to *Ppib*. Each circle in bar graphs represents an individual mouse, and bars show mean ± s.d. In line graphs, the mean ± s.d is shown. Statistical tests: two-way ANOVA (**a**,**e**,**f**,**j**), two-tailed Mann–Whitney test (**b**,**g**), two-tailed unpaired t-test (**c**,**h**,**i**) or one-way ANOVA with Benjamini–Hochberg correction for multiple comparisons (**k**–**m**).

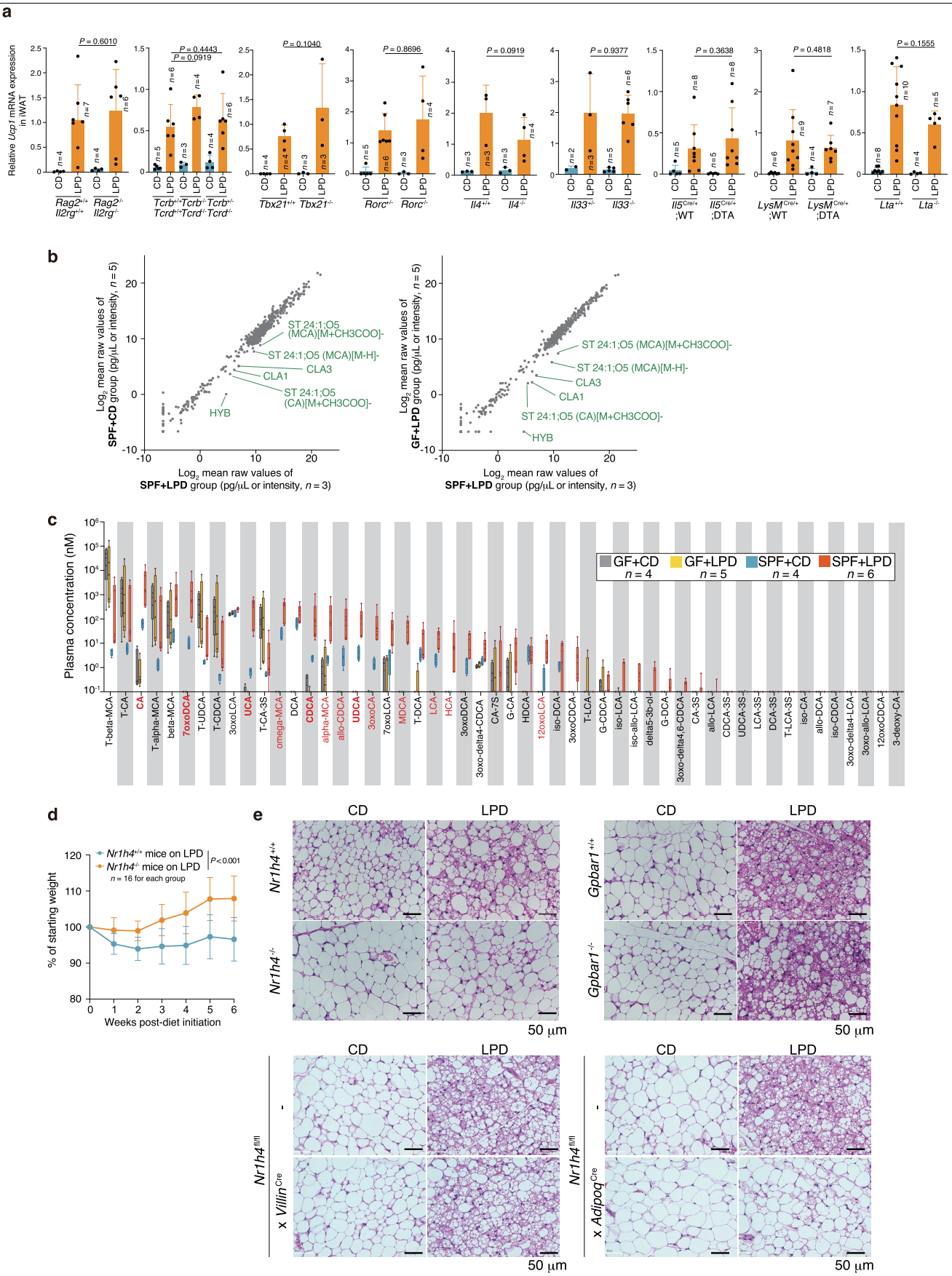

Extended Data Fig. 4 | See next page for caption.

Extended Data Fig. 4 | Role of bile acid–FXR signalling in LPD-mediated browning. a, Various immune cell subsets, including type 2 innate lymphoid cells (ILC2s), γδ T cells, macrophages, and eosinophils, have been implicated in WAT browning or activation of BAT. To assess their contribution to LPD-mediated browning, we examined a panel of SPF mutant mice deficient in various components of the immune system. Relative *Ucp1* mRNA expression in iWAT was used as a readout of browning. *Rag2*$^{-/-}$*Il2rγ*$^{-/-}$ mice, which lack both innate and adaptive lymphocytes, exhibited unimpaired iWAT browning when fed an LPD. Similarly, LPD-mediated browning was preserved in *Tcrβ*$^{-/-}$*Tcrδ*$^{-/-}$ mice (deficient in T cells), *Tbx21*$^{-/-}$ mice (deficient in type 1 immunity), *Rorc*$^{-/-}$ mice (deficient in type 17 immunity), *Il4*$^{-/-}$, *Il33*$^{-/-}$, or *Il5*-Cre;*Rosa*-DTA mice (deficient in type 2 immunity), *LysM*-Cre;*Rosa*-DTA mice (deficient in myeloid cells), and *Lta*$^{-/-}$ mice (deficient in lymphoid tissues). **b**,**c**, Eight-week-old GF and SPF B6 male mice were fed a CD or an LPD for 6 weeks. Non-targeted LC–MS/MS analysis (**b**) and targeted LC–MS/MS bile acid profiling (**c**) were performed on plasma samples. A LPD increased plasma levels of linoleic acid derivatives such as conjugated linoleic acids (CLA1 and CLA3) and 10-hydroxy-octadecanoic acid (HYB) (**b**), consistent with previous reports that linoleic acid metabolism promotes the proliferation of beige adipocyte progenitor cells[93]. In addition, several bile acids (highlighted in red) exhibited significantly higher plasma levels in SPF mice fed an LPD (SPF + LPD group) compared with the other three groups (**c**). **d**, Eight-week-old male SPF *Nr1h4*$^{+/+}$ mice and *Nr1h4*$^{-/-}$ mice were fed an LPD for 6 weeks. Longitudinal percent changes in body weight (mean ± s.d) are shown. **e**, Eight- to ten-week-old male SPF mice of the indicated genotypes were fed either a CD or an LPD for 6 weeks. Representative H&E-stained images of iWAT from two independent experiments are shown. Each circle in bar graphs and box plots represents an individual mouse, and bars show mean ± s.d. Box-plot centre lines indicate the median, boxes the interquartile range, and whiskers the data range. In line graphs, the mean ± s.d is shown. Statistical tests: one-way ANOVA with Benjamini–Hochberg correction for multiple comparisons (**a**), two-tailed Mann–Whitney test for each comparison (**c**) or two-way ANOVA (**d**).

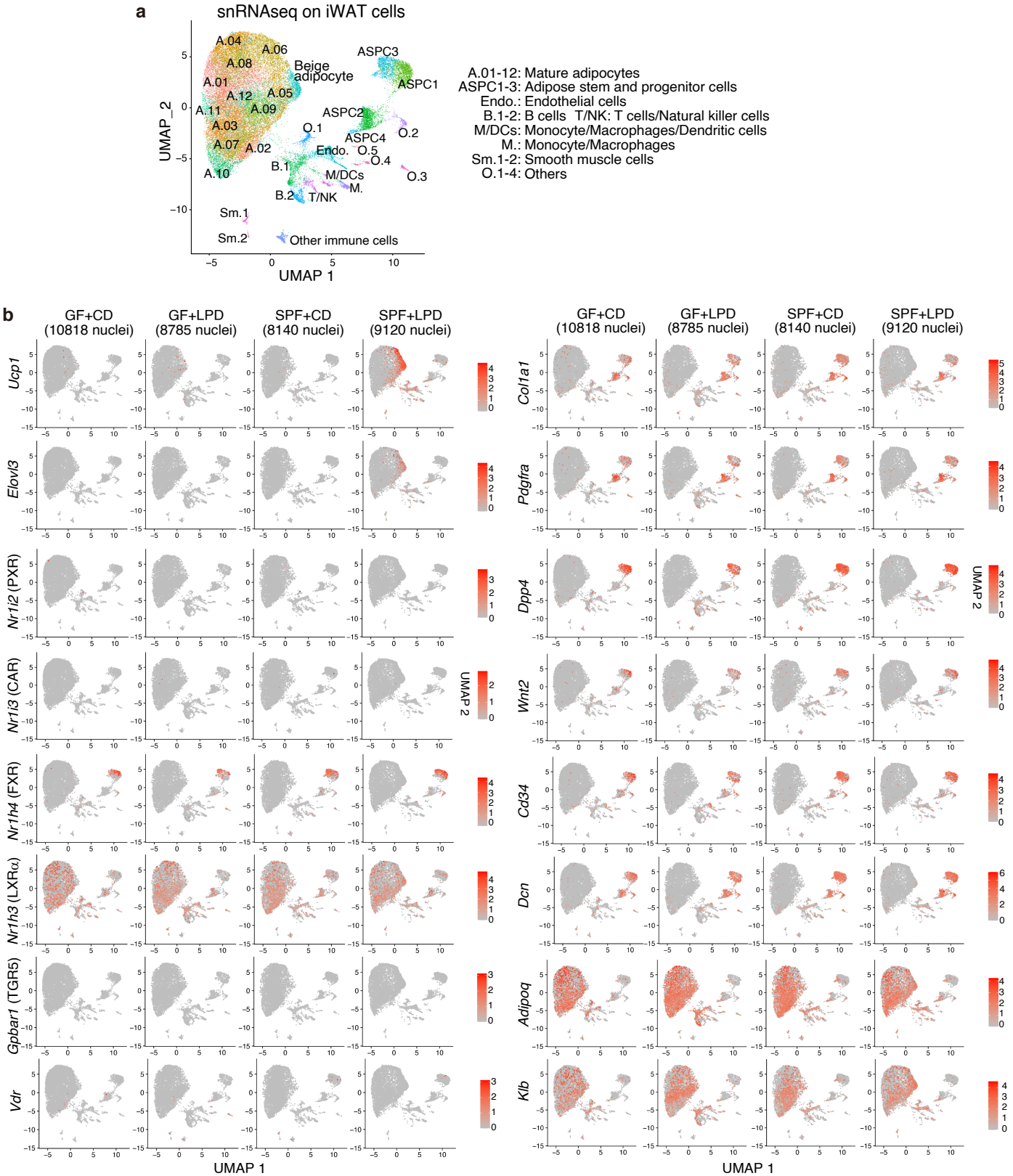

Extended Data Fig. 5 | ASPCs specifically express FXR in iWAT. snRNA-seq was conducted on iWAT cells from GF and SPF B6 male mice fed either a CD or an LPD for 6 weeks. Data were pooled from two independent samples, each consisting of nuclei from 3-4 mice. **a**,**b**, UMAP visualizations of the annotated cell populations (**a**) and indicated genes (**b**) are shown. Among bile acid receptors, pregnane X receptor (PXR, *Nr1i2*), vitamin D receptor (VDR), constitutive androstane receptor (CAR, *Nr1i3*), and TGR5 were not detectably expressed in iWAT cells, whereas liver X receptor alpha (LXRα, *Nr1h3*) was broadly expressed across multiple adipose cell clusters. In contrast, FXR (encoded by *Nr1h4*) expression was restricted to a cluster expressing ASPC markers, including *Dpp4*, *Col1a1*, *Pdgfra*, *Wnt2*, *Cd34*, and *Dcn*.

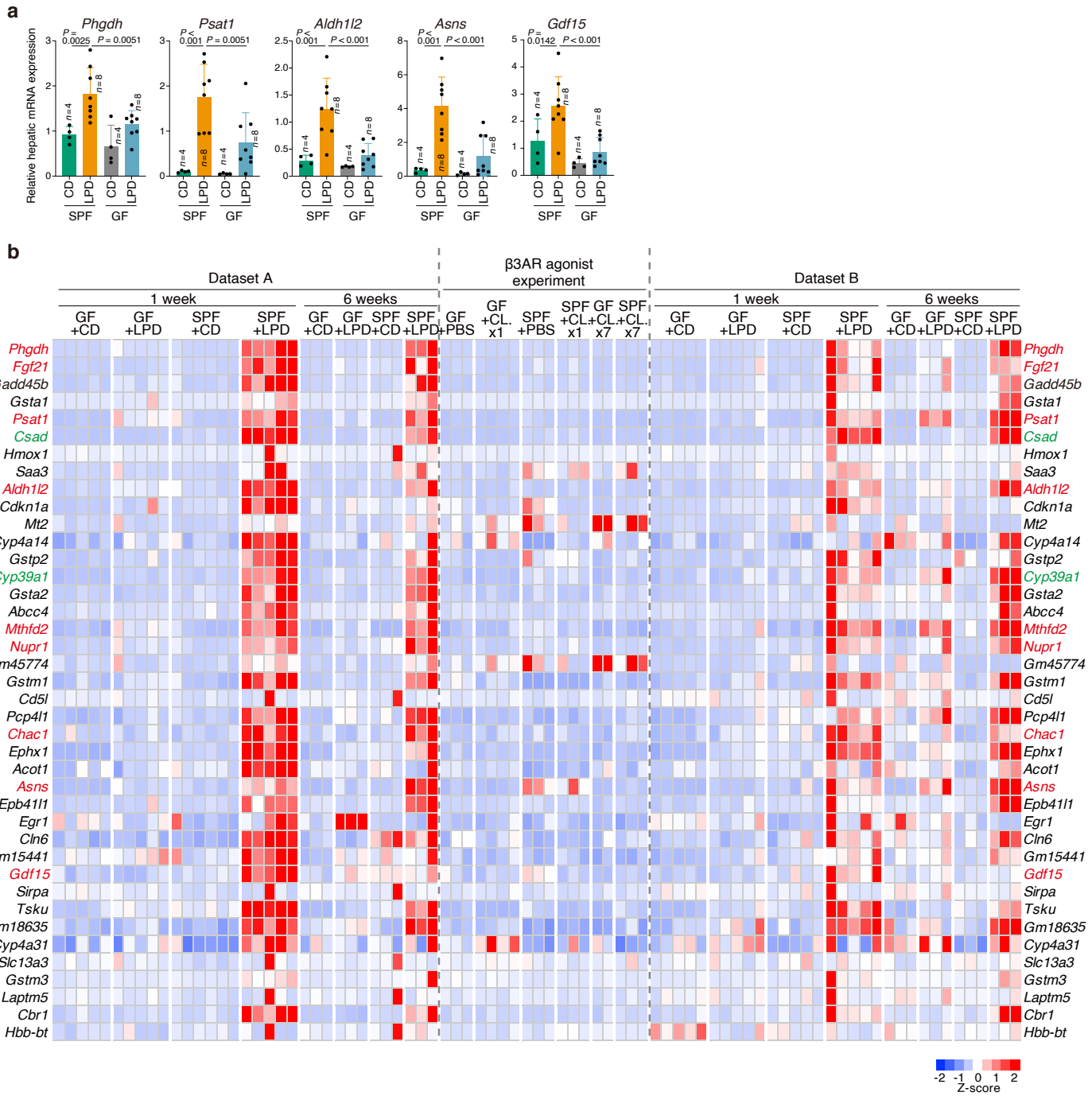

Extended Data Fig. 6 | The gut microbiota mediates LPD-induced alterations in the liver transcriptome. a,**b**, Eight-week-old GF and SPF B6 male mice were fed a CD or an LPD for 1 or 6 weeks. Liver RNA was extracted, followed by RT–qPCR of the indicated genes (**a**) and bulk RNA-seq (**b**). The heat map highlights genes with higher expression levels (≥5-fold change with RPKM ≥ 200) in LPD-fed SPF mice versus LPD-fed GF and CD-fed SPF mice. Data show two independent experiments (datasets A and B) as well as a positive control experiment in which β3-adrenergic receptor (β3AR) agonist CL316,243 was administered intraperitoneally (20 μg/mouse/day), either as a single dose ("CL.x1") or daily for 7 consecutive days ("CL.x7"). Genes previously reported to be ATF4-inducible are highlighted in red, while *Csad* and *Cyp39a1*, which have been implicated in bile acid production, are highlighted in green. Each circle represents an individual mouse, and bars show mean ± s.d. Statistical tests: one-way ANOVA with Benjamini–Hochberg correction for multiple comparisons (**a**).

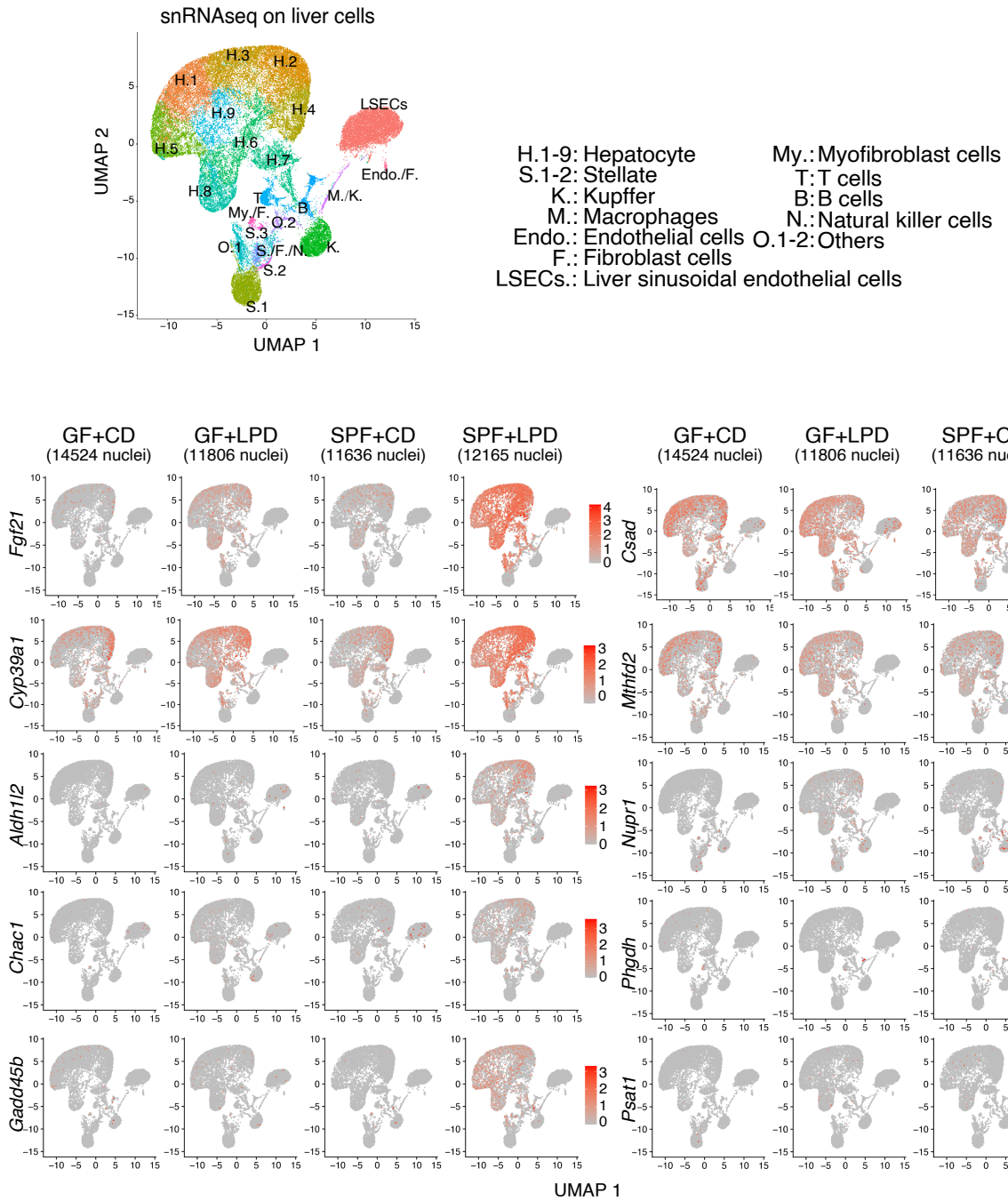

Extended Data Fig. 7 | LPD feeding upregulates ATF4-inducible genes in hepatocytes in a microbiota-dependent manner. snRNA-seq was performed on liver tissue from GF and SPF B6 male mice fed either a CD or an LPD for 9 weeks. Expression levels and distributions of the indicated genes are visualized by UMAP. Plots show pooled data from two library preparations, each derived from hepatocyte nuclei isolated from a single mouse.

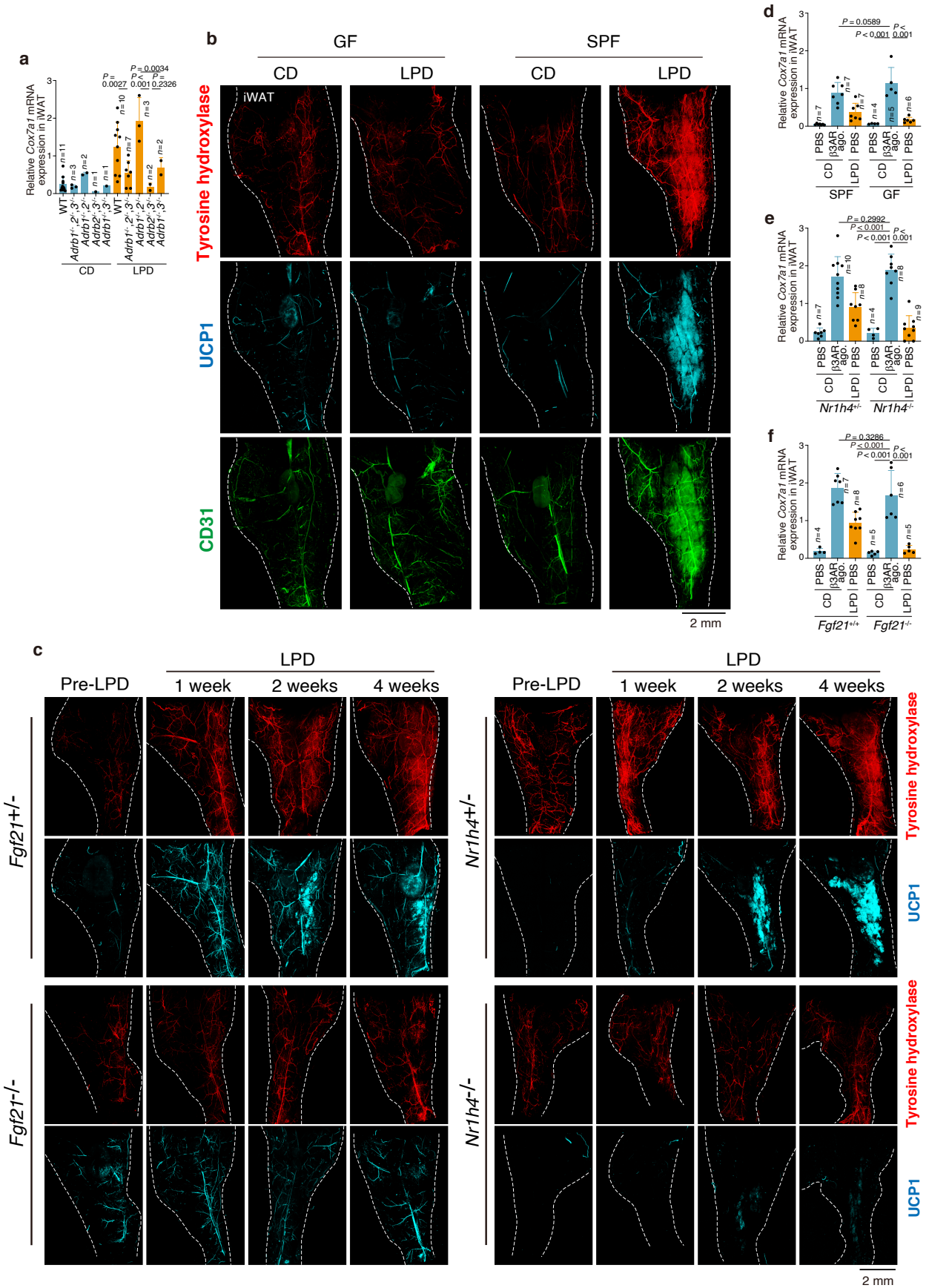

Extended Data Fig. 8 | See next page for caption.

Extended Data Fig. 8 | The microbiota mediates remodelling of sympathetic neurons and vasculature. a,**d**–**f**, *Cox7a1* expression in iWAT was quantified in SPF mice of the indicated genotypes after 6 weeks on a CD or an LPD. Each circle represents an individual mouse, and bars show mean ± s.d. Statistical tests: one-way ANOVA with Benjamini–Hochberg correction. **b**, GF and SPF B6 male mice were fed either a CD or an LPD for 6 weeks. Whole-mount immunostaining of iWAT with iDISCO tissue clearing was performed using antibodies against tyrosine hydroxylase (sympathetic nerves; red), UCP1 (blue), and CD31 (endothelial cells; green). **c**, *Fgf21*$^{+/-}$, *Fgf21*$^{-/-}$, *Nr1h4*$^{+/-}$, and *Nr1h4*$^{-/-}$ mice were fed an LPD for 1, 2, or 4 weeks, and whole-mount immunostaining of iWAT was performed using antibodies against tyrosine hydroxylase (red) and UCP1 (blue). Images were acquired using a light sheet microscope. Representative images from two independent experiments are shown, with dashed lines indicating the iWAT boundaries.

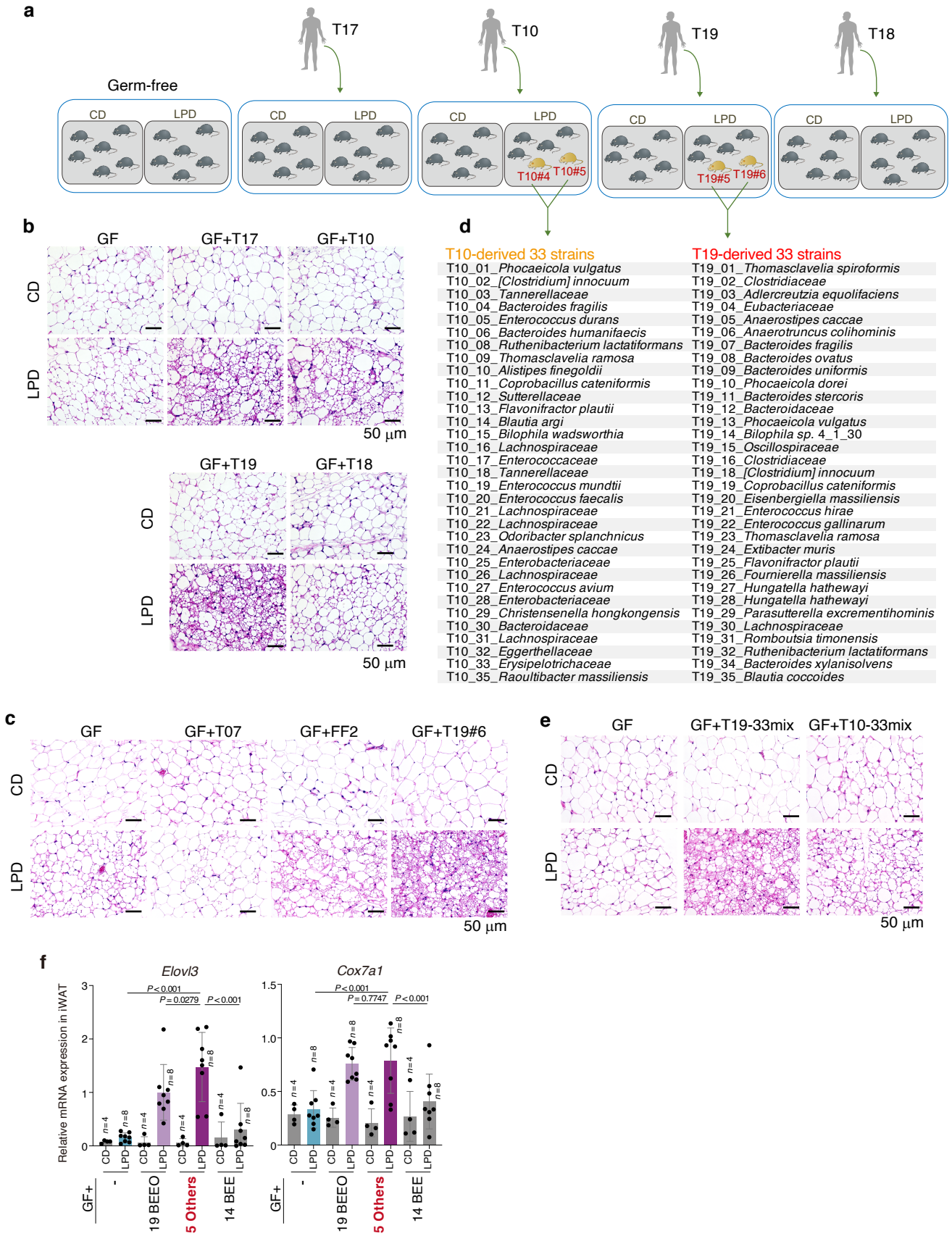

Extended Data Fig. 9 | See next page for caption.

Extended Data Fig. 9 | Isolation of beige-inducing bacterial strains from the human gut microbiota. a, Schematic illustrating the strategy used to isolate commensal strains that promote browning from human gut microbiota. **b**, GF B6 male mice were inoculated with faecal microbiota from human volunteers T17, T10, T19, or T18 and were fed a CD or an LPD for 6 weeks. Representative H&E-stained iWAT sections of the indicated groups from two independent experiments are shown. **c**, GF B6 male mice were inoculated with faecal microbiota from human volunteers T07 or FF2, or with caecal contents from mice colonized with T19 faecal microbiota, and were fed a CD or an LPD for 6 weeks. Representative H&E-stained iWAT sections from a single experiment are shown. **d**, Bacterial strains were isolated from caecal contents of mice T10-4, T10-5, T19-5 and T19-6. 33 strains were isolated from the T10-colonized mice, and an additional 33 strains were isolated from the T19-colonized mice. Lists of the 33 T10- or T19-derived strains, as determined by 16S rRNA sequencing, are shown. **e**, GF B6 male mice were colonized with the T10- or T19-derived 33-mixes and fed a CD or an LPD for 6 weeks. Representative H&E-stained iWAT sections from two independent experiments are shown. **f**, GF B6 mice were colonized with the indicated bacterial consortia—19 BEEO (a 19-strain group comprising *Bacteroides*, *Enterococcus*, *Erysipelotrichaceae*, and other phyla), 5 Others (strains from "other" phyla), or 14 BEE (the remaining 14 strains from the 19 BEEO group)—selected from the T19-derived 33-mix and fed a CD or an LPD for 4 weeks. mRNA expression of the indicated genes in iWAT, normalized to *Ppib*, was quantified by qPCR. Each circle represents an individual mouse, and bars show the mean ± s.d. Statistical analysis: one-way ANOVA with Benjamini–Hochberg correction.

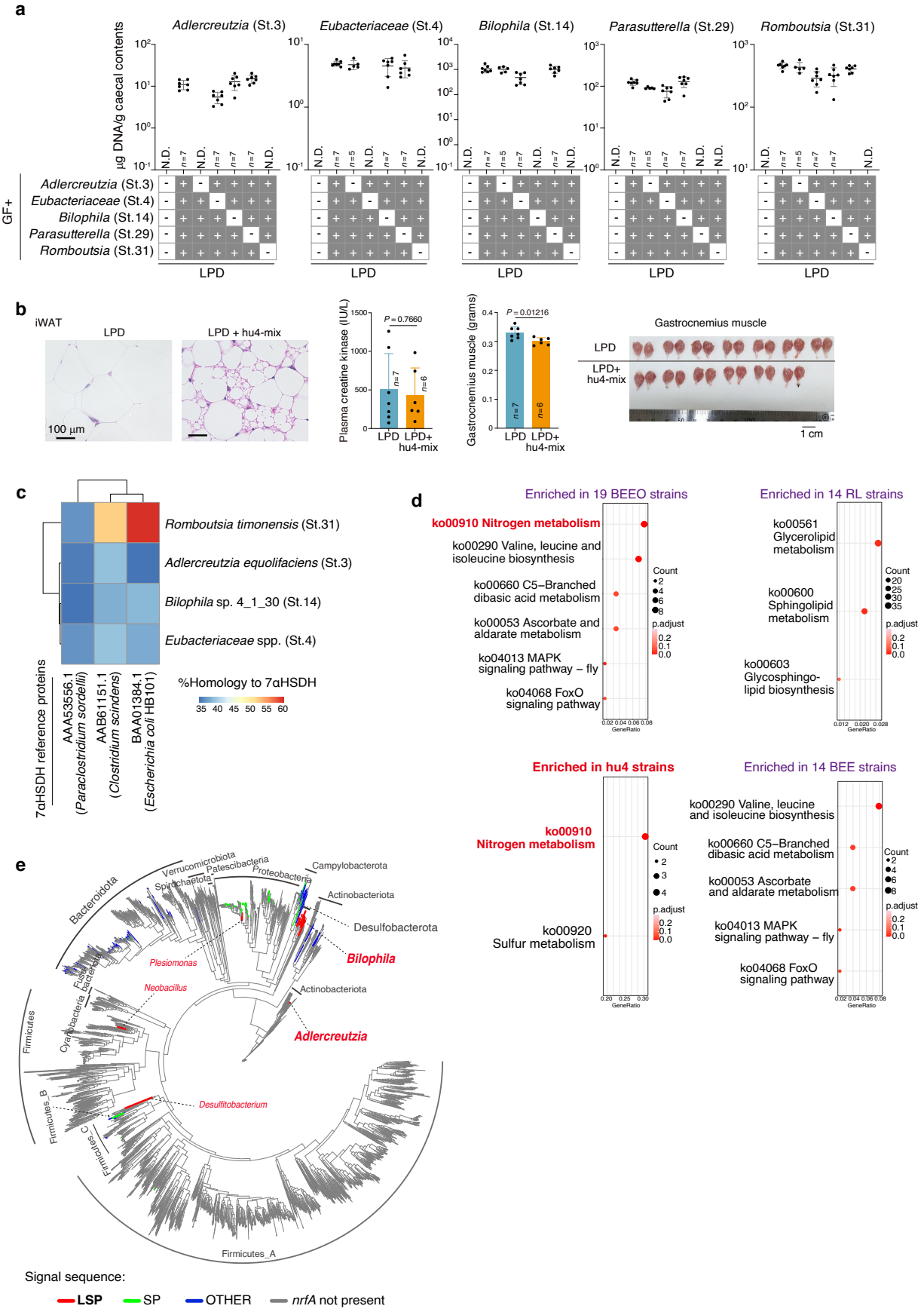

Extended Data Fig. 10 | See next page for caption.

Extended Data Fig. 10 | Characterization of four beige-cell-inducing human-derived bacterial isolates. a, GF B6 mice were inoculated with the indicated bacterial isolate mixtures (5 Others-mix or all possible 4-strain permutations thereof) or vehicle control and fed an LPD for 4 weeks. Plus (+) indicates inclusion, and minus (−) indicates exclusion of the indicated strain. Bacterial DNA from each strain was quantified in caecal contents by qPCR using strain-specific primers targeting 16S rRNA gene sequences. Each circle represents an individual mouse, and horizontal lines indicate the mean, ± s.d. N.D., not detected. **b**, GF mice were inoculated with faecal microbiota from human participant T07, fed a HFD for 4 weeks, and then switched to an LPD and given two oral doses of the hu4 strains or vehicle control. After 6 weeks of LPD feeding, H&E staining of iWAT was performed, plasma creatine kinase levels were measured as an indicator of muscle damage, and gastrocnemius muscle mass and gross morphology were assessed. Bars indicate the mean ± s.d, and statistical significance was determined by two-tailed unpaired *t*-test. **c**, Proteins homologous to the three previously defined reference 7α-hydroxysteroid dehydrogenase (7αHSDH) proteins were identified in the genome of each indicated strain, and the percent sequence homology of the best-matching hit in each strain to each of the three reference proteins is displayed as a heat map. **d**, GF mice were colonized with T19-derived 33-mix and fed a CD or an LPD for 4 weeks. Bacterial RNA was extracted from caecal contents and subjected to metatranscriptome sequencing. Pathway enrichment analysis was performed using the R package clusterProfiler (version 1.38.3), and KEGG pathways significantly enriched in the 19 BEEO, 14 RL, hu4, or 14 BEE subsets of the 33-mix under LPD versus to CD conditions are shown. Benjamini–Hochberg correction for multiple comparisons was used to calculate adjusted *p*-value. **e**, NrfA was annotated in all reference genomes from the Unified Human Gastrointestinal Genome (UHGG) using eggNOG, and signal sequences were analysed using SignalP. Species harbouring NrfA homologues with lipoprotein signal peptides (LSPs) are highlighted in red. SP, standard secretory signal peptide; LSP, lipoprotein signal peptide. LSPs are predicted to facilitate transport via the Sec translocon, cleavage by signal peptidase II, and anchoring to the inner membrane[94], thereby allowing NrfA to localise to the periplasm where it participates in the dissimilatory nitrate reduction to ammonium (DNRA) pathway. In this process, NrfA detoxifies nitrite and minimizes nitrogen loss by converting it into reusable, water-soluble ammonia instead of N_2 gas[56,95]. Among 266 genomes spanning nine phyla that encode *nrfA* homologue genes, only 10.5% contain LSPs, and the vast majority of LSP-containing *nrfA* homologues are found in the phylum Desulfobacterota, including *Bilophila* species. *Adlercreutzia* is the only genus within the phylum Actinobacteriota identified to carry a LSP-containing *nrfA* homologue (see also Supplementary Table 2).

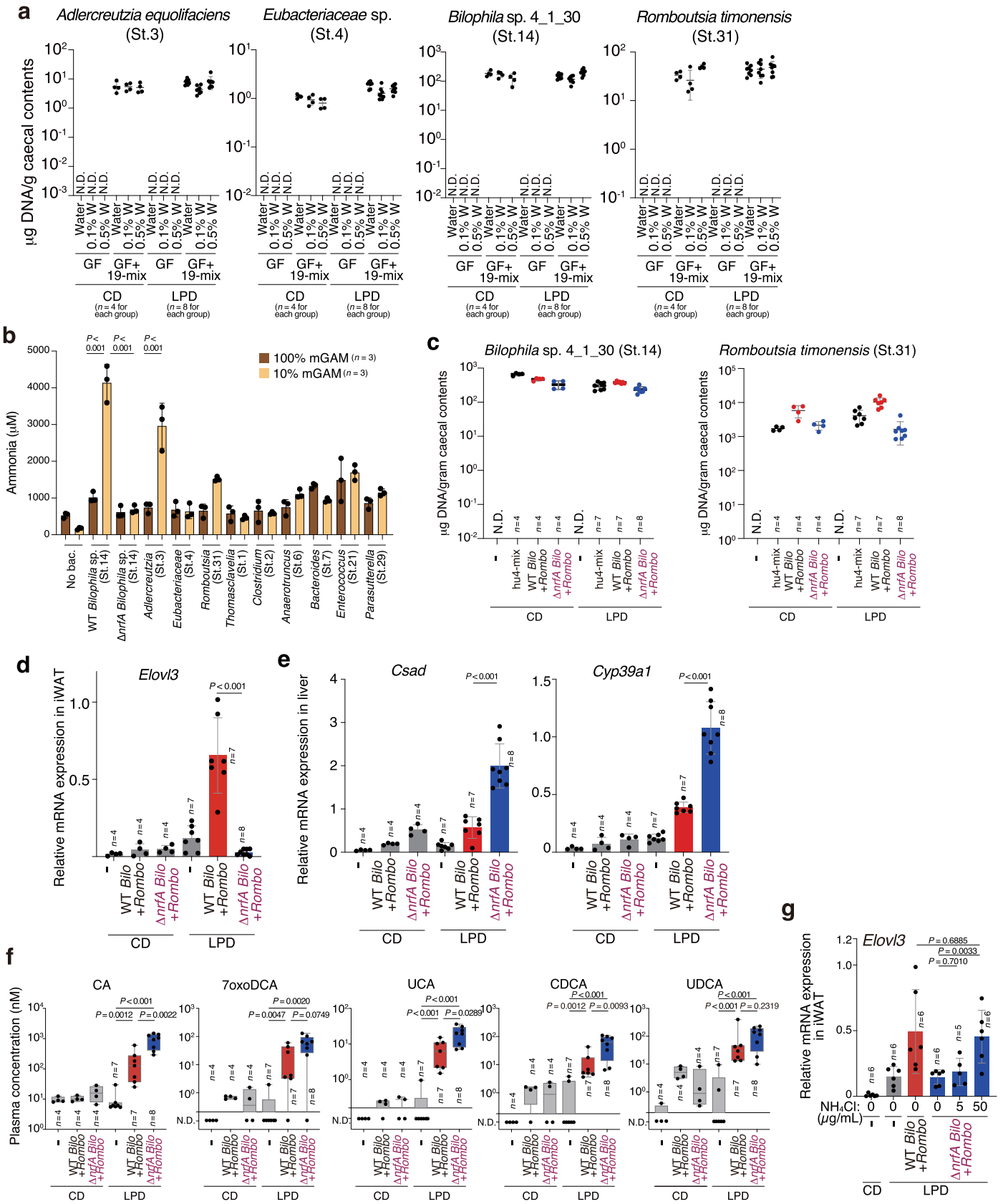

Extended Data Fig. 11 | See next page for caption.

Extended Data Fig. 11 | *Bilophila nrfA* contributes to LPD-mediated browning. a, GF B6 mice were colonized with the 19 BEEO-mix and fed a CD or an LPD for 3 weeks. During the last 2 weeks, mice were treated with 0.1% or 0.5% sodium tungstate dihydrate (W) via the drinking water. Bacterial DNA from each strain was quantified in caecal contents by qPCR using strain-specific primers targeting 16S rRNA gene sequences. **b**, Among the 33 T19-derived strains, 12 strains (including all members of the hu4-mix) were selected as phylogenetic representatives and cultured in 100% or 10% mGAM (diluted with Milli-Q-water) for 1 hour. Ammonia concentrations in the culture supernatants were measured using an ammonia detection kit ($n = 3$ biological replicates). Notably, *nrfA*-encoding, but not Δ*nrfA*, *Bilophila* and *Adlercreutzia* strains robustly produced ammonia. **c**–**f**, GF B6 mice were colonized with hu4-mix or with either *nrfA*-sufficient (WT) or *nrfA*-deficient (Δ*nrfA*) *Bilophila* sp. 4_1_30 (St.14) (*Bilo*) in combination with *R. timonensis* (St.31) (*Rombo*). Colonization density of each strain was quantified by qPCR using strain-specific 16S rRNA primers (**c**). Expression of *Elovl3* in iWAT (**d**), and *Csad* and *Cyp39a1* in the liver (**e**) were determined by qPCR and normalized to *Ppib*. Plasma bile acids were quantified by LC–MS/MS (**f**). **g**, Ammonium chloride (NH_4Cl) was administered to the indicated gnotobiotic mice via the drinking water, and *Elovl3* expression in iWAT was assessed. Circles represent individual mice (**a**,**c**–**g**) or wells (**b**). Horizontal lines (**a**,**c**) or the heights of each bar graphs indicate the mean ± s.d. Box-plot centre lines indicate the median, boxes the interquartile range, and whiskers the data range. Statistical tests: one-way ANOVA with Benjamini–Hochberg correction (**b**,**d**,**e**,**g**) or Mann–Whitney test (two-tailed) for each comparison (**f**). N.D., not detected.

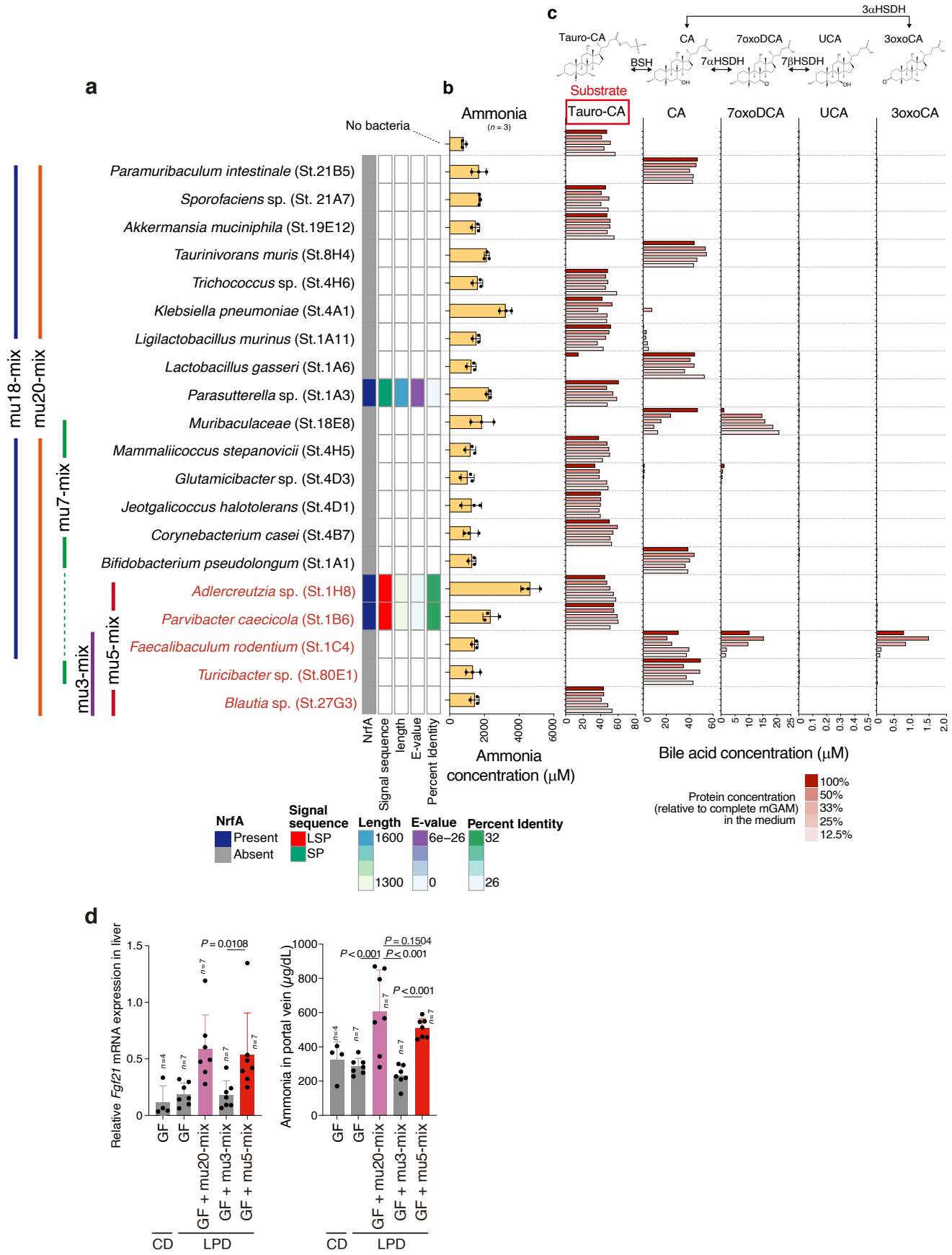

Extended Data Fig. 12 | See next page for caption.

Extended Data Fig. 12 | Ammonia production and bile acid conversion capabilities of 20 mouse-derived strains. a, Carriage of *nrfA* homologues and their signal sequences [lipoprotein signal peptides (LSPs) or Sec/SPI standard signal peptides (SPs)] was analysed across the genomes of the 20 mouse-derived strains. *nrfA* genes were annotated using eggNOG-mapper, and signal sequences were predicted with SignalP 6.0. "Percent identity" indicates sequence similarity to the *Bilophila* NrfA protein, as calculated by BLASTP. "E-value" denotes the expected number of chance alignments with an equal or higher bit score, as computed by BLASTP. "Length" indicates the length of the protein from each isolate that best aligns to NrfA as predicted by eggNOG-mapper. **b**, The 20 strains were cultured in 10% mGAM (diluted with Milli-Q water) for 1 hour, and ammonia concentrations in the culture supernatants were quantified using an ammonia detection kit ($n = 3$ biological replicates). **c**, Each strain was incubated with 50 μM taurocholic acid (tauro-CA) in medium containing varying protein concentrations (100% to 12.5% relative to complete mGAM) for 48 hours, and the resulting bile acids in the culture supernatants were analysed by LC–MS/MS. **d**, GF mice were colonized with the indicated mouse-derived bacterial consortia (mu20-, mu3-, mu5- or mu7-mix) and fed an LPD for 6 weeks. Hepatic *Fgf21* expression and portal vein ammonia concentrations were measured. Each circle represents an individual mouse, and bars show mean ± s.d. Statistical tests: one-way ANOVA with Benjamini–Hochberg correction.